Interactions Between Currents and the Spatial Structure of Aquatic Vegetation

By

Jeffrey T. Rominger

B.S. Civil & Environmental Engineering
University of Virginia, 2007

Submitted to the Department of Civil and Environmental Engineering
in partial fulfillment of the requirements for the degree of

Master of Science in Civil and Environmental Engineering
at the
MASSACHUSETTS INSTITUTE OF TECHNOLOGY
June 2009

Signature of Author .....
Department of Civil and Environmental Engineering
May 8, 2009

Certified by .....
Heidi M. Nepf
Professor of Civil and Environmental Engineering
Thesis Supervisor

Accepted by .....
Daniele Veneziano
Chairman, Departmental Committee for Graduate Students

Interactions Between Currents and the Spatial Structure of Aquatic Vegetation

By

Jeffrey T. Rominger

Submitted to the Department of Civil and Environmental Engineering
on May 8, 2009 in partial fulfillment of the requirements
for the degree of
Master of Science in Civil and Environmental Engineering

Abstract

Vegetation is present in nearly all aquatic environments, ranging from meandering streams to constructed channels and rivers, as well as in lakes and coastal zones. This vegetation grows in a wide range of flow environments as well, from stagnant water to highly turbulent flows dominated by waves and currents. Feedbacks between the dominant currents and the vegetation not only significantly alter the velocity structure of the flow, but play a large role in determining the spatial structure of the vegetation as well.

This thesis examines these interactions through field experiments, review of existing literature and theoretical and analytical models. The first study describes a set of experiments in which vegetation was added to the point bar of a stream meander during base flow. During the next flood event, this vegetation proved to be destabilizing as a portion of the vegetation scoured away and the cross section of the open channel showed clear patterns of erosion. The secondary circulation present in the meander was significantly altered as well.

In the second study, the relationship between tidal currents and the spatial distribution of seagrass meadows is examined. Seagrass beds range in their coverage from continuous meadows, to spotty swaths dominated by discrete patches. The relationship between this area coverage and tidal currents, explained by the principles of percolation theory, helps describe why certain distributions of seagrass within a meadow are more stable than others.

Drawing on the principles and examples established in the first two sections, the final section describes an analytical model for predicting vegetation coverage in a rectangular open channel. The model can allow for fixed banks, such as those in a concrete-lined channel, or can allow erosion of the boundaries, as is possible in natural streams. These two versions of the model show notably different results. Ultimately, this thesis presents multiple cases of the interactions between currents and aquatic vegetation and showcases an important example of a multi-disciplinary research approach in fluid mechanics.

Thesis Supervisor: Heidi M. Nepf
Title: Professor of Civil and Environmental Engineering

Acknowledgements

First and foremost, I would like to thank my advisor, Heidi Nepf, for her creativity, advice, expertise and patience over the past two years. I have learned and grown so much, and it would not have been possible without her work as my advisor. I would also like to thank her for acceptance of my diverse interests and her encouragement in pursuing those interests as they relate to fluid mechanics and as they apply to my future professional life.

Several students, former students and professors were very generous with their advice and assistance over the past two years. I would like to thank Anne Lightbody, Yukie Tanino, Mitul Luhar, Kevin Zhang, Mack Durham, David Gonzalez-Rodriguez, Marcos, Roman Stocker, Eric Adams, Ole Madsen and Chiang Mei for their instruction, time and thought.

I would like to thank my family and all of my friends who gave me support and enriched my personal (and academic) life over the past two years as well.

This work is based upon work supported by the National Science Foundation under Grant No. EAR 0738352. Any opinions, findings, and conclusions or recommendations expressed in this material are those of the authors and do not necessarily reflect the views of the National Science Foundation. Research assistance for the material presented in Chapter 2 was provided by Katie Kramarczuk, June Sayers, Alex Nereson, Johnathan Wacloff, Eric Johnson, and Mary Presnail. This work was also supported by the STC program of the National Science Foundation via the National Center for Earth-surface Dynamics under the agreement Number EAR-0120914.

Table of Contents

List of Figures

List of Tables

1. Introduction

1.1. *Brief Introduction to Aquatic Vegetation*

The immediate, hydraulic impact of aquatic and riparian vegetation is an increase in flow resistance and a reduction in conveyance capacity (Kouwen and Unny 1973; Kouwen, 1990; Wu et al 1999). Historically, many channels have been straightened and denuded of vegetation to accelerate the passage of peak flows, but these anthropogenic modifications have had unintended consequences on water quality, channel stability and stream ecology. For example, many studies show that aquatic macrophytes maintain and improve water quality by utilizing nutrients, producing oxygen and detaining heavy metals and other contaminants (e.g. Chambers and Prepas 1994; Kadlec and Knight 1996; Windham et al. 2003). Mars et al., reports that aquatic vegetation can effectively utilize excess nitrogen and phosphorous and recommends widespread planting as a remediation technique (1999). In addition to reducing nitrogen and phosphorous concentrations, aquatic vegetation sequesters heavy metals such as arsenic, mercury and lead in their root systems (Windham et al., 2003). Vegetation can also have positive impacts on water quality by reducing suspended solids and thereby reducing the contaminants that associate with these solids (Moore et al. 2004).

Vegetation has proved so effective at removing nutrients and solids from contaminated water that constructed wetlands are now a viable alternative to conventional wastewater treatment plants (Mitsch and Jorgensen 2004). Several case studies document that natural or constructed wetlands can remove over 80% of nitrogen and over 90% of total phosphorus, total suspended solids (TSS), 5-day biological oxygen demand (BOD5) and heavy metals along with many harmful pathogens (Sundaravadivel and Vigneswaran 2001, Kadlec 2003, Moore 2004). Beyond enhancing the removal of contaminants and solids in water bodies, aquatic and riparian

vegetation can also promote biodiversity by creating spatial heterogeneity in the flow (Kemp et al. 2000; Crowder and Diplas 2002).

1.2. *Aquatic Vegetation as an "Ecosystem Engineer"*

Whereas vegetation was historically removed from channels, today vegetation is often added to channels not just to improve water quality, but also to stabilize the banks and alter the flow patterns. Several studies show how the roots of certain species, ranging in scale from grasses to trees, can increase the mechanical stability of stream and riverbanks (Abernethy and Rutherford 2000; Simon and Collison 2002). By reducing near-bed velocity, in-stream and floodplain vegetation can both reduce erosion and promote deposition. Therefore the addition of vegetation is often advocated as a restoration technique, not only for its ability to remove contaminants from the water column, but also for its ability to increase the mechanical stability of banks and coastlines (Mars et al. 1999; Abernethy and Rutherford 1998; Pollen and Simon 2005; Tanaka 2009). Also, coastal marshes and mangroves provide coastal protection by damping waves and storm surge (*e.g.* Turker et al. 2006, Massel et al. 1999, Othman 1994).

Aquatic vegetation is often labeled an "ecosystem engineer," which is best defined as an organism that alters its surrounding environment (Jones et al. 1994). Several geomorphologic studies document the ability of vegetation to influence channel shape, promote sediment deposition and carve distinct habitats out of dynamic flow environments. Tal and Paola (2007) specifically document the ability of vegetation to stabilize banks and to transform a channel from a braided planform into a single-thread channel. Fagherazzi (2006) described vegetation's ability to stabilize salt marshes through enhanced sediment deposition and a reduction in wave energy. As an obstruction in the water, aquatic vegetation exerts a drag force on the flow and

thus diverts water to areas with less drag (this is described in the next section in detail). By diverting a portion of the flow, the vegetation diminishes the velocity in the region with vegetation and therefore reduces the forces that cause erosion while simultaneously promoting sediment deposition. Through both processes, the bed becomes more stable. Fonseca et al. (1983) observed that finite patches of seagrass were associated with local bed maxima and attributed this to enhanced particle retention within the meadow. By reducing the forces that cause erosion and creating conditions that allow sediment to settle and accumulate, vegetation can help the bed become more stable. This positive feedback, described in several of the studies cited above, promotes "sheltering", wherein the individual plants are protected by the characteristics of the overall vegetation canopy.

The growth and propagation of aquatic vegetation is not without limits, though. Unstable and rapidly moving sediment can be detrimental to vegetative growth, as high turbulence in the plant canopy can be as well. Chambers et al., observed a strong negative correlation between macrophyte biomass and current velocities in a river setting, with little vegetation present above an apparent threshold of 1 m/s (1991). Similarly, Nilsson found the percentage of bare ground along a reach increased with increasing current velocities in the free stream (1987). These thresholds are important feedback mechanisms that control the growth of vegetation in high-energy environments.

1.3. *Stream Restoration*

Many of these principles come together and are applied in stream restoration. The restoration of degraded waterways is a burgeoning industry in the United States, with several millions of dollars spent every year specifically on restoring local fisheries (NRC 1996, Ronie et

al. 2002). The United States has 3.5 million miles of rivers, and as of 1978, an estimated 70-90% of all of these riparian areas in the U.S. were extensively altered (Kaufmann et al. 1997). One of the most telling definitions of riparian zones describes them as "an interface between man's most vital resource, namely, water, and his living space, the land" (Odum 1981). Restoration most often seeks to reduce or erase the negative impacts that humans have wrought on the stream through mismanagement, alteration or destruction due to the overarching need for resources. This is accomplished through reestablishing the natural ecosystems and the natural equilibrium that existed prior to the changes made by society. The reestablishment of natural ecosystems requires some understanding of the forces governing a stream's dynamic equilibrium. Restoration goals often include bank stabilization, re-creation of floodplains, habitat creation and pollutant filtering (Kondolf 1995). Restoration projects can also seek to mitigate anticipated damages to streams due to construction and development projects. Other goals often termed as "restoration projects" may include simply increasing channel capacity or creating favorable recreation areas (Kondolf 1995). Addressing many of the possible goals, several current restoration techniques involve the addition of vegetation or other roughness elements in the riparian zone. These techniques can be effective, but are often piecemeal in nature, addressing narrow, local issues like bank stabilization and creation of small habitats. Better understanding of the governing physics is needed to more effectively restore streams.

1.4. *Physical Characteristics of Aquatic Vegetation*

Aquatic vegetation is highly heterogeneous, with variations across individual plants and species, as well as larger-scale variations in the density and height of aquatic vegetation canopies. At the scale of individual plants, i.e. the stem scale, there are variations in stiffness,

buoyancy and the stem geometry. Different species vary from being completely rigid to highly flexible. At the scale of the canopy, the variable spacing between plants is parameterized by an average spacing and stem density. Canopy height is divided into two general categories. Emergent aquatic vegetation occupies the entire water column, growing up to the free surface, and in many cases, extending into the air above the water surface. Submerged vegetation occupies only a fraction of the water column, allowing the flow to pass over the canopy. In this thesis, I am primarily interested in the interactions at the canopy-scale, and therefore I describe the canopy based on its mean height and average stem density while ignoring the stem-scale variations in geometry.

We describe the canopy's density using its frontal area per unit volume, a. For most species of aquatic vegetation, there is a characteristic stem width or diameter, d_{plant}, from which $a = md_{plant}$, where m is the number of stems per unit area of the bed. Although the stem density can vary spatially, a mean spacing between the stems is described using,

$$s = \sqrt{\frac{d_{plant}}{a}} \,. \tag{1.1}$$

The frontal area per unit volume, a, is used to describe the solidity of terrestrial canopies, $\lambda = ah$ (e.g. Grimmond and Oke 1999, Jimenez 2004). Often a canopy's density is expressed more explicitly with its solid volume fraction, $\phi = ad_{plant}$ and the complementary porosity, $n = 1 - ad_{plant}$. Aquatic canopies exhibit a wide range of densities, varying several orders of magnitude, with $a = 0.0001$ to $1\ cm^{-1}$, where the lower limit can describe the understory of sparse kelp forests, and the higher limit describes denser channel vegetation or mangroves (*e.g.* Kouwen and Unny, 1973; Chandler et al., 1996; Ciraolo et al., 2006). Marsh grasses are relatively sparse with

$\phi \approx 0.01$, stem diameters d_{plant} = 0.1 cm to 1 cm, and a = 0.01 to 0.10 cm^{-1} (*e.g.* Valiela et al., 1978; Leonard and Luther, 1995; Lightbody and Nepf, 2006; Hena et al., 2007). The understory of kelp forests (the layer below the dense mat of fronds near the surface) can have a frontal area per unit volume, a = 0.0001 to .1 cm^{-1}, where the lower limit is found most often in deep water forests (Jackson 1997, Gaylord et al. 2007). Mangrove forests, or mangals, are some of the densest aquatic canopies, with a solid volume fraction as high as $\phi \approx 0.45$, root diameters d_{plant} = 4 cm to 9 cm, and a = 0.2 cm^{-1} (Mazda et al., 1997; Furukawa et al., 1997). In many canopies, the frontal area per unit volume varies significantly with height above the bed. This is often exemplified in canopies where the plant morphology varies from a bare stem near the bed, branching into leafier and denser material closer to the surface to maximize exposure to sunlight. In this thesis I restrict the investigation to morphologies that are approximately constant over the height of the canopy.

1.5. *Momentum Equations*

Due to the stem scale heterogeneities present in the flow, a double-averaging scheme is employed to average over horizontal spatial fluctuations, as well as short-time fluctuations (e.g. Raupach and Shaw 1982). The velocity is averaged horizontally over a scale equivalent to a few the stem spacings, s, to remove fluctuations near the stems and the stem wakes. The time average removes random turbulence and stem-scale shedding fluctuations. First, the instantaneous velocity and pressure (p) fields are decomposed into the time average (overbar) and deviations from the time-average (single prime). The time-averaged quantities are further decomposed into the spatial mean in a plane parallel to the bed (angle bracket) and deviations from that spatial mean (double prime). The vertical velocity, w, is assumed to be small

compared to the longitudinal and lateral velocities, u and v, respectively. The case studies presented in this thesis are restricted to canopies of high porosity, wherein $n \approx 1$. Therefore the resulting momentum balance equation is (e.g. Nikora et al. 2007)

$$\underset{\text{(i)}}{\frac{D\langle\bar{u}\rangle}{Dt}} = \underset{\text{(ii)}}{gS} \underset{\text{(iii)}}{-\frac{1}{\rho}\frac{\partial\langle\bar{p}\rangle}{\partial x}} \underset{\text{(iv)}}{+\frac{\partial}{\partial y}\bar{\tau}_{xy}} \underset{\text{(v)}}{+\frac{\partial}{\partial z}\bar{\tau}_{xz}} \underset{\text{(vi)}}{-F_D}. \tag{1.2}$$

where the shear stress terms are given by

$$\underset{(\text{iv}_a)\ (\text{iv}_b)\ (\text{iv}_c)}{\bar{\tau}_{xy} = \nu\frac{\partial\langle\bar{u}\rangle}{\partial y} - \overline{u'v'} - \overline{u''v''}} \tag{1.3}$$

$$\underset{(\text{v}_a)\ (\text{v}_b)\ (\text{v}_c)}{\bar{\tau}_{xz} = \nu\frac{\partial\langle\bar{u}\rangle}{\partial z} - \overline{u'w'} - \overline{u''w''}} \tag{1.4}$$

Here, term (i) is the material derivative of the longitudinal velocity and represents both the instantaneous and convective accelerations of $\langle\bar{u}\rangle$, term (ii) is the component of gravity parallel to the bed where S is the pressure gradient, ρ is the density of the fluid and ν is the kinematic viscosity. Term (iii) is the longitudinal pressure gradient. Term (iv) is the spatially-averaged lateral shear stress, comprised of the viscous stress (iv_a), the turbulent Reynolds stress (iv_b) and an additional stress, called the dispersive stress (iv_c), associated with spatial correlations in velocity. The dispersive stress is negligible compared to (less than 10% of) the turbulent stress for ah >=0.1; and increases only to 30% at ah = 0.03 (Poggi et al., 2004). Although the

dispersive stress makes some contribution in sparse canopies, the Reynolds' stress is the dominant stress term for nearly all aquatic canopies. Term (v) is the vertical shear stress, comprised of the same components as the lateral shear stress. Since I assume that the canopy density is uniform in the vertical direction, terms (v_b) and (v_c) can be neglected as well. The final term in the equation, term (vi), is the drag force the vegetation exerts on the flow.

Each of the three case studies presented in this thesis describes a different flow environment, ranging from streamflow in a meandering channel, tidal currents through a seagrass meadow to unidirectional currents in a straight channel. Each requires certain assumptions or slightly different notations for the momentum balance and the resulting equations will be presented in each section, respectively.

1.6. *Reynolds Number*

The Reynolds number is a dimensionless comparison of the inertial forces to the viscous forces, terms (i) and (vi), respectively, in the momentum equation (Equation 1.2). Using the stem diameter as the characteristic length scale, the stem Reynolds number is defined as,

$$\mathrm{Re}_{\mathrm{stem}} = \frac{\langle \bar{u} \rangle d_{plant}}{\nu}. \tag{1.5}$$

Depending on the type of environment, the depth of the flow, h, is also often used as the characteristic length scale, defining, Re_h. In surface flow wetlands, the velocities can be as low as m/day in order to maximize treatment time with Reynolds numbers near $O(1)$. In tidal inlets, velocities are typically of O(1 m/s) with with Re ~ $O(10^4)$. Open channel flows can have velocities up to O(10 m/s), especially during flood conditions. For the three case studies

presented in this paper, the Reynolds number is generally greater than $O(10^3)$ (e.g. Fonseca and Bell 1998, Rominger et al. 2009), and therefore viscous forces are often negligible.

1.7. *Vegetative Drag Force*

In open channel flows, resistance is most often modeled with a bed friction factor or roughness coefficient at the channel's wetted perimeter. In channels with aquatic vegetation, the stems exert a drag force on the flow that is often several orders of magnitude greater than the bed resistance. It is difficult to treat vegetation as added roughness since the vegetative drag can act over the entire depth of the flow, therefore this force needs to be parameterized in the governing equation. By averaging the drag force over the stem-scale variations, the mean drag force can be modeled using a quadratic drag law (e.g. Finnigan 2000),

$$F_D = \begin{cases} \dfrac{C_D a \langle \bar{u} \rangle \left| \langle \bar{u} \rangle \right|}{2} & \text{for vegetated areas} \\ 0 & \text{for unvegetated areas} \end{cases} \tag{1.6}$$

where C_D is the canopy drag coefficient. The drag force has a quadratic, as opposed to linear, dependence on $\langle \bar{u} \rangle$ due to the high Reynolds number of most environmental flows (Tanino and Nepf 2008).

1.8. *Overview of Thesis Contents*

Previous studies document the impact of existing vegetation (McBride et al. 2007, Shiono et al. 2009a, Shiono et al. 2009b), but do not investigate the possibility of enhancing that impact by choosing the specific placement of vegetation in the stream. Further, certain planting

locations and densities may prove to be inherently destabilizing, e.g. promoting erosion. Frissell and Nawa (1992) analyzed the failure of hundreds of roughness elements and in-stream structures, finding many of them incompatible with the local hydraulics of the streams. Specifically, structures increased local turbulence, caused scour holes to form, or were washed downstream during high flows. Similarly, to have successful replanting and restoration of channels using vegetation, how placement and planting density impact channel stability needs to be better understood. **Chapter Two** of this thesis provides insight into how the addition of vegetation at a specific location alters flow and channel stability. This study documents a set of experiments conducted in a constructed outdoor stream channel, wherein several variables could be controlled simultaneously. In this outdoor laboratory, the initial density and placing of vegetation was prescribed and then monitored for changes using a variety of techniques.

The second study presented in this thesis (**Chapter Three**) documents the feedback between tidal currents and the spatial structure of an eelgrass meadow in North Carolina. This study advances the results put forth by Fonseca and Bell (1998) and describes the feedbacks that exist between the distribution of plants in a seagrass meadow and the average tidal currents of the site. I ultimately describe how certain distributions of seagrass are inherently more stable than others and what the mechanisms are that drive the seagrass to these stable densities. The results of this section provide a new perspective on the natural organizations of seagrass meadows and the tendencies of these meadows in current-dominated environments.

Complementing these first two studies in **Chapter Four** is an analytical model that describes the natural feedbacks that prevent vegetation from encroaching beyond a certain limit into river or stream channels. This model builds on the conclusions of the previous two chapters and describes why certain vegetation densities and/or planting locations may be inherently

unstable. This model ultimately seeks to describe stable densities and amounts of vegetation in a channel based on certain stream parameters. This work is useful for streams/open channels or for restoration and stabilization projects in existing streams.

The interactions between aquatic vegetation and dominant stream and tidal currents have direct effects on the spatial structure of vegetation and for the velocity profile in a channel or seagrass bed. These interactions have important implications for local habitats, channel planform, sediment stability and the overall health of the ecosystem. It is the goal of this thesis to describe the influence of aquatic vegetation on unidirectional currents as well as the feedback mechanisms through which currents influence the growth and geometry of aquatic vegetation.

2. The Effects of Added Vegetation on Sand Bar Stability and Stream Hydrodynamics[1]

2.1. *Introduction*

Aquatic vegetation typically grows in shallower and/or slower moving sections of the flow and is therefore often found in a layer parallel to the open flow in streams, in a narrow band fringing lakes and ponds and in a similar narrow band in coastal zones. In streams and rivers, this vegetation can occupy a significant fraction of the cross section and can strongly affect flow and transport in the stream. The exchange of momentum and mass between the open channel and the vegetated layer is an important problem, and was shown to be dominated by coherent structures that form at the vegetation edge (White 2006). Further, the differing sources of sediment supply to vegetation, transport via these coherent structures and advection from upstream, are currently being investigated (L. Zong, personal communication, March 12, 2009). In this section, I investigate the effects that vegetation in a stream meander has on the hydrodynamics and the transport of sediment in the meander. Moreover, I comment on how the changes in flow structure impact the stability of the vegetation, the point bar and the overall stream cross section.

2.2. *Description of Outdoor StreamLab*

These experiments were conducted in the Outdoor StreamLab (OSL), an experimental facility built on a retired spillway adjacent to the University of Minnesota's St. Anthony Falls Laboratory in downtown Minneapolis. During 2008, within the facility's 40-m by 20-m

[1] This chapter is currently in review in the Journal of Hydraulic Engineering (Rominger et al. 2009), as "The Effects of Added Vegetation on Sand Bar Stability and Stream Hydrodynamics." Reprinted here with permission of ASCE.

Riparian Basin, a sand-bed stream was constructed with three meander bends that have an average wavelength of 25 m and a sinuosity of 1.3 (Figure 2-1). The system can provide water discharge up to 2100 L/s, although flows for this set of experiments were considerably smaller. Through the summer of 2008, a base flow of 38 L/s was maintained in the stream. Bank-full flood events, representative of the average flood magnitude in natural channels, occurred at approximately weekly intervals, each lasting 9 hours with a flow of 208 L/s. The surface gradients, derived from the survey data, were S = -0.006 and -0.007 for the flood level and base level flows, respectively.

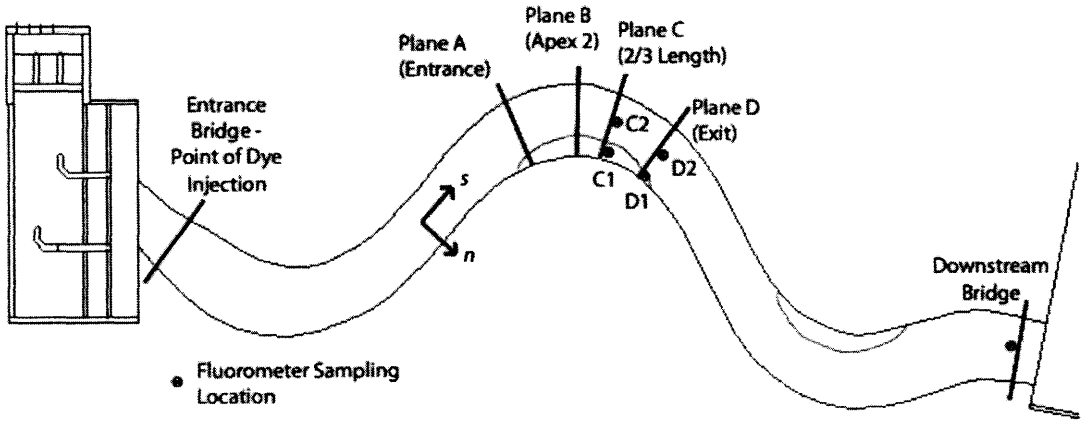

Figure 2-1: Plan view of the Riparian Basin of the Outdoor Stream Lab showing the streamwise coordinate system and indicating velocity and fluorometer measurement locations.

The banks of the channel were fixed in geometry and position with coconut fiber matting, but the bed of the channel was mobile, and consisted of coarse-grained sand (median grain size: D_{50} =

0.7 mm). A recirculating sediment system recycled bedload sediment lost from the downstream end back to the upstream end of the stream. During the first flood event, point bars formed from the mobile bed material near the inner bank of the second and third meander bends (See Figure 2-2). These point bars formed within the first few hours of the first flood event on July 10, 2008, and remained as roughly stable artifacts during the base flow and subsequent flood events in July (Figure 2-3). As described below, vegetation was then added to the point bar in meander 2, and changes in flow and channel morphology were observed through detailed measurements.

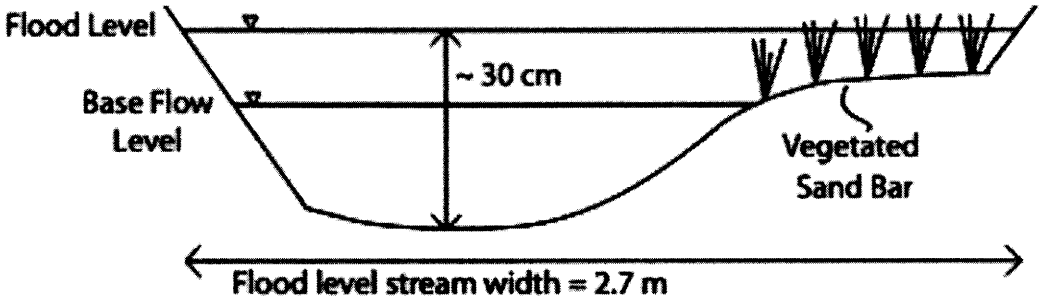

Figure 2-2: Diagram of the stream cross-section at the apex of Meander 2 with the vegetation added to the area of the sand bar emergent at baseflow. The dimensions provided are the approximate design dimensions and varied somewhat over the course of the experiments.

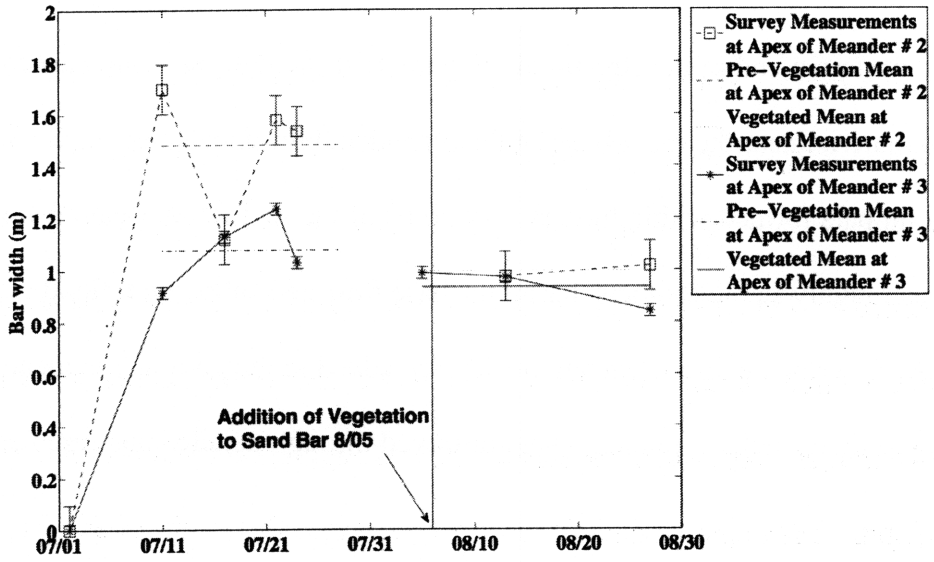

Figure 2-3: The width of the point bar developed over time, beginning with the first flood event on July 10, 2008, and also with the addition of vegetation to the point bar in Bend #2 on August 5, 2008. These widths were derived from survey data points taken at the apex of Meander 2. The pre-vegetation mean width of the emergent point bar is 148 ± 11 cm. The vegetated mean width is 99 ± 2 cm.

2.3. *Stream Coordinate System and Momentum Equations*

In meandering streams, it is useful to define a coordinate system that follows the curvature of the stream, with the downstream coordinate tangent to the stream centerline. This coordinate system is left-handed, orthogonal and curvilinear, similar to systems defined by Smith and McLean (1984) and Dietrich and Smith (1983) and consists of an s-axis, tangent to the centerline of the stream and positive in the downstream direction, an n-axis, perpendicular to the stream centerline and positive towards the right bank, and a vertical axis, z, positive in the upwards direction with $z = 0$ at the water surface. The time-average velocity field is denoted (u, v, w) in the directions (s, n, z), respectively. The depth-averaged force balance equations in the downstream and cross-stream directions within the vegetation are then:

$$\left(\tau_{zs}\right)_b = -\frac{\rho g h}{(1+N)}\frac{\partial \eta}{\partial s} - \rho\frac{1}{1+N}\frac{\partial}{\partial s}\langle u^2\rangle h - \rho\frac{\partial}{\partial n}\langle uv\rangle h - 2\rho\frac{\langle uv\rangle h}{(1+N)R} - \frac{1}{2}\rho C_D a h\langle|u|\rangle\langle u\rangle \quad (2.1)$$

(A1) (A2) (A3) (A4) (A5) (A6)

$$-\left(\tau_{zn}\right)_b = \rho g h\frac{\partial \eta}{\partial n} - \rho\frac{\langle u^2\rangle h}{(1+N)R} + \rho\frac{1}{1+N}\frac{\partial}{\partial s}\langle uv\rangle h + \rho\frac{\partial}{\partial n}\langle v^2\rangle h + \rho\frac{\langle v^2\rangle h}{(1+N)R} - \frac{1}{2}C_D a h\langle|v|\rangle\langle v\rangle \quad (2.2)$$

(B1) (B2) (B3) (B4) (B5) (B6) (B7)

Terms A1 and B1 represent the boundary shear stress, η is the super-elevation of the water surface, h is the total depth of the water column, ρ is the density of water, g is the acceleration due to gravity, R is the local radius of curvature of the stream and the non-dimensional coordinate $N = n/R$. Note that since these equations are depth-averaged, the angle bracket now indicates both a spatial average over a length equivalent to multiple plant stems as well as an average over the depth of the water column.

To the leading order, the dominant terms in the cross-stream force balance are often B2 and B3, the cross-stream pressure gradient and the centrifugal force, respectively. Near the bottom of the water column, bed friction (term A1) causes a lower streamwise velocity, and thus a lower centrifugal force and therefore the pressure gradient, which is uniform over depth, drives a secondary flow toward the inside of the meander, i.e. toward the point bar. Near the top of the water column, the velocity is higher, resulting in a large centrifugal force that exceeds the pressure gradient, causing the secondary flow to be outward, away from the point bar. In this section I examine how the addition of vegetation to a point bar changes this secondary circulation, and consider the effects this has on water and sediment supply to the sand bar.

2.4. *Experimental Methods*

Velocity measurements were made during each of the repeated 9-hour, bank-full flood events. A sideways-looking Nortek Vectrino Acoustic Doppler Velocimeter (ADV), was used to simultaneously measure velocity in the s, n and z (u, v and w) directions at different cross sections along the length of the stream. The ADV was mounted on a motorized traverse oriented perpendicular to the local stream direction, i.e. along the local n - axis. At each cross section, velocity was measured at roughly ten (10) points in the horizontal, n - axis, and a varying number of points in the vertical, z-axis, due to the varying depth. The highest data points were within two centimeters of the surface, and the lowest points were within 5 cm of the bed. The velocity was recorded at each point for between 120 to 240 seconds at 25 Hz. The velocity data was filtered to exclude erroneous values with low correlation coefficients or low signal-to-noise ratios (SNRs). The most common cause of these erroneous data points was obstructions in the sampling volume such as stream debris or a solid surface like the streambed or bank. Each transect was aligned perpendicularly to the streambanks, and the transect position was marked with stakes and surveyed to ensure alignment throughout the summer. Checking the total flowrate at each transect against the flowrate delivered from the upstream headbox further ensured alignment. Note: ecological experiments being conducted simultaneously in the OSL limited the bank-full flood events to 9 hours in length and a periodicity of approximately 1 per week. These time constraints were the main limiting factors in the number of velocity measurements that could be gathered.

Two types of tracer tests, using Rhodamine WT, provided information regarding the transport parameters of the stream at the reach-scale as well as locally around the point bar. First, to measure reach-averaged parameters, dye was injected as a planar source near the mouth of the

stream and a fluorometer was set up near the downstream bridge (Figure 2-1). I diluted 2 ml of Rhodamine WT into a 500 ml solution and injected the solution over the stream's cross-section over a period of approximately 1 second (~instantaneous). A submersible recording fluorometer (SCUFA, Turner Designs) recorded the dye concentrations of water at the downstream bridge at a rate of 1 Hz. To estimate the reach-scale longitudinal dispersion and the retention time, the downstream concentration records were analyzed using the method of moments (e.g. Murphy et al., 2007). Second, to estimate the difference in transport time-scales between the vegetated and unvegetated regions in the second meander, an identical mixture of dye was injected instantaneously as a planar source near the mouth of the stream and fluorometers were set up in Planes C and D (Figure 2-1). The SCUFA was set at mid-depth in the middle of the vegetated sand bar (points C1 and D1), and a Seapoint Sensors Fluorometer, sampling at 7.5 Hz, was set up in the same plane at the midpoint of the open region (points C2 and D2 in Figure 2-1). The two fluorometers were synchronized by hand using a stopwatch.

Floods began on July 10, 2008 and an approximately steady bathymetry was established during the first flood. Following the third flood, bank-side vegetation was introduced on the right bank of the stream. This vegetation was initially added only to the bends on July 22, and added to the riffle sections as well one week later. Surveys using a Leica Total Station were used to gather geometric information about the channel geometry as it developed over the summer. However, the bank-side vegetation showed little to no influence on the overall channel geometry or on the velocity profiles. This is most likely due to the steepness of the banks, and the very small area of flow exposed to this vegetation during the floods (less than 50 cm of an average 2.8-m cross sectional width). The bank-side vegetation was therefore considered negligible in all subsequent analyses.

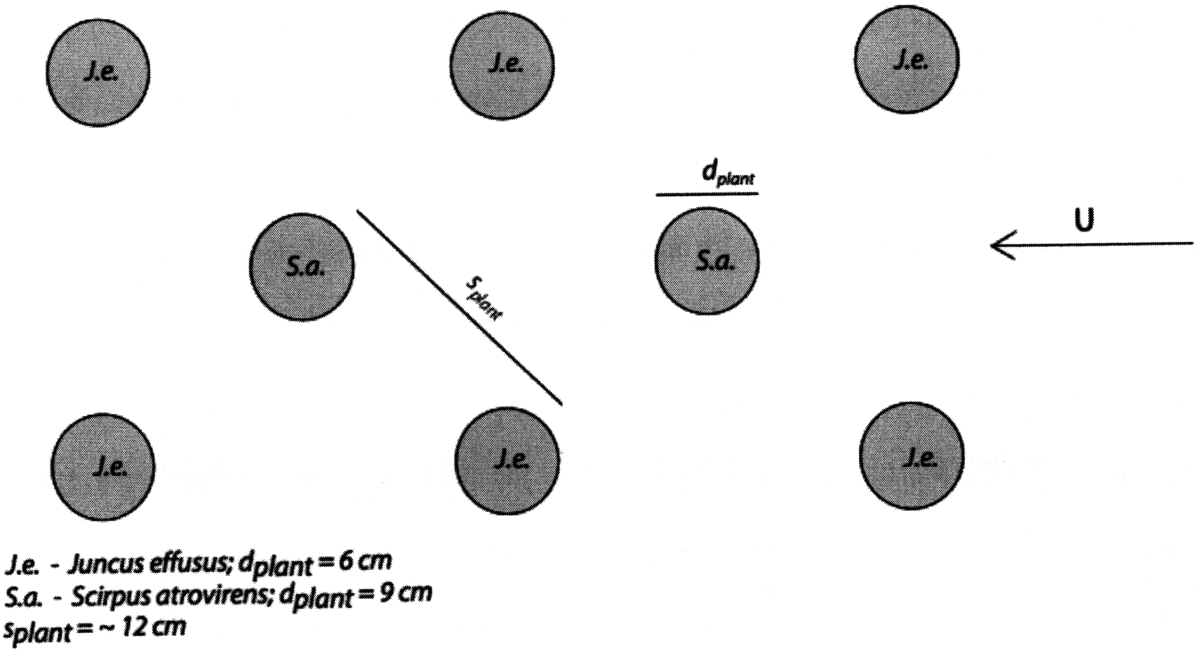

Figure 2-4: Plan view schematic of the vegetation array on the point bar in meander #2. The length, d_{plant}, refers to the effective width of the plant (averaged over its height), which is the combined width of all of the stems from a single plug projected onto the streamflow. The spacing, s_{plant}, refers to the average distance between the centers of two plugs.

On August 5, 2008, two reed species, *Juncus effusus* and *Scirpus atrovirens* were planted on the portion of the sand bar in the second meander that was exposed at base flow. This vegetation was planted in a uniform, staggered array that produced a vegetated frontal area per unit volume of $a = 5.2\ m^{-1}$, where $a = md_{plant}$, $m = 69\ m^{-2}$, and $d_{plant\ (avg)} = .075$ m (See Figure 2-4). Throughout the subsequent floods, the velocities and the reach-scale transport parameters were monitored for changes using the methods described above.

2.5. *Results and Discussion*

As expected, a secondary circulation was observed in the meander bends prior to the addition of vegetation. This circulation was most intense near the apex of the meander (Plane B of Figure 2-1), with a strong lateral outflow near the water surface and a return current near the bed of the stream (Figure 2-6b). The secondary circulation predominantly occupied the deeper part of the cross section, with smaller lateral, v, and vertical velocities, w, over the point bar. The depth-averaged streamwise velocity, $\langle u \rangle$, was highest near the outer bank of the meander and smallest over the point bar (Figure 2-6a).

After nearly one month of flow, including five floods, the point bar in the second meander was planted with emergent vegetation during base flow conditions. During the first flood event after the planting (August 6, 2008), the cross-sectional geometry changed rapidly due to the flow disturbance created by the plants (Figure 2-3). The outermost row of plants scoured away, as well as part of the next outermost row, removing approximately 50 cm of the emergent point bar's width along with most of the vegetation in this zone. This loss in point bar area, observed in the early stages of the flood, was confirmed by photographic and survey data. Similar measurements for the unvegetated point bar in Meander 3 showed little to no loss in emergent bar area, confirming that the losses observed in the second point bar were due to the added vegetation. An estimated 25-30 cm of vegetation was lost at this transect (Figure 2-5). The plants that were not scoured away in the first hours of the first flood were stable for the remainder of the summer flood schedule.

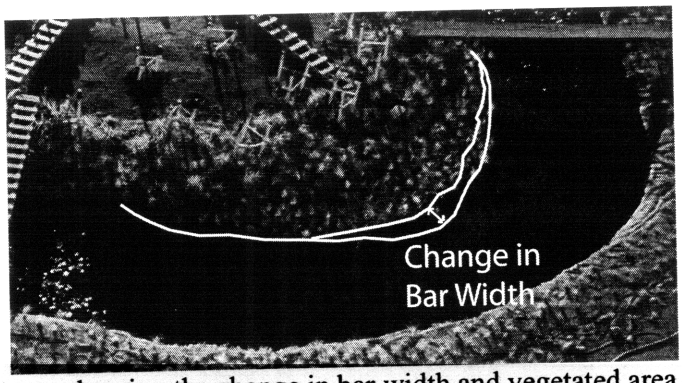

Figure 2-5: Overlaid images showing the change in bar width and vegetated area following the addition of vegetation. The outermost line represents the original point bar perimeter.

Both the depth-averaged streamwise velocity and the secondary circulation at the apex of meander 2 changed significantly after the vegetation was added (Figure 2-7). First, the depth-averaged streamwise velocity decreased over the bar and increased in the open region (Figure 2-7a). Second, the secondary circulation increased in strength, but was confined to the deepest section of the channel. The strength of the circulation can be characterized by the depth-averaged centrifugal force, i.e. term B3 (e.g. as in Kitanidis and Kennedy, 1983), which increased by 30% after the addition of vegetation to the bar (Figure 2-8). Finally, over the point bar, a strong outward flow (toward the outer bank) now extends over the entire depth of the water column.

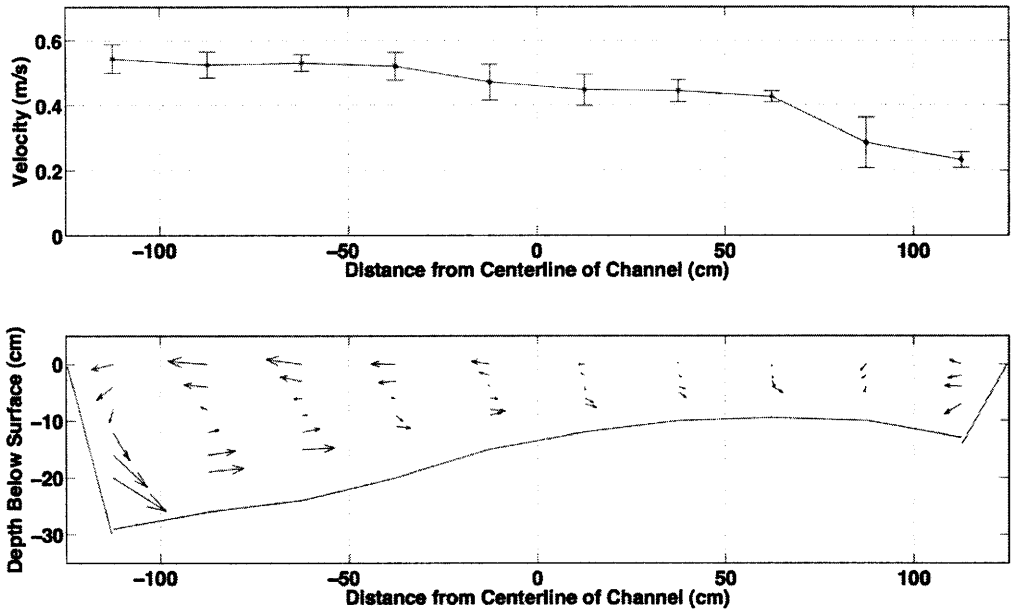

Figure 2-6: Velocity Measurements at Apex 2 on July 16, 2008. (a) Depth averaged downstream velocity, $<u>$, and (b) velocity components in the lateral and vertical directions, v and w, showing the secondary circulation in the n-z plane. The cross-sectional outline shows the measured bed profile, measured by hand from the stream surface.

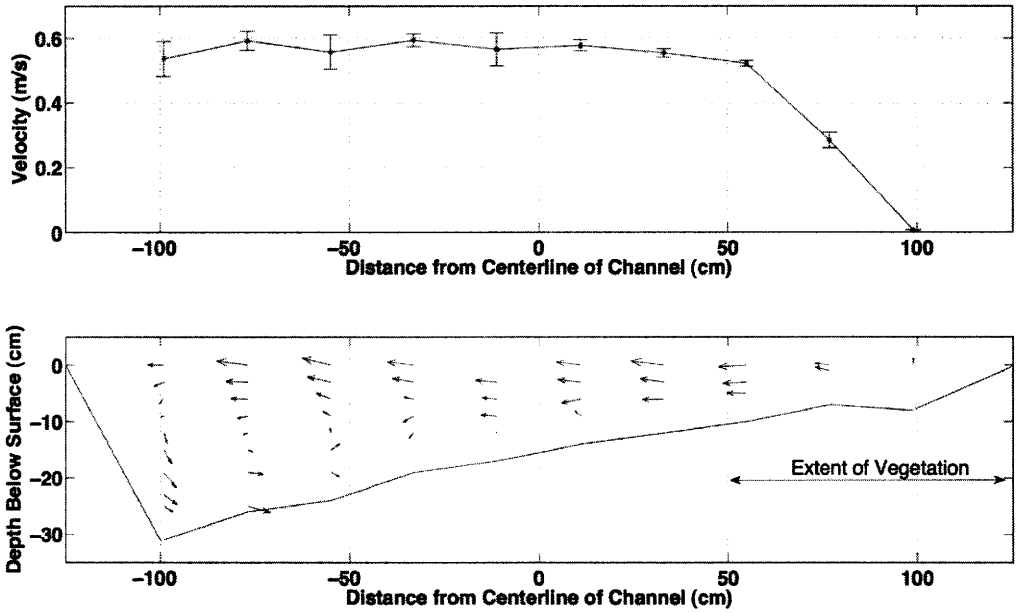

Figure 2-7: Velocity Measurements at Apex 2 with the vegetated sand bar on August 26, 2008. (a) Depth averaged downstream velocity, $<u>$, and (b) velocity components in the lateral and vertical directions, v and w, showing the secondary circulation in the n-z plane. Note the lateral outflow present over the entire stream depth near the right bank. The cross-sectional outline shows the measured bed profile, measured by hand from the stream surface.

The difference in the velocity field before and after the insertion of vegetation occurs because the vegetation increases the hydraulic resistance over the point bar. Defining the bed stress by a bed drag coefficient, $(\tau_{zs})_b = -\frac{1}{2}\rho C_f |\langle u \rangle| \langle u \rangle$, I can compare the hydraulic resistance provided by the bed (term A1) with that provided by the vegetation (term A6), by comparing the terms C_f ($\approx .002$, for a sand bed) and $C_D ah$ ($\approx$ 0.8, assuming C_D = O(1)). This comparison indicates that the addition of vegetative drag (term A6) increases the total drag on the bar by two orders of magnitude, significantly retarding the flow and causing a lateral diversion toward the open channel. As the flow is diverted away from the region of high drag, the downstream velocity accelerates near the edge of the vegetation, causing the observed scour. Specifically, the velocity at the vegetation edge (y = 50 cm) increases from 45 cm/s before the addition of vegetation (Figure 2-5a) to 55 cm/s after the addition of vegetation (Figure 2-7a).

These changes in flow are explained by consideration of the spatial acceleration terms in the cross-stream momentum balance. As water shoals over the point bar, an effect that is magnified by the presence of vegetation, the downstream slope of the water surface is reduced. A concomitant acceleration of the flow in the deeper portion of the channel can increase the downstream slope in this region of flow. The combined effect of these changes in the downstream surface slope is a reduction in the cross-stream surface slope (i.e. the cross stream pressure gradient) near the apex. This phenomenon is also observed as flow shoals over a bare point bar, but it is greatly magnified by the two orders of magnitude increase in resistance introduced with the vegetation. For a further discussion of the effects of spatial accelerations on the surface slope and a very helpful diagram, see Dietrich and Smith (1983). The result is that after the vegetation is added, the centrifugal force exceeds the cross-stream pressure gradient over the entire depth over point bar, causing a lateral flow toward the open channel and outer

bank that extends over the water depth in the vegetated region, *i.e.* there is no return flow at the bed (Figure 2-7b). Importantly, the return current near the bed is now limited to only the deepest parts of the channel (Figure 2-7b), in contrast to the conditions before the vegetation (Figure 2-6b), in which the return flow extended onto the bar. This implies that the addition of vegetation changes the secondary flow in such a way as to cut off sediment supply from the open channel to the bar.

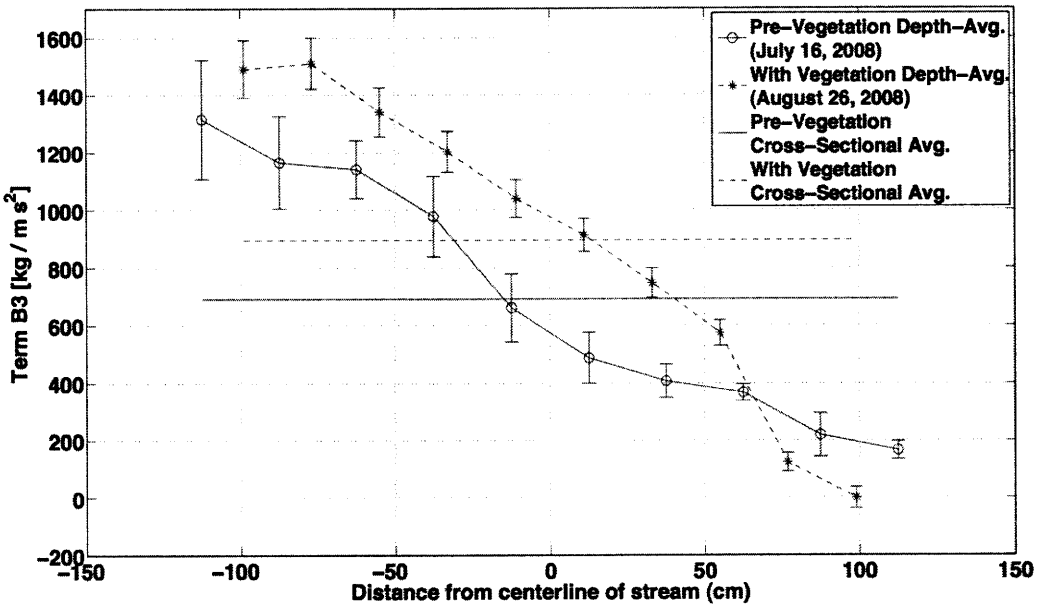

Figure 2-8: The depth averaged centrifugal force and the cross-sectionally averaged centrifugal force at the apex of Meander # 2 from before and after the vegetation was added to the system.

Finally, measurements of the bed geometry taken before and after the vegetation was added show how the depth-profile changed (Figures 2-6b, 2-7b and 2-9b). Approximately 5 cm of sediment was deposited within the vegetation and between 0 and 4 cm of erosion occurred near the edge of the vegetation. Erosion (0 to 5 cm) also occurred in the deeper parts of the cross section near the outer bank.

2.5.1. *Implications for Planting Stability*

Several studies suggest that plant growth can be inhibited by flow. As discussed above, both Chambers et al. (1991) and Nilsson (1987) both found clear negative correlations between current velocities and vegetative cover. Chambers documented a clear threshold of 1 m/s beyond which very little vegetation was present, suggesting the mechanical strength of the sediment and/or the plant was exceeded. These studies imply that particular planting strategies will be less successful if they lead to locally enhanced velocities. To gain insight into this problem, I consider whether the observed loss of the introduced vegetation in our study is consistent with our physical understanding of plant stability.

There are two documented physical mechanisms that limit the invasion and propagation of vegetation into a stream channel. First, for an unconsolidated sandy bed, the substrate becomes mobile above a certain shear stress. Rapid scouring of the bed can preclude the growth of aquatic vegetation that depends on the substrate for stability (Fonseca et al., 1983). Second, plants have an inherent lodging velocity that defines the point at which the plant itself fails under physical stresses. This value is a function of the stem flexural stiffness, geometry and natural roughness of the plant (Duan et al. 2002). For the mobile sand bed found in the OSL, the scouring threshold was likely reached well before the lodging velocity. The plants lost during

the flood came out as intact plugs, with no obvious damage to the plant material. This implies that the plants dislodged because the substrate around them was eroded, so that changes in the sediment stability will guide the understanding of this loss of vegetation.

The Shields Parameter, ψ, describes the ratio of destabilizing (drag) and stabilizing forces (settling) for non-cohesive sediment. This parameter is defined as

$$\psi = \frac{\tau_b}{(\rho_s - \rho)gd_{grain}} = \frac{\rho C_f \langle u^2 \rangle}{(\rho_s - \rho)gd_{grain}} \tag{2.3}$$

Here, ρ_s is the sediment density, C_f is the coefficient of friction of the bed and d_{grain} is the sediment grain diameter. I can evaluate the changing stability of the bed by comparing the Shields Parameter before and after the vegetation was added. Because the sediment is unchanged, it can be assumed that both the settling forces and the bed friction coefficient do not change. It is then convenient to form the following ratio, to describe the changes in bed stability:

$$\frac{\psi_{veg.}}{\psi_{unveg.}} = \frac{u^2_{veg.}}{u^2_{unveg.}} \tag{2.4}$$

The areas in the vegetated cross section where erosion was observed correspond to a Shields Parameter ratio of greater than 1 (Figure 2-9). Similarly, the areas in which deposition occurred correspond to a Shields Parameter ratio of less than 1. The correspondence between the Shields Parameter ratio and the observed erosion/deposition patters suggests that the vegetation changed the stability of the bed by altering the local flow speed and thus the local bed stress. This is consistent with the observation above, that the plants lost were removed intact, i.e. the sediment

eroded away around the plug. Further, this set of experiments reinforces the theory that high energy and rapid sediment scour can preclude vegetative growth and propagation. Not only did changes in the bed profile show strong agreement with the comparison of Shields Parameters, but also with the areas where vegetation was lost from the planted array. It is important to note that this ratio of the Shields Parameters indicates tendencies only. It does not suggest that certain areas will erode indefinitely and other areas will continue to accrete.

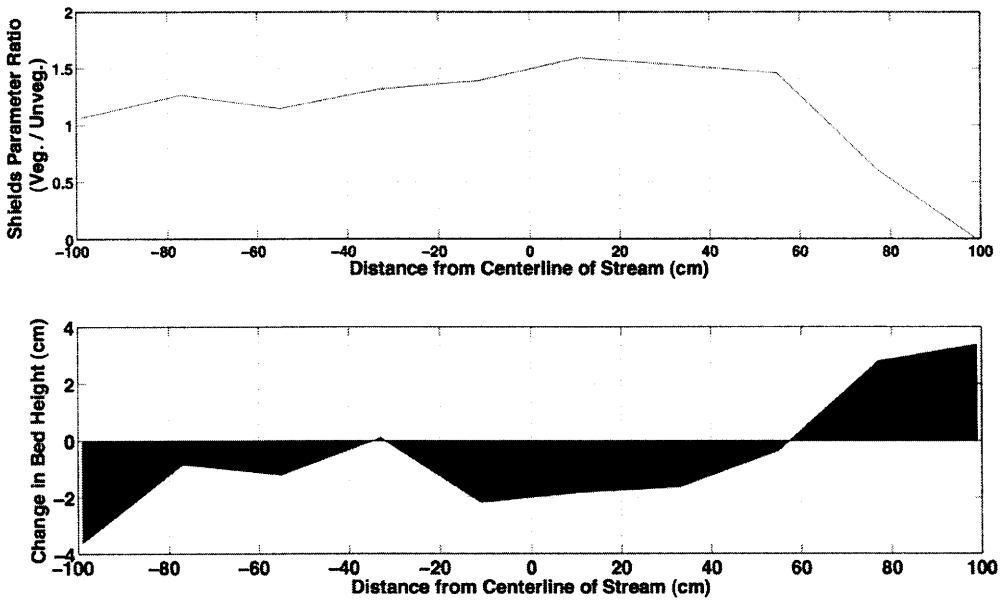

Figure 2-9: (a) The ratio of the Shields Parameters $\psi_{veg.}/\psi_{unveg.}$ showing the tendency of the system towards either deposition (< 1) or erosion (> 1) and (b) the change in the bed height following the addition of vegetation to the system.

2.5.2. *Water Supply to the Vegetated Bar*

The availability of suspended sediment on the bar, as well as the water quality on the bar, both depend upon the supply of new water to this region. The tracer measurements made near

the vegetated bar allowed us to draw conclusions about the advective and diffusive transport near the bar. Figure 10 shows the residence time distributions at two longitudinal positions for dye passing through the vegetation (fluorometer positions C1 and D1 in Figure 2-1) and dye passing through the open channel (fluorometer positions C2 and D2 in Figure 2-1). The arrival time of the peak dye concentration is delayed in the vegetation compared to the arrival time of the peak concentration in the open channel. The delays observed at cross-sections C and D (Figure 2-1) are $\Delta T_{Plane\ C} = 18 \pm 10$ sec. and $\Delta T_{Plane\ D} = 27 \pm 3$ sec.

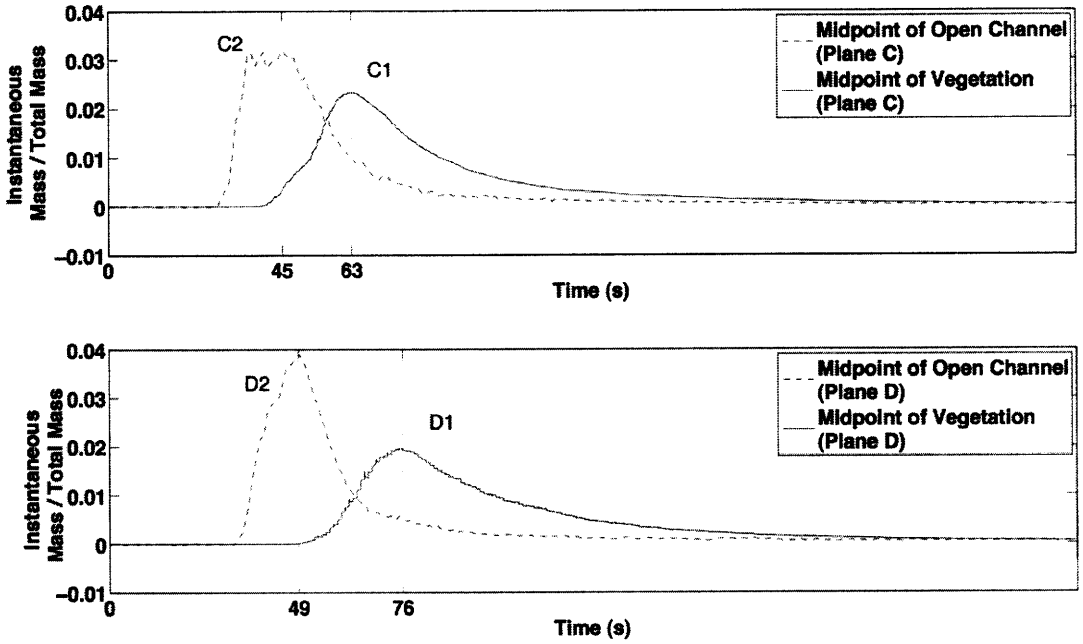

Figure 2-10: Residence time distributions of dye passing through the open channel and vegetated regions in (a) Plane C and (b) Plane D.

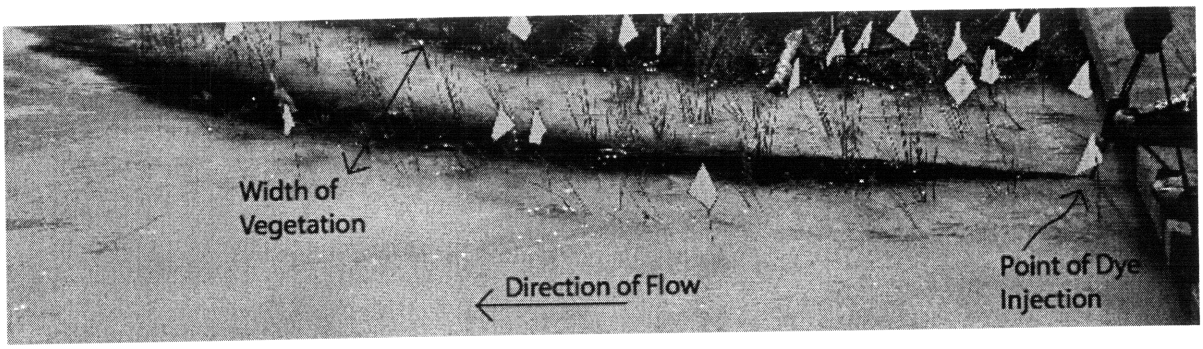

Figure 2-11: A continuous injection of Rhodamine WT (black in the exaggerated contrast image). Note that the tracer cannot spread across the width of the vegetation because the observed diffusion is offset by an outward advection from the bank toward the open channel.

If the vegetated region is a distinct advection zone, with little diffusive exchange with the open channel, then the delay in the dye passage, $\Delta T_{Plane\,C}$, should be approximately two thirds of $\Delta T_{Plane\,D}$, because Plane C is 2/3 the distance between Plane A (leading edge of the vegetation) and Plane D. Assuming fluid acceleration is relatively small in this region, the observed timescales agree with this hypothesis, suggesting that dye enters the sand bar at the upstream edge and advects in streamlines roughly parallel to the bank with little lateral exchange with the open water. Further, I can estimate the lateral diffusivity, D, from photographs of the dye evolution along the channel (e.g. as in Nappo et al. 2008). Then, using the width of the vegetation, $b_v = 0.7$ m, the lateral diffusive velocity, $D / b_v = 0.004$ m/s, was found to be much smaller than the measured lateral velocity, $v = -0.12$ m/s. Although some mixing was observed near the interface of the vegetation, the turbulent diffusion was not large enough to offset the significant outward lateral advection, such that diffusion provides a negligible scalar flux to the bar. Therefore, longitudinal advection from the upstream portion of the vegetated sand bar is the dominant source of new water to the bar, and thus the only potential sediment supply as well. These findings are confirmed by photographs of dye streamlines within the vegetation, showing

little lateral mixing across the boundary (See Figure 2-11).

2.5.3. *Coherent Structures in the Stream*

In flows adjacent to a porous layer, periodic coherent vortices can form and grow at the interface (Drazin and Reid 1981, White 2006). These vortices have been observed in a wide range of flows from laminar flow regimes adjacent to porous media to turbulent flows adjacent to submerged aquatic vegetation (Jimenez et al. 2001). As in the Outdoor StreamLab, the resistance caused by the vegetation creates a sharp lateral velocity gradient across the vegetation interface. In shear layers such as these that possess an inflection point in the velocity profile, coherent vortices can form from a Kelvin-Helmholtz type instability (Raupach and Shaw 1982, Ghisalberti and Nepf 2002, White and Nepf 2007). These vortices are responsible for large momentum fluxes across the vegetation interface and can be responsible for the transport of scalars such as contaminants, seeds and other suspended particles as well. Linear stability theory gives a prediction for the frequency of these periodic vortices as

$$\frac{f_n \theta}{\overline{U}} = 0.032 \tag{2.5}$$

where f_n is the frequency, θ is the width of the shear layer and $\overline{U}$ is the average velocity across the shear layer (Ho and Huerre 1984). To check for the presence of coherent structures in the Outdoor StreamLab, I analyzed the frequency components of the velocity records for a single, pronounced frequency. I checked the velocity records at every cross-stream point in both Planes B and D (Figure 2-1) and then correlated the power spectral densities to enhance any unique frequencies. After correlating ten periodograms, there is a slight peak in Plane B at 0.34 Hz, but

there is no dominant frequency (Figure 2-12). Following the same procedure in Plane D, the correlated periodogram shows a stronger peak at 0.19 Hz (Figure 2-13), which suggests that coherent structures have formed in the stream by the tailing edge of the vegetation. Using Equation 2.5, a shear layer width of $\theta = 0.08$ m, which is reasonably predicts this frequency. But, these coherent structures are only visible after correlating the periodograms from all ten of the cross-stream locations.

Since these vortices transport high momentum fluid from the open channel into the vegetation and vice versa, they can significantly affect the lateral diffusivity, D, of scalars in the flow. This exchange can be an important source of sediment supply to the bar (L. Zong, personal communication, March 12, 2008; White 2006). In this case, though, the impact of these vortices on transport along the patch length was minimal, as their formation was not observed until near the tailing edge of the patch (Figures 2-12 and 2-13 below).

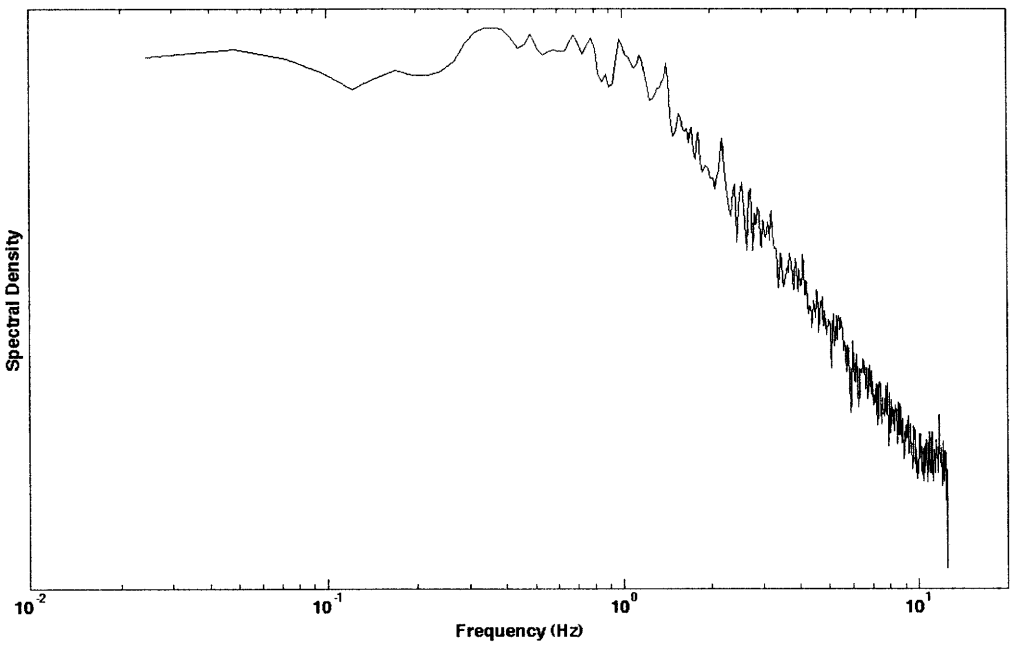

Figure 2-12: The correlated periodogram for the velocities at the Apex of Meander 2 (Plane B). This figure shows a slight peak at 0.34 Hz, but does not show definitive evidence of coherent structures. The spectral density units on the vertical axis are arbitrary.

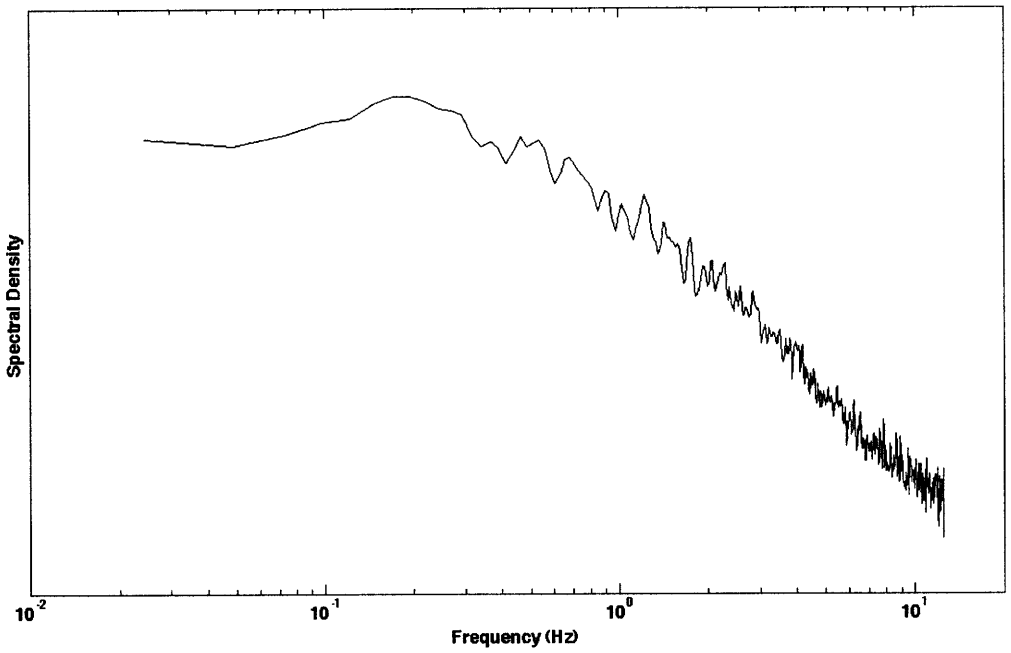

Figure 2-13: The correlated periodogram for the velocities at the Exit Plane of Meander 2 (Plane D). This figure shows a more pronounced peak at 0.19 Hz, which suggests coherent structures have formed by the tail-edge of the patch of vegetation. The spectral density units on the vertical axis are arbitrary.

2.5.4. *Reach-Scale Longitudinal Dispersion*

Aris (1956) came up with a way to describe the longitudinal turbulent dispersion coefficient using the method of moments. This technique expresses K_x in terms of the spatial variance of the concentration distribution. Using the following moment generating equation

$$M_i = \int_{-\infty}^{\infty} t^i C(t) dt \tag{2.6}$$

where M_i is the ith moment of the concentration distribution, $C(t)$ is the concentration distribution, i.e.,

$$M_0 = \text{total mass} \tag{2.7}$$

$$\mu = \frac{M_1}{M_0} = \text{center of mass}, \tag{2.8}$$

the temporal concentration variance is

$$\sigma_t^2 = \frac{M_2}{M_0} - \left(\frac{M_1}{M_0}\right)^2. \tag{2.9}$$

Using the assumption of "frozen turbulence" first postulated by Taylor (1935) and described by Fischer et al. (1979), the temporal concentration variance can be related to the spatial concentration variance, σ_x^2, in the following manner

$$\sigma_x^2 = \sigma_t^2 U_c^2 \tag{2.10}$$

$$U_c = \frac{L_x}{\mu} \tag{2.11}$$

where *Lx* is the distance between the sampling point and the point of injection. Therefore, the longitudinal dispersion coefficient is

$$K_x = \frac{1}{2}\frac{d\sigma_x^2}{dt} \approx \frac{\sigma_x^2}{2\mu}. \tag{2.12}$$

The reach-scale tracer tests indicated that the longitudinal dispersion coefficient (K_x = 5.1 ± 0.2 x 10^{-4} m^2s^{-1}) did not change, within uncertainty, after the addition of vegetation at the banks and on the bar (Figure 2-14). There was also no significant change in the residence time distribution following the addition of the vegetation (See Appendix A.3). Although the vegetated sand bar creates a large slow-zone, only about 10% of the flow encounters this region, with the remaining flow diverted around it. The flow needs to encounter multiple such zones, so that a larger fraction of the flow experiences a slow-zone, in order to observe an impact on reach-scale dispersion.

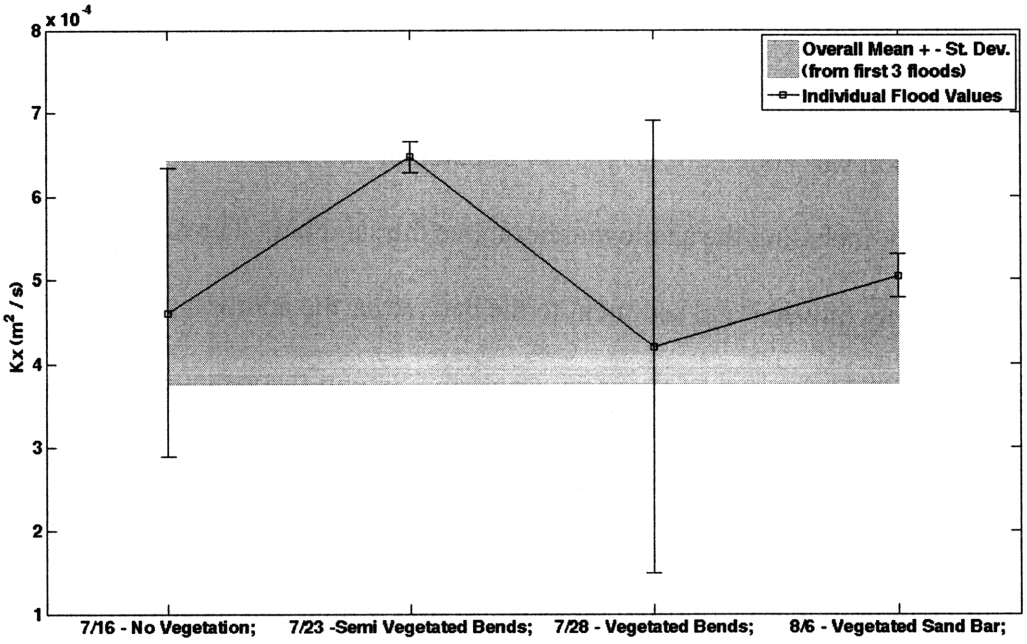

Figure 2-14: Changes in the longitudinal dispersion coefficient of the stream as vegetation was incrementally added to the channel. The error bars represent the standard deviation.

2.6. *Conclusions*

In this set of experiments, vegetation was added to a fully-developed sandy point bar near the convex bank of a stream meander. The vegetation was planted during base flow on the emergent portion of the bar. Both the flow field and the bed topography changed dramatically between conditions before and after the addition of the vegetation. Following the addition of vegetation, erosion occurred near the lateral edge of the vegetation, resulting in a 33% loss of emergent bar width at the apex at base flow. However, deposition occurred further into the vegetation, near the inner stream bank. These distinct positions of local erosion and deposition can be explained by the local changes in velocity and thus, local changes in the Shields parameter which governs sediment motion. Areas where the Shields parameter ratio was greater than unity correspond to regions of erosion and areas where the ratio was less than unity correspond to areas of deposition. The observations suggest that the spatial accelerations caused by the presence of the vegetation shifted the sand bar area to a new geometric equilibrium.

The addition of vegetation also altered the pattern of secondary flow in the meander. Before the vegetation was added, the secondary circulation in the meander extended across the width of the stream, including the shallow areas above the sand bar. The return current near the bed acted as a supply of water and sediment to the bar. After the addition of the vegetation, the secondary circulation was present only in the deepest section of the meander, near the outer, concave bank, and the flow above the sand bar was outward over the entire water column. Importantly, the vegetation altered the secondary circulation sufficiently to cut off a source of water and sediment to the bar. Further, the outward flow within the vegetation was sufficient to offset diffusive transport from the main channel onto the vegetated bar, effectively cutting off the bar from diffusive flux from the main channel, thereby eliminating another potential source of

sediment and exchange. The water within the vegetation enters near the upstream edge and follows the streamlines approximately parallel to the bank before exiting the vegetation near the downstream edge. Based on the observed flow pattern, the main source of sediment to the bar was from sediment that enters near the upstream edge.

Some of the vegetation was added to a zone in which it could not physically thrive and locally detrimental to the stability of the channel geometry. The enhanced velocities in the open channel scoured the outer edge of the point bar, not only removing sediment, but most of the vegetation in the outer rows. The strength of the secondary circulation also increased significantly. In a completely natural channel, this would have likely enhanced erosion of the outer bank, accelerating the meander growth. This could not occur in our channel because the banks were fixed in position by buried fiber matting. Overall, this study illustrates the hydrodynamic impact of aquatic vegetation on the point bar region in a stream meander, and how the changes in flow structure may impact the stability of the vegetation, the point bar and the overall stream cross section.

3. Structure-Flow Feedbacks in Seagrass Meadows[2]

3.1. *Brief Introduction to Seagrass Meadows and their Structure*

Seagrass meadows play an important role in coastal zones, dissipating wave energy, helping to stabilize sediment and protecting against storm surges (Koch et al. 2009). Beyond simply exerting drag on currents, seagrass meadows can also significantly dampen waves in the near-shore region. Certain studies have documented reductions in wave height and wave energy due to seagrasses of 20% and 40%, respectively (Bradley and Houser 2009, Fonseca and Cahalan 1992). By reducing wave energy and by physically sheltering the bed, seagrass meadows can help reduce erosion rates and can increase sediment accumulation within the bed (Chen et al. 2007). Now, as coastal protection becomes more of a concern, the restoration of seagrass meadows and the understanding of the structure of these meadows is becoming increasingly important and a priority for coastal communities (Short et al. 2002, Bradley and Stolt 2006, Neenhuis et al. 2002).

Under natural conditions, aquatic vegetation is organized in different geometries, ranging from lush meadows to distributed, discrete patches. The different geometries are the result of many factors, including access to sunlight, nutrient availability, and the physical stresses associated with waves and currents (Fonseca et al, 1983; Zimmerman et al., 1997, Koch, 2001). Fonseca and Bell (1998) examined the relationship between flow and meadow structure for two species: *Zostera marina* (eelgrass) and *Halodule wrightii* (shoalgrass). They used aerial photographs to map seagrass cover, and then correlated the fractional coverage with three environmental factors: current speed, wave exposure, and water depth. The seagrass cover ranged from isolated patches of 1 m^2 (the resolution of the surveys) to lush, continuous canopies

[2] This chapter appears in Luhar et al. (2008) as Section 4: Case Study 2. Reprinted here with permission of Springer.

of at least 2500 m^2 (50 m by 50 m areas – the grid size) (Figure 3-1). In this study, a negative correlation was found between fractional coverage and all three environmental factors, but the strongest correlation was with the maximum tidal current. Other studies have found aquatic vegetation biomass to be most strongly correlated with fetch (a measure of wave exposure) (Coops et al. 1991, Duarte and Kalff 1990). In areas not exposed to strong currents, wave exposure would likely affect seagrass cover the most, but waves were not as significant at this site. Similarly, Fonseca et al. (1983) found a strong negative correlation between maximum tidal current and the height/length ratio for seagrass patches. Here, I present a flow model that provides insight into the the strong negative correlation between fractional coverage and current speed observed by Fonseca and Bell (1998).

In tidal regions, the current speed is determined by the balance between the tidal forcing and the drag exerted by the bed and/or vegetation. The tidal forcing is a function of the maximum tidal amplitude and the resulting slope of the water surface. Higher drag within the vegetation can divert flow to open areas, resulting in reduced flow within the canopy and accelerated flow in the open areas (Gambi et al., 1990, Rominger et al. 2009). This diversion of the flow to open areas tends to be self-reinforcing, as the reduced flow within the canopy creates favorable conditions for continued growth, while the accelerated flow in the open areas creates a high-energy environment that can damage plants and prohibits growth (Scoffin, 1970; Fonseca and Fisher, 1986; Duan et al., 2006). However, in order for this feedback to operate, the open areas must have sufficient continuity to form channels. I appeal to percolation theory to understand the connectivity of these channels and the fractional coverage at which they occur.

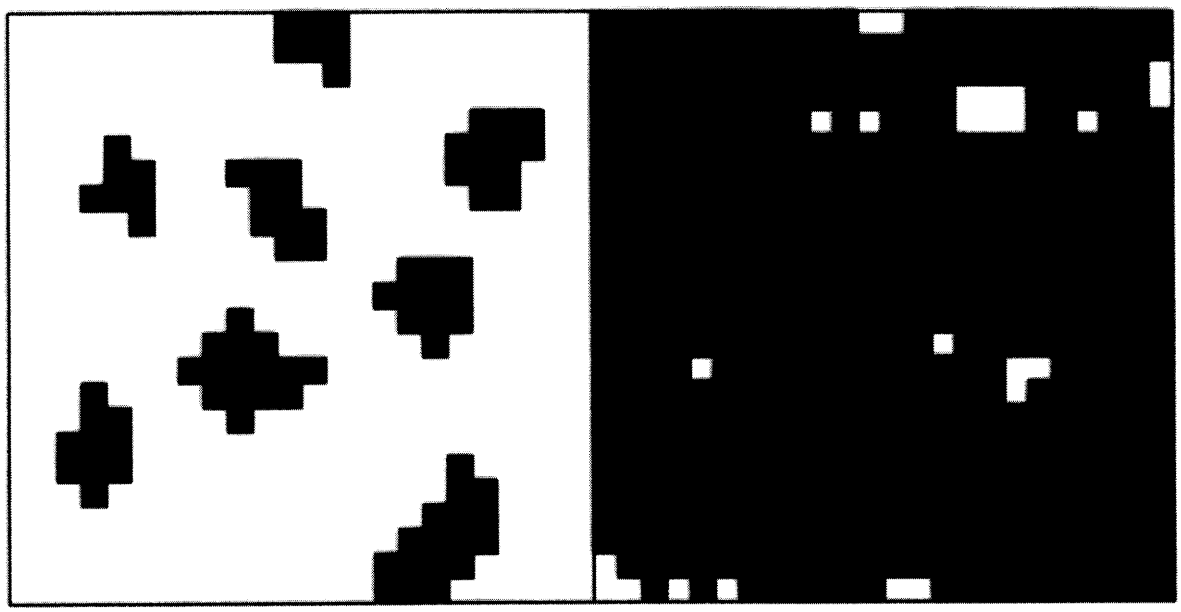

Figure 3-1: Two contrasting seagrass meadows resolved onto square grids. (a) A sparse meadow dominated by discrete patches (the black areas) and (b) a nearly continuous meadow with a few spots absent of vegetation. These two diagrams are representative of some of the results seen in Fonseca and Bell (1998).

3.2. *Percolation Theory and Distinct Flow Regimes in Seagrass Meadows*

Percolation theory describes the connectivity of randomly placed elements in a grid. In this sense, connectivity is described as the existence of a connected path of conducting elements across a domain. The fractional value of conducting elements that must be present for the grid to be connected can be described for many different geometries using probability. For a two-dimensional rectilinear grid, the critical fraction of conducting elements is well documented at 0.59274, also known as the percolation threshold (Stauffer 1985, Lee 2008). These same principles can be applied to the connectivity of a landscape comprised of open channels and submerged aquatic vegetation as conducting and insulating elements, respectively.

As in Fonseca and Bell (1998), the fractional area occupied by vegetation will be described by A_v / A, where A_v is the bed area covered by vegetation within a total area A.

Starting with full coverage, $A_v / A = 1$, imagine removing randomly placed pockets of vegetation. When only a few unvegetated regions exist (large A_v / A), they are unlikely to be connected and channels will not be able to form. According to percolation theory, randomly placed landscape elements become statistically connected when they represent 59.3% of the area. That is, the open regions must reach ~60% of the area before significant channeling will occur. This corresponds to a vegetative cover of ~40%. It is important to note, however, that this limit was derived for randomly placed landscape elements. The growth and propagation of vegetation is not a purely random process. Whether propagation occurs via sexual or vegetative reproduction, there is an inherent bias to grow adjacent to existing plants, i.e. through the lateral growth of rhizomes below the bed or via the dispersal of spores in the flow (Sintes, et al., 2005; Marba and Duarte, 1998). This natural tendency may shift the area fraction at which channelization occurs.

We use the limits prescribed by percolation theory to describe two flow regimes within the seagrass landscape, *i.e.* landscapes with ($A_v / A < 0.4$) and without ($A_v / A > 0.4$) connected channels (i.e. Figure 3-1). As in Fonseca and Bell (1998), the flow is assumed to be driven by tidal variation in the surface elevation, $S = \partial H / \partial x$, which is assumed to be uniform over the entire region of interest. The driving force is balanced by the drag associated with the vegetation and the bed. When $A_v / A < 0.4$ connected channels are present, and separate momentum balances are possible within the channels and within the vegetation. Assuming steady, uniform conditions, and taking the depth-average, the momentum balance reduces to,

$$\rho g S = \tfrac{1}{2} \rho C_D a \frac{h}{H} U_v^2 \quad \text{for } A_v/A < 0.4 \text{ in vegetation} \tag{3.1a}$$

$$\rho g S = \tfrac{1}{2} \rho \frac{C_f}{H} U_o^2 \quad \text{for } A_v/A < 0.4 \text{ in channels} \tag{3.1b}$$

The depth-averaged velocity within the vegetation and channels is denoted U_v and U_o, respectively. The turbulent stress at the bed is modeled with a bed-drag coefficient, C_f, and averaged over the depth of the flow, H.

The tidal forcing, ρgS, was estimated from data provided in Fonseca and Bell (1998). Let U_o^* equal the current observed in the absence of vegetation ($A_v / A = 0$), and let U_v* equal the current observed in regions will full coverage ($A_v / A = 1$). Using the observed values for U_v* and U_o^*, (3.1a) and (3.1b) can be solved simultaneously for ρgS, and the drag ratio, $C_D ah / C_f$. The resulting drag ratio, $C_D ah / C_f = 25$, is comparable to that derived from previously observed values for a and h and independently estimated values of C_D and C_f (Werner at al., 2003; Ghisalberti and Nepf, 2006; Tanino and Nepf, 2008). The maximal tidal forcing, ρgS, can now be used in (3.1a) and (3.1b) to evaluate U_c and U_v for $A_v / A = 0$ to 0.4. Note that (3.1a) assumes uniform conditions, and it is therefore not suitable for very short patches of vegetation. As flow enters a patch, it requires a distance $L_x \approx B$, where B is the patch width, to adjust to the vegetative drag and attain the momentum balance implied by (3.1a). For patches shorter than this adjustment length, the flow within the vegetation will not have a sufficient length to adjust and will remain elevated, *i.e.* $U_v \approx U_c$, possibly eroding the entire patch.

According to the percolation threshold, when $A_v / A > 0.4$ there are no continuous channels. Because the open regions are unconnected, they do not provide a flow path along which Equation 3.1b applies. Instead, the essentially contiguous, but spotty, coverage of vegetation dictates a uniform mean velocity, U, in all regions, both open and vegetated. The depth- and area-averaged momentum balance then becomes,

$$\rho g S = \tfrac{1}{2}\rho C_D a \frac{h}{H}\frac{A_v}{A}U^2 \quad \text{for } A_v/A > 0.4 \tag{3.2}$$

Using (3.1) and (3.2), the velocities U_o, U_v, and U are estimated for the full range of area coverage (Figure 3-2). For $A_v / A < 0.4$, the area-average velocity is

$$U = \left(\frac{A_v}{A}\right)U_v + \left(1 - \frac{A_v}{A}\right)U_c. \tag{X}$$

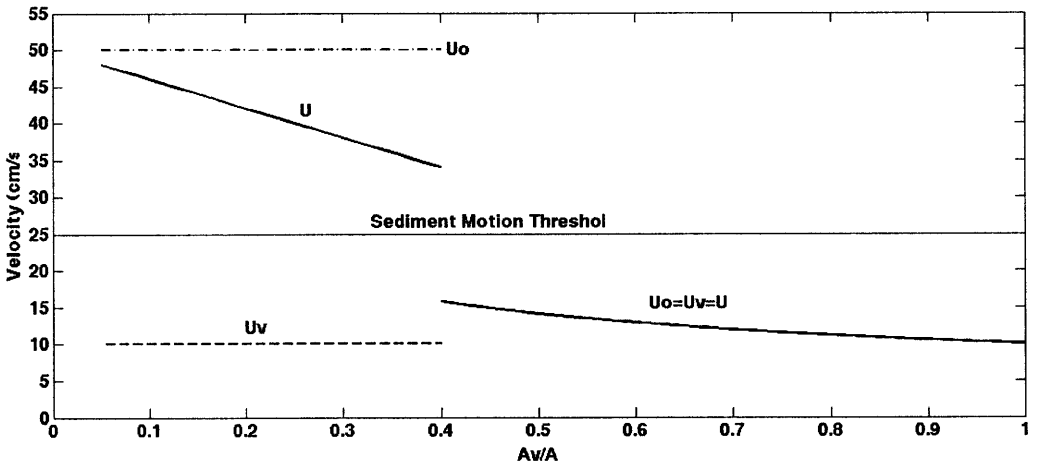

Figure 3-2: Velocity in the open channels, U_o, in the vegetation, U_v, and the spatially-averaged velocity, U, modeled by Equations 3.1 and 3.2.

3.3. *Results and Discussion*

Although the models are discontinuous at $A_v / A = 0.4$, I expect a smooth transition in natural systems. The tidal forcing here is calibrated to the conditions observed in Fonseca and Bell (1998), and the modeled, average velocity, U, agrees in magnitude with the velocity

observed in that paper. In the modeled system, sediment motion is initiated at $U \geq 25$ cm/s (Fonseca and Bell, 1998), and this threshold is also shown in the figure. The model suggests that when channels are present ($A_v / A < 0.4$) sediment motion will occur within the channels but not within the vegetation (Figure 3-2). However, when channels are absent ($A_v / A > 0.4$), sediment motion does not occur either in the vegetated or unvegetated regions. As discussed in the next paragraph, these transitions in behavior can explain the higher probability of occurrence for meadows with area fraction close to the channelization limit (40%).

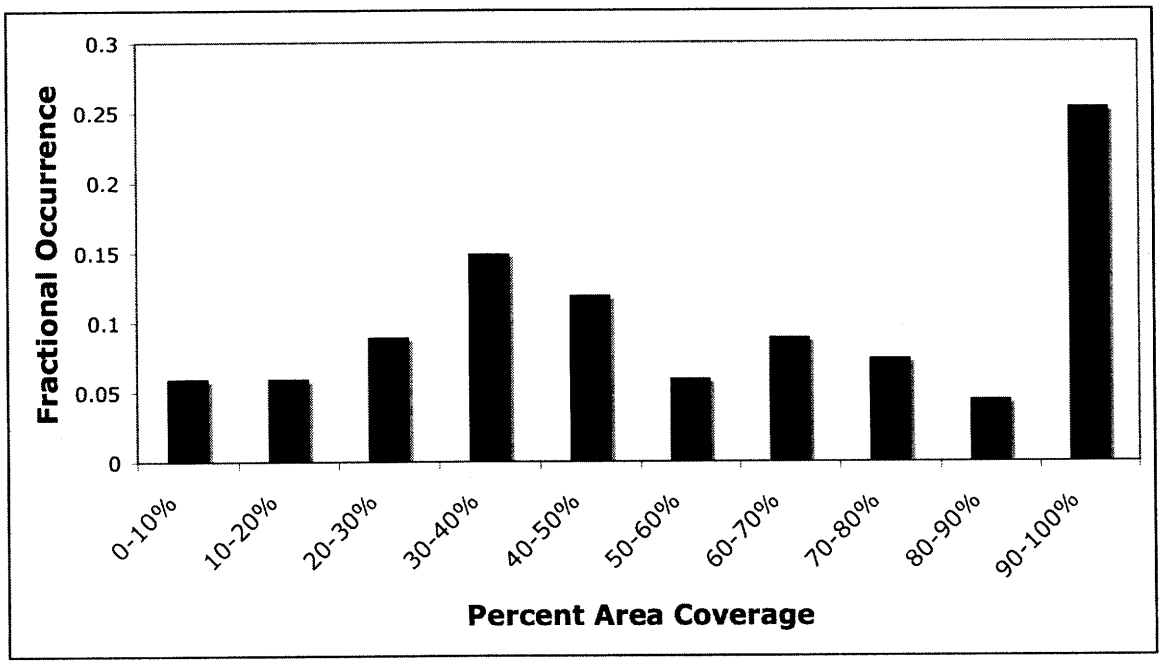

Figure 3-3: The probability density bar plot of fractional area coverage, A_v / A, based on observations in seagrass meadows. Peaks near 40% and 100% suggest that these coverage percentages represent stable landscapes. The data was adapted from Fonseca and Bell (1998).

Using data published in Fonseca and Bell (1998), a histogram of the observed fractional coverages, A_v / A, was constructed (Figure 3-3). The histogram shows two peaks, near 100% and

another near the channelization limit of 40%. These peaks suggest that 100% and 40% represent stable conditions. The model described above explains this stability. Above an area faction of 40%, the velocity in all regions remains below the limit for sediment motion. This means, if a disturbance generates regions of open area, but A_v / A remains above 0.4, the open areas will likely be able to refill, as the local velocity remains depressed and conducive for growth. That is, area cover percentages between 40 and 100% are unstable, with re-growth pushing conditions back to 100% coverage. However, if a disturbance drives the area fraction below 40%, channels can form, and the velocity in the channels increases above the threshold for sediment motion (Figure 3-2), which inhibits re-growth and stabilizes the channels, and stabilizing A_v / A near or just below 40%. Finally, as area coverage approaches zero, individual patches become too short to decelerate the oncoming flow, so that the in-canopy velocity remains above the threshold for sediment motion, and these patches will likely be eroded. Specifically, isolated patches of seagrass of length less than $L_x \approx B$ are unstable. In this system of seagrass $L_x \sim 1$ m. This implies there is another, minimum threshold in area coverage, below which the vegetation coverage is unstable and tending to 0%. Finally, as mentioned above, the inherent tendency of new vegetation to grow near existing vegetation will alter the critical threshold at which channelization occurs. Since the vegetation and the open areas are no longer randomly placed, vegetation will likely need to occupy more than 40% of the bed area to eliminate channels. The exact value is unknown, as vegetative growth and propagation has not yet been modeled in this context.

3.4. *Conclusions*

The spatial horizontal structure of seagrass meadows is controlled by a series of

feedbacks between the natural growth of the plants and the destabilizing forces of the currents, similar to the results of the Outdoor StreamLab experiments presented in Chapter 2. For vegetation area fractions below the critical threshold of $A_v / A \approx 0.40$, there is a connected network of channels with velocities above the sediment motion threshold. These channels are therefore self-reinforcing, in that vegetation cannot easily propagate into them. The vegetated areas are able to divert flow to these channels and thus there are reduced velocities within the canopies themselves, thereby implying stability. Beyond the critical threshold of $A_v / A \approx 0.40$, the open areas in seagrass meadows are no longer connected and the velocity across the entire meadow is roughly equivalent. Therefore, above $A_v / A \approx 0.40$, the vegetation will be able to propagate into the open areas, tending to create a continuous meadow.

These results have important implications for artificial plantings of seagrass beds and for protection of existing seagrass beds. If such a critical area fraction exists, above which the vegetation can form continuous meadows, and below which reinforced open channels exist, this threshold must be taken into account when seeding new beds. The ultimate goal of a restoration project may be continuous coverage, but inserting plants in a density below this critical threshold could result in perpetually fragmented meadows. Conversely, in order to achieve a continuous meadow, one may only need to plant plugs at slightly above the critical threshold in order to eliminate the connectivity of channels. Furthermore, if the seagrass patches are so small or so sparse that they cannot decelerate the flow sufficiently, they will be unstable. This case study illustrates the important implications that percolation thresholds can have in coastal seagrass meadows and, moreover, demonstrates the importance of understanding physical feedback mechanisms in the ecological sciences.

4. Models of the Interactions between Vegetation and Open Channel Flows

4.1. *Introduction to Aquatic and Riparian Vegetation in Open Channels*

Riparian vegetation is common along streams, channels and rivers of many different geometries and flow magnitudes. This vegetation typically covers the river bank down to the base flow level, and depending on the flow characteristics such as depth, turbidity and speed, can propagate further into the channel from the bank. Some species typically found in the riparian zone are *Juncus effusus* (common rush), *Scirpus atrovirens* (dark green bulrush), *Scirpus cyperinus* (wool grass) and many species in the *Carex* or *Eleocharis* genera. Many other species of aquatic vegetation grow directly in the channels themselves, such as several in the *Ranunculus*, *Potamogeton* and *Ceratophyllum* genera. Both types of vegetation can occupy large fractions of the channel cross sections and have a significant impact on the hydrodynamics (e.g. Green 2005a, Green 2006, Rominger 2009).

When vegetation is present in a channel, it is usually the main source of resistance in the flow, often several orders of magnitude larger than bed roughness (Green 2005b). The stems create a drag force on the flow through the viscous shear stress on the surface of the stem and through the pressure drop across the stem or array of stems. In high Reynolds number flows, such as in the three case studies presented in this thesis, the contribution from the pressure drop across rigid vegetation dominates the total drag force (Tanino and Nepf 2008). Although, in flexible canopies, the plants can streamline themselves to reduce separation causing viscous forces to play a larger role. Several studies have demonstrated that in addition to the density of vegetation, the spatial distribution of the vegetation plays a significant role in determining the overall flow resistance (Li and Shen 1973, Fisher and Reeve 1994, Green 2005a). For example,

if vegetation is evenly distributed throughout a channel cross section, it will have more of an impact on the flow than vegetation clumped near the channel edges even for the same overall area fraction or volume fraction of vegetation. In this section I consider only the theoretical overall area fraction of vegetation and ignore the potential for spatial heterogeneities.

4.2. *Model 1: Fixed Channel Cross Section*

4.2.1. *Governing Equations*

As currents encounter stands of aquatic or riparian vegetation, they are partially diverted around the plants because of the drag force the plants exert on the flow. This leads to reduced velocities within the vegetation, but enhanced velocities in the unvegetated regions due to the diverted flow. As discussed in the first case study, as the flow velocity increases beyond a certain threshold, the channel substrate can be eroded, precluding the further growth of vegetation. This suggests that for a theoretical fixed flow rate, Q, that must pass through the channel, the cross section can never become fully blocked by vegetation. In this model for flow through a partially-vegetated, straight channel, I hold the flow rate constant, as Q must be set by the hydrology of the local watershed and cannot be a function of the amount of vegetation in the channel. Therefore the governing equations for this model are,

$$-\rho g S = \tfrac{1}{2}\rho C_D a \langle \overline{u}_v \rangle \left| \langle \overline{u}_v \rangle \right| - \frac{\partial}{\partial y}\tau_{xy} \quad \text{(within vegetation)} \tag{4.1}$$

$$-\rho g S = \tfrac{1}{2}\rho C_f / h \langle \overline{u}_o \rangle \left| \langle \overline{u}_o \rangle \right| + \frac{\partial}{\partial y}\tau_{xy} \quad \text{(outside vegetation)} \tag{4.2}$$

$$Q = \langle \overline{u}_o \rangle h_o b_o + \langle \overline{u}_v \rangle h_v b_v \tag{4.3}$$

where the shear stress created at the vegetation/open channel interface is dominated by the turbulent Reynolds stress (Term iv_b in Equation 1.3). I denote the depth-averaged velocities in the vegetation and open channel using $\langle \overline{u}_v \rangle$ and $\langle \overline{u}_o \rangle$, respectively, which employ the spatial and time averaging discussed in §1.5. The variables, h_o, b_o, h_v and b_v refer to the heights and widths of the open channel and vegetated region, respectively, (See Figure 4-1 Below). In natural streams, the potential gradient, $\rho g S$, is a combination of the bed slope (and hence the local topography) and the slope of the water surface driving the flow. In this model, we do not distinguish between the bed and surface slopes and simply treat $\rho g S$ simply as the potential gradient, which can increase as vegetation grows into the channel. As described in the introduction section on the momentum equations, it is assumed that the vegetation canopies have a porosity large enough, such that $n \approx 1$.

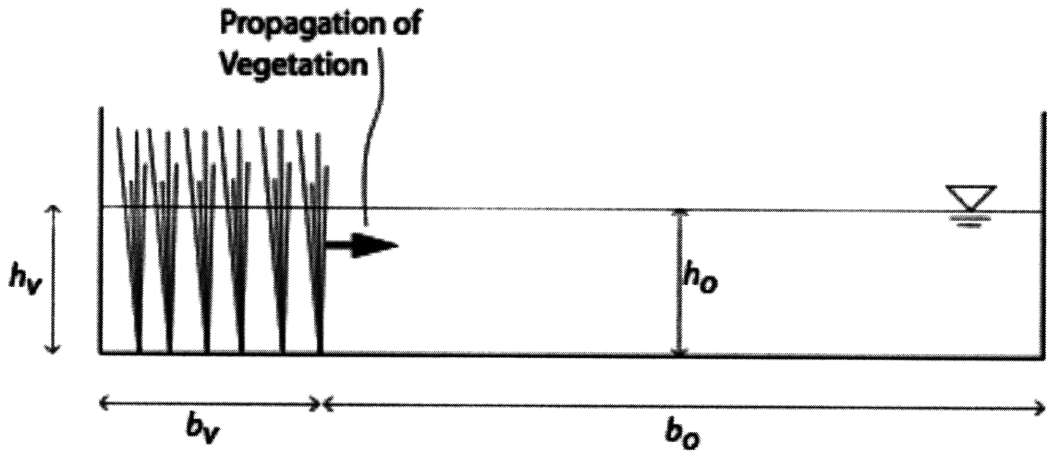

Figure 4-1: Schematic cross section of a theoretical, straight, rectangular channel, partially filled with vegetation. In this iteration of the model, the depth within the vegetation and the open channel, h_v and h_o, respectively, are equal and constant.

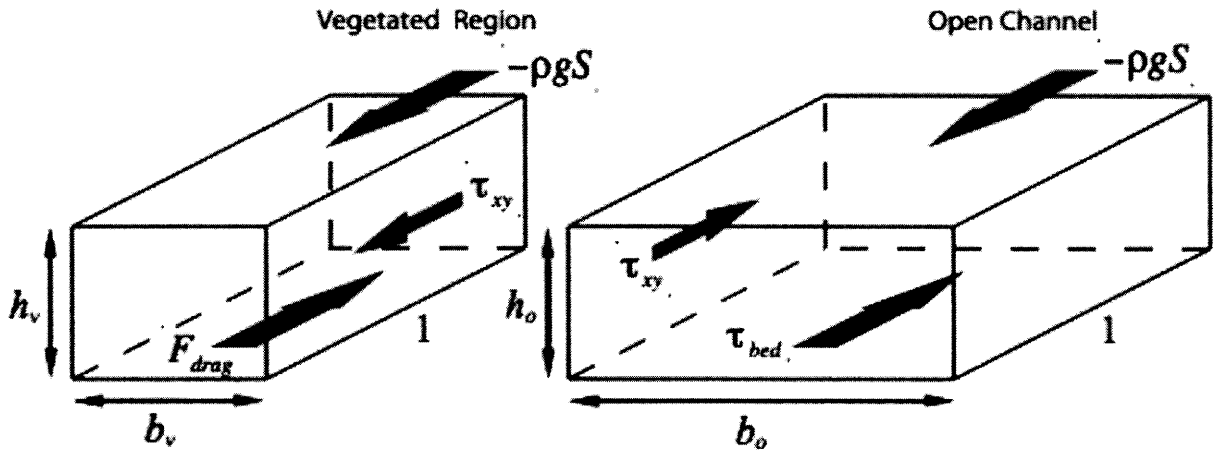

Figure 4-2: Control volume schematics for both the vegetated region and the open channel. The thick arrows represent components of the momentum balance, and S represents the potential gradient.

Since the turbulent Reynolds stress is a correlation of the deviations from the mean velocities, it can not be explicitly modeled, therefore I adopt the following closure scheme, based on the difference in mean velocities,

$$\tau_{xy} = -\rho\overline{u'v'} = \rho\left(\langle\overline{u}_o\rangle - \langle\overline{u}_v\rangle\right)^2 . \tag{4.4}$$

Prior studies confirm that the Reynolds stress is proportional to the velocity difference making this closure scheme (Equation 4.4) reasonable (White and Nepf 2008). If $h_o = h_v = constant$, Q is set by the hydrology and constant, and the total width of the channel $W = b_o + b_v = constant$, I can vary the width of the vegetation to determine its effect on the channel velocities. In actual channels, vegetation can propagate into the channel during an extended period of base-flow or it

can be added artificially during a restoration project. In the following example the flow rate is defined $Q = 0.2$ m^3/s, $W = 2.5$ m, $h_o = h_v = 0.18$ m and $C_D a = 5$ m^{-1}, which are the design values from the OSL, discussed in Case Study 1. Using the closure scheme above (Equation 4.4), I can solve these two coupled momentum balances analytically for $\langle \overline{u}_v \rangle$ and $\langle \overline{u}_o \rangle$ while varying b_v.

4.2.2. *Results and Discussion*

These results show that as the fractional width of vegetation, b_v / W, increases from 0.0 to ~0.24, the velocity in the open channel increases steadily, while the velocity within the vegetation sharply decreases. As the width fraction increases beyond ~0.24, the velocity within the vegetation begins to increase as the velocity in the open channel increases as well. As the fractional width of the vegetation approaches 1.0, the velocity in the open channel and the velocity in the vegetation converge at $\langle \overline{u}_v \rangle = \langle \overline{u}_o \rangle = 0.44$ m/s, the same velocity that is seen if $b_v / W = 0$. This is due to the fact that the cross sectional area of the channel is held constant along with Q. In reality, as the vegetational area increases, the added resistance will cause the depth of flow to increase and increase the size of the effective cross section.

As the vegetation occupies a larger fraction of the channel, the overall drag force exerted on the flow increases, which thus "shelters" the vegetation and results in a reduced velocity within the vegetation canopy. But, as the fractional width of vegetation increases further, the flow within the canopy begins to increase again. This is due to the flow being constrained by the size of the cross section.

The *critical* Shields parameter, ψ_{cr}, describes the point of neutral stability for particles (See Equation 2.3). At $\psi = \psi_{cr}$, the destabilizing forces balance the stabilizing forces, and the sediment particles are at state of dynamic equilibrium, i.e. the sediment motion threshold. For

$\psi > \psi_{cr}$, I define another threshold above which vegetation cannot grow, i.e. the vegetation erosion threshold (Rominger et al. 2009). In reality, this threshold can be a function of the sediment characteristics, the mechanical properties of the vegetation or a combination the sediment and vegetation characteristics unique to the site. For the purposes of this example, this threshold is set at $\langle \overline{u}_{crit} \rangle = 0.53$ m/s, which was the velocity observed near the edge of the vegetation in Outdoor StreamLab experiments at which point significant dislodging of plants was observed.

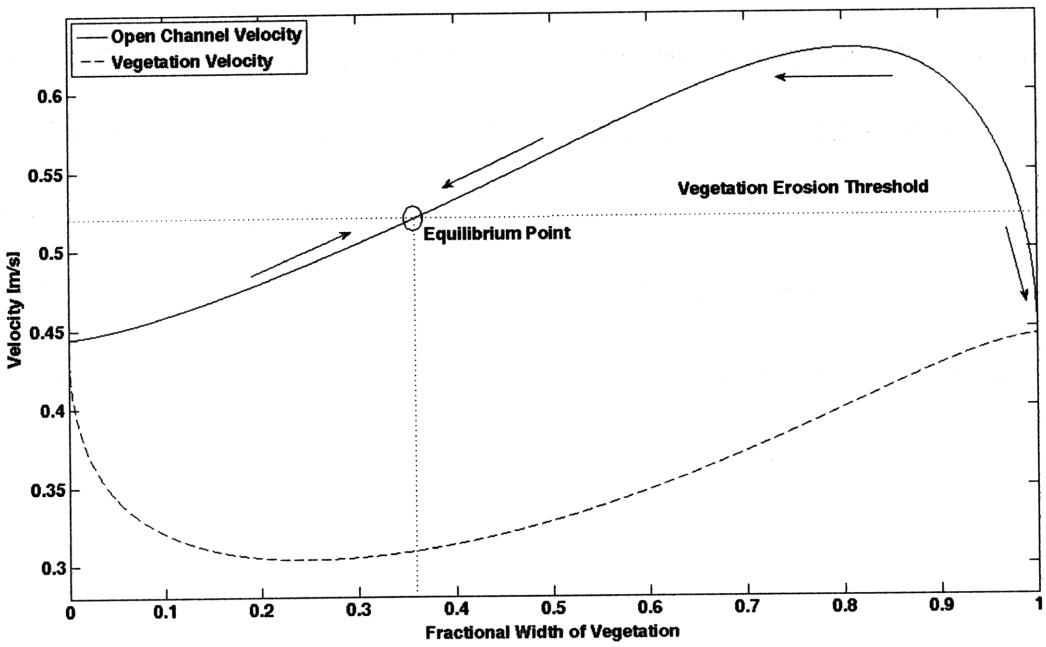

Figure 4-3: *Model 1* results showing the velocity in both the open channel and in the vegetation, as a function of the fractional width of the channel occupied by vegetation.

As the velocity in the open channel increases above this threshold, I assume vegetation can not encroach any further into the stream, because the rapid flow in the open channel has

either created a rapidly mobile bed, or the vegetation itself cannot withstand the force of the flow above this threshold. The crossing of this threshold corresponds to a specific fractional width of vegetation, which in this case is $b_v / W = 0.36$ (Figure 4-3). If vegetation were inserted into a channel and occupied a fractional width larger than 0.36, or if vegetation was able to grow beyond this fraction due to some natural perturbation, the flow would theoretically dislodge the outermost stems until $b_v / W \leq 0.36$ and $\langle \overline{u}_o \rangle \leq 0.53$ m/s. Conversely, if vegetation were to occupy a fractional width $b_v / W < 0.36$, the vegetation would be able to propagate until $b_v / W = 0.36$. These two competing forces, the potential of the flow to erode and dislodge vegetation, and the tendency of the vegetation to propagate further into the channel converge at a point of stability, where $b_v / W = 0.36$ (Figure 4-3).

According to this model, if the vegetation occupies more than 97% of the channel it can theoretically propagate until it fully covers the channel. This would create a second point of stability at $b_v / W = 1.0$. This second point of stability is unrealistic, though, because as the vegetative drag increases, the depth of flow will increase as well and, in the case of a stream channel, overtop the banks and spread out onto the floodplain. Furthermore, the vegetation cannot be perfectly rigid and would bend under the force of the flow, becoming submerged and creating a layer of flow above the vegetated layer. These nonlinear phenomena would play a more significant role as $b_v / W \geq \sim 0.50$, but are not accounted for in this model.

4.3. *Model 2: Erodible Channel Cross Section*

4.3.1. *Governing Equations and Iterative Procedure*

In this second formulation, instead of simply adding vegetation to the channel and observing the responses of the open channel and in-vegetation velocities, I impose the critical

vegetation erosion threshold of $\langle \overline{u}_{crit} \rangle = 0.53$ m/s on the system and allow erosion to occur to maintain $\langle \overline{u}_o \rangle \leq \langle \overline{u}_{crit} \rangle$. In this formulation, vegetation is incrementally added to an initially rectangular channel and the response of the channel is observed at each step. If the initial width of added vegetation results in $\langle \overline{u}_o \rangle > \langle \overline{u}_{crit} \rangle$, then the channel can adjust by eroding the three boundaries of the open channel, i.e. the vegetation interface, the bed and the outer bank (Figure 4-4). The erosion of the open channel assumes that this model takes place in an ideal channel with boundaries of infinite, uniform sediment. The same momentum equations that are used in *Model 1* (Equations 4.1-4-3) are used here and an iterative procedure for varying the width of the vegetation, b_v, the depth of the open channel, h_o, and the total width of the channel, W, to account for the changing cross section. In this model, $h_o = h_v$ initially. I solve these two coupled momentum balances analytically for $\langle \overline{u}_v \rangle$ and $\langle \overline{u}_o \rangle$, but at each step, check if $\langle \overline{u}_o \rangle \geq \langle \overline{u}_{crit} \rangle$. If this is true, the vegetation , the bed of the open channel and the outer bank of the open channel then incrementally erode until $\langle \overline{u}_o \rangle = \langle \overline{u}_{crit} \rangle$. Therefore at each step, although a certain amount of vegetation is added to the channel, a portion of that vegetation can erode along with the unvegetated boundaries of the channel.

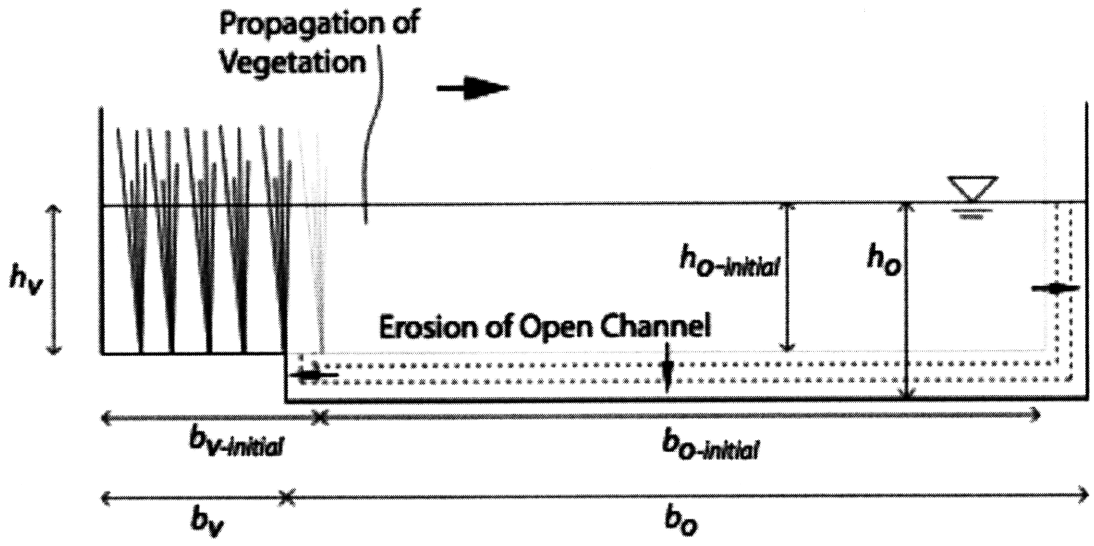

Figure 4-4: Schematic cross section of a theoretical rectangular channel, partially filled with vegetation, with the open channel subject to erosion. In this iteration of the model, an initial amount of vegetation is added to the channel. If this geometry proves to be unstable, the boundaries of the open channel, including some of the vegetation, erode until equilibrium is reached.

4.3.2. *Results and Discussion*

Although vegetation is added to a certain fraction of the cross section initially, part of this vegetation may be unstable. As the channel adjusts, a portion of the vegetation erodes along with the bed and outer bank of the open channel. This erosion results in a new, smaller fractional width of vegetation in the channel, both due to the erosion of vegetation and the increase in the total channel width. The results below are plotted in dimensional form because the ultimate width of vegetation and the width fraction are dependent on the initial values of the stream cross section and the overall flow rate.

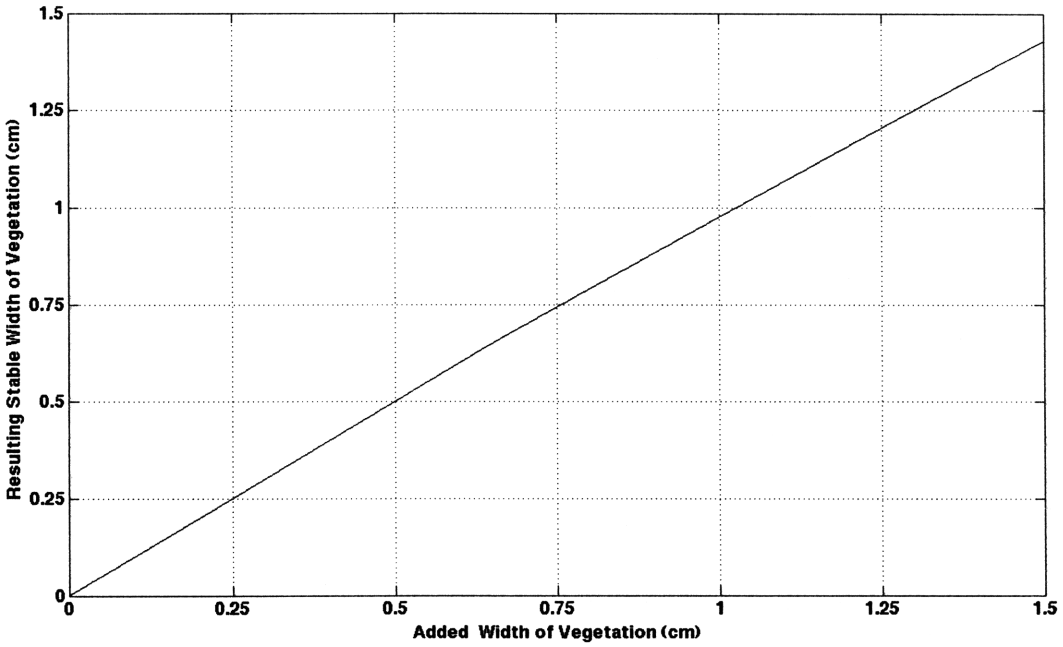

Figure 4-5: The relationship between the initial width of added vegetation in the channel, $b_{v\text{-}initial}$, and the resulting stable width of vegetation, b_v. The slope of this line is 1 initially, but beyond the critical width of vegetation, the slope drops below 1, showing a smaller width of vegetation is stable than the amount added.

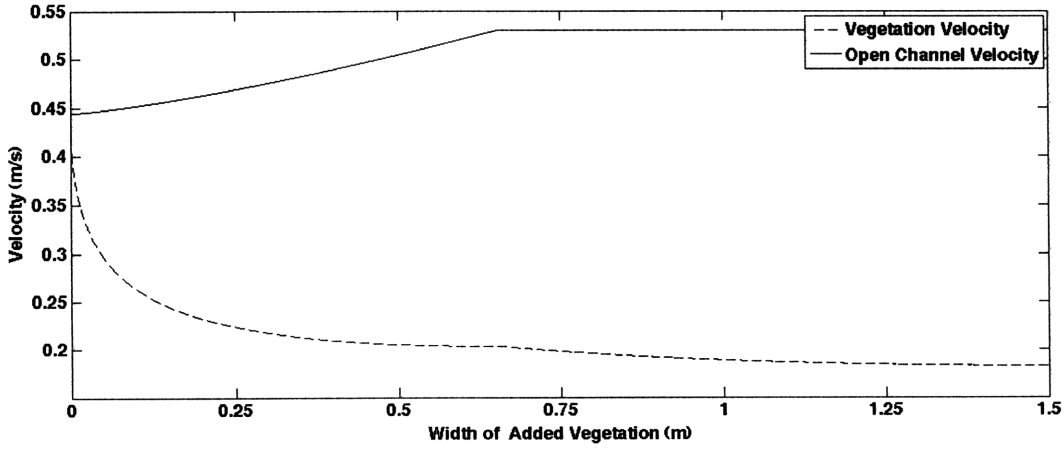

Figure 4-6: *Model 2* results showing the velocity in the open channel and within the vegetation as a function of the width of "added" vegetation. When the width of added vegetation equals 0.654 m, the initial cross section is no longer stable and begins to adjust to maintain $\langle \overline{u}_o \rangle = \langle \overline{u}_{crit} \rangle$.

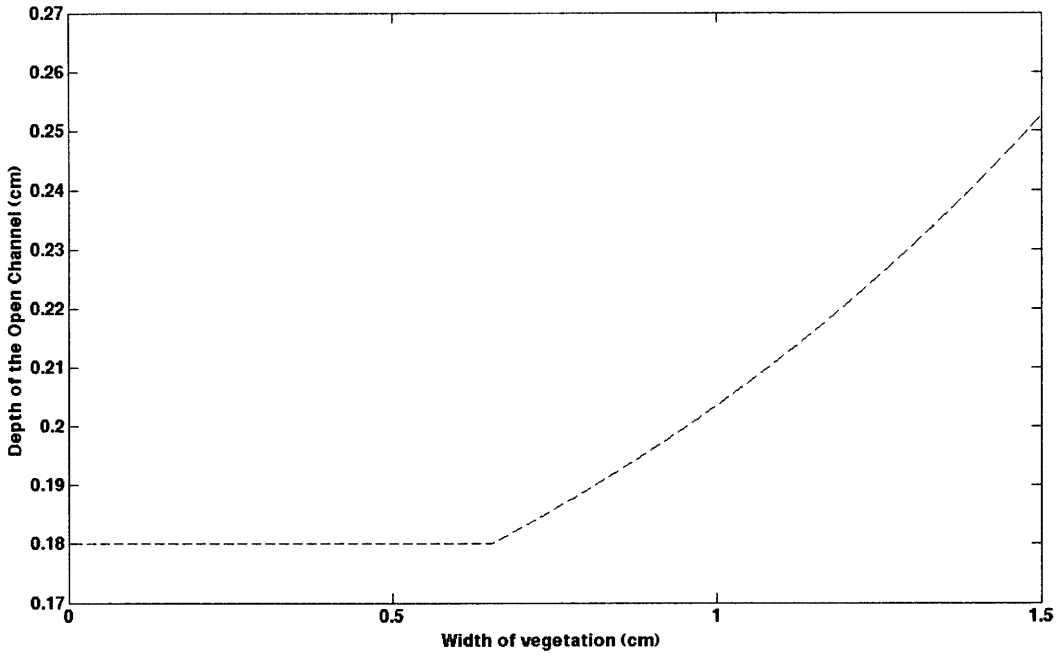

Figure 4-7: Depth of the open channel v. width of vegetation added to the channel. Once vegetation increases past the critical point, high velocities in the open channel begin to scour the bed.

These results are interesting in that there is no single "stable" width of vegetation. For any width of vegetation added to the channel, the channel adjusts through erosion of the bed, the outer bank and a portion of the added vegetation. This model thus depends highly on the initial geometry of the cross section. For example, as Figure 4-5 shows, if 1.25 m of vegetation is added to the 2.5 m wide channel, or 50% of the initial channel width, only 1.206 m of vegetation will remain stable, and the overall channel width will increase to 2.54 m. But, 1.25 m of vegetation can be stable provided that 1.3 m of vegetation is initially added to the 2.5 m wide channel. By adding the potential erosion of the sediment and the vegetation into the model, these results show that nearly any width of vegetation added to the channel can be stable, provided the open channel can freely adjust to accommodate the added flow.

Figure 4-6 shows widths of vegetation up to 0.658 m result in open channel velocities below the critical velocity, and therefore do not alter the cross section. As $b_{v\text{-}initial}$ increases beyond 0.658 m, $\langle \overline{u}_o \rangle$ increases beyond $\langle \overline{u}_{crit} \rangle$, and the channel adjusts to a new geometric equilibrium in order to reduce $\langle \overline{u}_o \rangle$ to $\langle \overline{u}_{crit} \rangle$ (e.g. Figure 4-4 Schematic). Figure 4-7 shows the response of the streambed in the open channel to added vegetation. Once vegetation is added beyond the critical point, sediment starts to erode in the bed open channel, greatly increasing the depth (and thus the cross-sectional area) which reduces velocities back below the threshold.

The sediment characteristics themselves need to be taken into account as well. This model assumes a critical velocity of $\langle \overline{u}_{crit} \rangle = 0.53$ m/s, beyond which sediment erodes rapidly and vegetation cannot grow. This velocity was observed at the edge of the vegetation in the Outdoor StreamLab, yet it is highly empirical. For the purposes of the theoretical model above, this example threshold value is used to demonstrate the interactions that occur between the vegetation and the channel flow when velocities exceed such a threshold, but it is dependent on the local sediment and vegetation properties. Therefore, for each channel, this threshold will be different and some knowledge of the sediment and vegetation is necessary for the application of this model.

Overall, I can conclude several points from this theoretical model. The first model indicates that for a given channel cross section and flowrate, and for a certain critical threshold that is dependent on the sediment characteristics, there is a single stable width of vegetation that can exist. The vegetation will tend to grow into the channel until the velocity at the edge of the vegetation reaches this threshold. If the vegetation grows beyond this width due to some perturbation, like an extended period of low flow, the high velocities in the open channel will cause erosion and drive the vegetation back to this point of stability. The second model, which

allows the cross section to erode when the critical velocity is exceeded, indicates that there may not be a single stable width of vegetation for a given channel. Vegetation can still grow outwards to a point of stability, but if vegetation is added beyond this width, it will only erode partially, while the rest of the open channel erodes to accommodate the increased flow. Therefore, this leads us to conclude that many different widths of vegetation can be stable for a given cross section and flowrate. Model 2 demonstrates that this vegetation can induce erosion in the unvegetated sections of the channel, which in turn imparts some stability on the vegetation itself.

4.4. *Underlying Assumptions and Limitations of the Models*

Natural channels are much more complex than the models presented in this section. The vegetation could grow in dense patches and cause the flow to form a complex series of channels through these patches. Depending on the plant species, the roots may change the local critical Shields parameter, and thus, the critical threshold beyond which vegetation cannot grow. For example, a complex and established root structure may greatly increase the threshold velocity that will erode vegetation. The sediment in the channel may be highly heterogeneous, or there may be only a finite amount of erodible sediment, i.e. the channel could flow through incised rock or be reinforced with rip rap or concrete. This model relies on the assumption that all three surfaces erode at the same rate. There may be a layer of bedrock or a discrete change in sediment characteristics below the streambed and this may limit vertical erosion. Also, as in the Outdoor Streamlab, the bed may be erodible, but the banks of the channels may be fixed in position by artificial structures or by rocks and debris and the channel may be limited in its ultimate width. Moreover, the velocities in these models are not only time-averages but averaged over the

fractional cross sectional areas of either the vegetation or the open channel. The true velocity profile in a channel would have velocities slightly higher than $\langle \overline{u}_v \rangle$ at the edge of the vegetation that could lead to further erosion (e.g. White and Nepf 2007). The strong secondary circulations present in meandering channels are not currently accounted for by this model either.

Regardless of these complexities that are found in natural channels, the models presented in this section can be useful tools for determining the responses of channels to the growth or addition of vegetation. The parameters of a given channel, such as the overall flowrate and dimensions, can be input to the model which can describe the tendencies towards erosion of the banks and/or stabilization of the vegetation. Laboratory experiments and field observations can be used to confirm that this model captures the essential physics of the propagation of vegetation into a channel.

4.5. *Comparison with OSL Data*

Currently the experiments in Case Study 1 are the only known data that describe the change in a channel cross section following the addition of vegetation. In the Outdoor StreamLab, the cross section showed erosion of the bed in the open channel as well as erosion of the added vegetation, which qualitatively agrees with the model put forth in this section. Nearly 1.25 m of vegetation was added to the emergent area of the point bar at base flow, in an approximately 2.8 m wide stream. This amount of vegetation in the cross section proved to be unstable during the periodic floods and 25-30 cm of vegetation was eroded laterally (Figure 2-5) while nearly 50 cm of emergent width of the point bar was eroded (Figure 2-3). Figure 4-8 shows that approximately 2 cm of vertical erosion occurred simultaneously in the open channel along with 25 – 30 cm of lost vegetation. Before the vegetation was added to the stream, the

average velocity in the open channel was near 49 cm/s. This average velocity increased to 56.8 cm/s following the addition of vegetation. By using the OSL design parameters in the model and comparing this experimental data with the model output, I have a rough estimate of the model's efficacy in predicting stream behavior following the addition of vegetation.

The model predicts that if 1.25 m of vegetation is added to the channel then the channel bed will erode 5 cm, and the vegetation will simultaneously erode 5 cm. Clearly the vegetation eroded at a much faster rate than the bed of the open channel. This could be due to much higher local velocities and turbulence intensity immediately at the patch edge, which the model cannot resolve. The model presented here only resolve spatially averaged velocities. This could also be due to the fact that the roots did not have adequate time to stabilize the sediment and the plant plugs acted like bridge piers, causing scour holes to form around them (e.g. Breusers et al. 1977). The model also predicts that the open channel velocity will increase from 45 cm/s to 53 cm/s after the addition of vegetation (Figure 4-6). This prediction essentially captures the changing velocities in the actual channel due to the added vegetative drag force. Within the vegetation, the model predicts $\langle \bar{u}_v \rangle$ = 18.4 cm/s. Figure 4-9 shows that the true velocity within the vegetation is not uniform over the width and decreases to nearly stagnant flow near the inside bank of the meander.

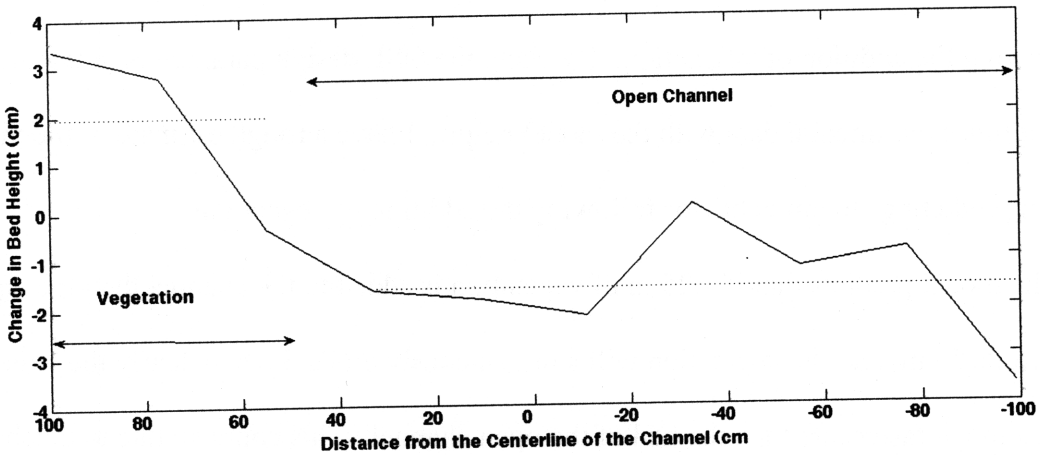

Figure 4-8: The change in bed height at the Apex of Meander 2. In the open channel, the depth increased by an average of 2 cm. Note the horizontal axis is plotted in reverse order to compare with the model output.

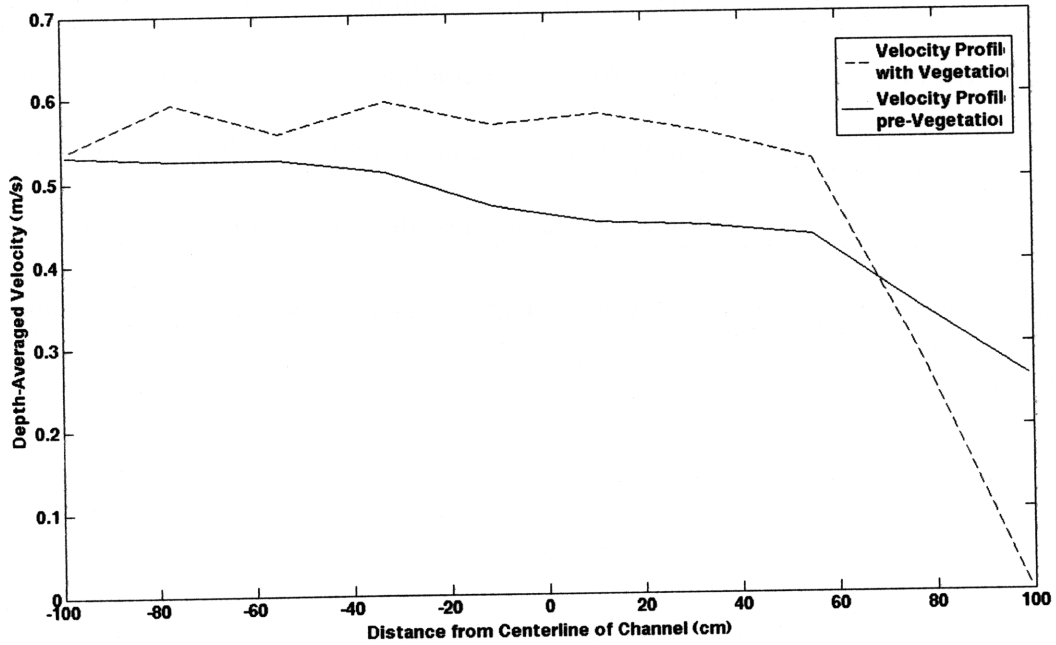

Figure 4-9: Comparison of the downstream velocities at the Apex of Meander 2. The average velocity in the open channel increases from 49.3 cm/s to 56.8 cm/s following the addition of vegetation.

The model predicts the changes in the changes in velocities well, but cannot explain the rapid and drastic loss of vegetation that was seen in the Outdoor StreamLab. These changes were further complicated by the interactions between the vegetated point bar and the strong secondary circulation in the meander. This secondary circulation was an important sediment supply to the point bar and had cross-stream velocities that were nearly 25% of the downstream velocity. Above all, the mechanisms of vegetation dislodging and erosion are not well understood, nor are the effects that vegetation has on bulk sediment properties. Furthermore, each plant species has slightly different mechanical properties and root structure. For models to capture changes in a stream cross section more accurately, much more needs to be understood about the vegetation and how it anchors itself in moving flows.

5. Conclusions

This thesis describes the interactions between currents and aquatic and riparian vegetation in multiple environments, and the resulting effects on the spatial distribution of this vegetation and the changes in flow patterns. Chapter two describes experiments in which vegetation was added to the point bar in the meander of a constructed stream. This vegetation was above the water level at base flow but interacted with the flow during the episodic floods. I monitored the vegetation for changes in its coverage as well as the three dimensional velocities in the stream for significant changes in the flow patterns. A portion of this vegetation eroded within the first flood event, and the secondary circulation was permanently altered, effectively decreasing the supply of sediment and water the point bar. Furthermore, a portion of the sand bar as well as the streambed in the open channel showed significant erosion, suggesting that the addition of vegetation was initially destabilizing to the stream meander. This study's results are important for stream restoration efforts in that these efforts often include the addition of vegetation to stabilize banks and landforms. By documenting a case in which the addition of vegetation helped promote erosion, this study calls into question widespread planting in favor of more targeted, appropriate plantings.

In Chapter Three, I document the hydrodynamic influence on the spatial distribution of plants in a seagrass meadow. Ranging from discrete, unconnected patches, to continuous swaths of vegetation, seagrass meadows show great variation in area coverage and distribution. This study shows how seagrass, in the presence of strong tidal currents, organizes itself in either nearly continuous meadows, or more patchy distributions near a specific area fraction of coverage. By drawing on the principles of percolation theory, which describes the connectivity of landscape elements, I can predict that this fractional threshold is near 40%. These results are

important for restoration efforts as many local governments have recognized the importance of seagrass meadows in coastal zones for their role in bed stability, coastal protection, nutrient uptake and habitat creation. By understanding some of the physics that govern their spatial growth, planting and management efforts can be better informed and more efficient.

In the final section of this thesis, Chapter 4, I build a model that predicts the interactions between aquatic vegetation and flow in a straight rectangular channel. The first version of this model has fixed boundaries, while the second version allows erosion when the flow reaches a critical level. By assuming a certain set of sediment parameters (which are site-specific in the field) the first model predicts a maximum fraction of the channel that can be occupied by vegetation. If the vegetation were to grow beyond this point, the velocities during the periodic flood events would erode the vegetation back to the critical point. The second model does not show a single maximum width of vegetation, but does predict if vegetation will cause erosion in the open channel. Despite being unable to capture some of the complexities of natural systems, these models are useful tools again for stream and river management, as well as for flood management using open channels.

There are many branches of science studying the coupling between hydrodynamics and ecology, yet these interactions are still not well understood. Quite often, hydrodynamicists and aquatic ecologists simply operate in mutually exclusive realms. With the combination of field experiments, theoretical development and analytical models assembled in this thesis, I present several examples of the interactions between aquatic vegetation and currents and how these interactions affect the spatial structure of the vegetation. Moreover, by tying together the physics of currents with the survival and growth of one of the most important elements of aquatic ecosystems, its vegetation, I hope to reinforce this cross-collaboration between these two

disciplines and provide research from which real-world applications can be derived.

6. Areas for Future Research

There are several clear extensions of this work, and several areas where further study will bolster or assist the theory and results presented in this thesis.

- The most natural extension of the work in the Outdoor StreamLab is to put plants in at different parts of the channel and observe their impact on the flow. Also, once the coconut fiber reinforcement in the banks decomposes, the vegetation will impact the channel differently, possibly by enhancing turbulence near the outer bank in the meander, causing the stream meander to grow in amplitude. This is an area ripe for inestigation.
- With more time in the Outdoor StreamLab, more velocity profiles can be taken in the second meander to more completely understand the velocity structure in this section. With ecological experiments limiting the floods to 9 hours in duration at a periodicity of approximately 1 flood per week, velocity measurements are strictly limited by the amount of time the stream is at flood level.
- Flume-scale experiments could be conducted in a constructed basin, or in a rectangular flume with a sinuous "liner" that allows meandering stream dynamic to be investigated. Flume-scale experiments would eliminate the time constraints of operating in the OSL and/or operating in the field.
- These results can also be used a experimental confirmation for numerical models. Currently researchers at the St. Anthony Falls Laboratory are using velocity profiles from this thesis to confirm a 3D numerical model for streamflow. The interplay between experiments and modeling is especially promising in this case, as vegetation could be added at different points in the numerical model to visualize their effects on

the stream.

- A more thorough field investigation of seagrass meadows would help build on the results of Chapter 3. Specifically, the nature of channels and the feedbacks that maintain these channel could be studied more closely. Fonseca and Bell (1998) only measured velocities in a spatially averaged sense over a 2500 m^2 area. Multiple targeted velocity measurements would better capture the two distinct flow regimes described in § 3.2.
- The model presented in Chapter 4 could be confirmed with experiments in straight, rectangular channels in a flume, or could be compared to field data if enough streams with significant amounts of vegetation in them could be surveyed and described.
- Building further on the conclusions and limitations of the model in Chapter 4, the point at which channels overtop is an interesting problem, as the flow is no longer constrained by the channel. By confirming vegetation's effect on the stream surface slope, flood waters spreading out onto a floodplain can be better predicted.
- Finally, all three studies presented in this thesis encounter a threshold beyond which vegetation cannot grow. Surely, this value is a function of the local sediment and the properties of the vegetation, but it has still not been adequately described. Currently, only observations of critical velocities exist. No detailed surveys have been done on this critical threshold for a specific type of vegetation, nor for a specific sediment size and type. These observations would be very helpful for these and many future results.

References

Abernethy, B. and I.D. Rutherford. 1998. Where along a river's length will vegetation most effectively stabilise stream banks? *Geomorphology*, **23**, 55-75.

Aris, R. 1956. On the dispersion of a solute in a fluid flowing through a tube. *Proc. R. Soc. Lond.* **A235**, 67-77.

Breusers, H.N.C., Nicollet, G., and H.W. Shen. 1977. Local scour around cylindrical piers. *J Hydr. Res.* **15**(3), 211-252.

Chambers, P. and E. Prepas. 1994. Nutrient dynamics in riverbeds: the impact of sewage effluent and aquatic macrophytes. *Water Res. Res.* 28:453–464. doi:10.1016/0043-1354(94)90283-6.

Chambers, P.A., Prepas, E.E., Hamilton, H.R., and M.L. Bothwell. 1991. Current velocity and its effect on aquatic macrophytes in flowing waters. *Ecol. Appl.,* **1**(3), 249-257.

Chandler M, Colarusso P, and R. Buchsbaum. 1996. A study of eelgrass beds in Boston Harbor and Northern Massachusetts Bays. Office of Res and Devel, US EPA, Narragansett.

Ciraolo G, Ferreri G, LaLoggia G. 2006. Flow resistance of Posidonia Oceanica in shallow water. *J. Hydraul. Res.* 44(2):189–202

Coops, H., Boeters, R., and H. Smit. 1991. Direct and indirect effects of wave attack on helophytes. *Aquat. Bot.* **41**, 333-352.

Crowder, D.W. and P. Diplas. 2000. Using two-dimensional hydrodynamic models at scales of ecological importance. *J. of Hydr.,* **230**, 172-191.

Crowder, D.W. and P. Diplas. 2002. Vorticity and circulation: spatial metrics for evaluating flow complexity in stream habitats. *Can. J. Fish. Aquat. Sci.,* **59**, 633-645.

Dietrich, W.E and J.D. Smith. 1983. Influence of the Point Bar on Flow Through Curved Channels. *Water Res. Res.,* **19**(5), 1173-1192.

Diplas, P., Dancey, C.L., Celik, A.O., Valyrakis, M., Greer, K. and T. Akar. 2008. The role of impulse on the initiation of particle movement under turbulent flow conditions. *Science.* **322**, 717-720.

Duan, J.G., R.H. French and J. Miller. 2002. The lodging velocity for emergent aquatic plants in open channels. *J. of Amer. Water Res. Assoc.*, **38**(1), 255-263.

Duan J., Barkdoll B. and R. French. 2006. Lodging velocity for an emergent aquatic plant in open channels. *J. of Hydraul. Eng.* 132(10):1015–1020. doi:10.1061/(ASCE)0733-9429(2006)132:10(1015)

Duarte, C.M. and J. Kalff. 1990. Patterns in the submerged macrophyte biomass of lakes and the importance of the scale of the analysis in the interpretation. *Can. J. Fish Aquat. Sci.* **47**, 357-363.

Finnigan, J. 2000. Turbulence in plant canopies. *Annual Review of Fluid Mechanics*, **32**, 519-571.

Fischer, H.B., List, E.J., Koh, R.C.Y., Imberger, J. and N.H. Brooks. 1979. *Mixing in inland and coastal waters*. 483 pp., Elsevier, New York.

Fisher, K.R. and C.E. Reeve. 1994. Impact of aquatic vegetation cutting. In *2nd International Conference on River Flood Hydraulics*, White WR, Watts J (eds.): 439-447.

Fonseca, M.S. 1998. Exploring the basic pattern expression in seagrass landscape. PhD thesis, University of California, Berkeley.

Fonseca, M.S. and S.S. Bell. 1998. Influence of physical setting on seagrass landscapes near Beaufort, North Carolina, USA. *Mar. Ecol. Prog. Ser.* **171**, 109–121. doi:10.3354/meps171109

Fonseca, M.S. and J.S. Fisher. 1986. A comparison of canopy friction and sediment movement between four species of seagrass with reference to their ecology and restoration. *Mar. Ecol. Prog. Ser.*, **29**, 15-22.

Fonseca, M.S., Zieman, J.C. Thayer, G.W., and J.S. Fisher. 1983. The role of current velocity in structuring eelgrass (*Zostera marina* L.) meadows. *Est., Coast. and Shelf Sc.*, **17**, 367-380.

Frissell, C.A., and R.K. Nawa. 1992. Incidence and causes of physical failure of artificial habitat structures in streams of Western Oregon and Washington, *North American Journal of Fisheries Management*, **12**, 182-197.

Furukawa, K.,Wolanski, E., and H. Mueller. 1997. Currents and sediment transport in mangrove forests. *Estaur. Coast. Shelf. Sci.* 44:301–310. doi:10.1006/ecss.1996.0120

Gambi, M.C., Nowell, A.R.M., and P.A. Jumars. 1990. Flume observations on flow dynamics in *Zostera marina* (eelgrass) beds. *Mar. Ecol. Prog. Ser.* 61:159–169. doi:10.3354/meps061159.

Ghisalberti, M. and H. Nepf. 2005. Mass transfer in vegetated shear flows. *Environ. Fluid. Mech.* **5**(6):527–551. doi:10.1007/s10652-005-0419-1.

Ghisalberti, M. and H. Nepf. 2006. The structure of the shear layer over rigid and flexible canopies. *Environ. Fluid. Mech.* **6**(3):277–301. doi:10.1007/s10652-006-0002-4.

Green, J. 2005a. Comparison of blockage factors in modelling the resistance of channels containing submerged macrophytes. *River Res. Appl.* **21**:671–686. doi:10.1002/rra.854

Green, J. 2005b. Modelling flow resistance in vegetated streams: review and development of new theory. *Hydrol. Process.* **19**, 1245-1259. doi: 10.1002/hyp.5564

Green, J. 2006. Effect of macrophyte spatial variability on channel resistance. Adv. Water Resour. **29**:426–438. doi:10.1016/j.advwatres.2005.05.010.

Grimmond, C.S.B. and T. Oke. 1999. Aerodynamics properties of urban areas derived from analysis of surface form. *J. Appl. Meteorol.* **38**:1262–1292. doi:10.1175/15200450(1999)038<1262:APOUAD>2.0.CO;2.

Ho, C.M. and P. Huerre. 1984. Perturbed free shear layers. *Ann. Rev. Flu. Mech.* **16**, 365-422. doi:10.1146/annurev.fl.16.010184.002053.

Jackson, G.A. 1997. Currents in the high drag environment of a coastal kelp stand off California. *Cont. Shelf Res.* **17**(15), 1913-1928.

Jimenez, J. 2004. Turbulent flows over rough walls. *Annu. Rev. Fluid Mech.* **36**, 173–196. doi:10.1146/annurev.fluid.36.050802.122103.

Jimenez, J., Uhlmann, M., Pinelli, A. & G. Kawahara. 2001. Turbulent shear flow over active and passive porous surfaces. *J. Fluid Mech.* **442**, 89–117.

Kadlec, R.H. and R.L. Knight. 1996. *Treatment Wetlands*. Lewis Publishers, Boca Raton, FL.

Kemp, J., Harper, D., and G. Crosa. 2000. The habitat-scale ecohydraulics of rivers. *Ecological Engineering*, **16**,17-29.

Kitanidis, P.K. and J.F. Kennedy. 1984. Secondary current and river-meander formation. *J. Fluid Mech.*, **144**, 217-229.

Koch, E.W. 2001. Beyond light: physical, geological, and geochemical parameters as possible submersed aquatic vegetation habitat requirements. *Estuaries*. **24**, 1–17. doi:10.2307/1352808

Koch, E.W., Barbier, E.B., Silliman, B.R., Reed, D.J., Perillo, G.M.E., Hacker, S.D., Granek, E.F., Primavera, J.H., Muthiga, N., Polasky, S.P., Kenned, C.J., Kappel, C.V., and E. Wolanksi. 2009. Non-linearity in ecosystem services: temporal and spatial variability in coastal protection. *Front Ecol Environ*. **7**(1): 29–37, doi:10.1890/080126.

Kondolf, G.M. and E.R. Micheli. 1995. Evaluating stream restoration projects. *Env. Management*. **19**(1), 1-15.

Kouwen, N. 1990. Modern Approach to Design of Grassed Channels, *J. Irrigation and Drainage.*

118(5), 733-743.

Kouwen, N., and T. Unny. 1973. Flexible Roughness in Open Channels. *J. Hydraul. Div.* **99**(HY5), 713-728.

Lee, M.J. 2008. Pseudo-random-number generators and the square site percolation threshold. *Physical Review E.* 1539-3755/2008/**78**(3)/031131(11).

Leonard, L. and M. Luther. 1995. Flow hydrodynamics in tidal marsh canopies. *Limnol. Oceanogr.* **40**:1474–1484.

Li, R-M. and H.W. Shen. 1973. Effects of tall vegetation of flow and sediment. *Journal of the Hydraulics Division of the American Society of Civil Engineers.* **99**(HY5), 793-814.

Lightbody, A. and H. Nepf. 2006. Prediction of velocity profiles and longitudinal dispersion in emergent salt marsh vegetation. *Limnol. Oceanogr.* **51**:218–228.

Luhar, M., Rominger, J., and H. Nepf. 2008. Interaction between flow, transport and vegetation spatial structure. *Environ. Fluid Mech.* **8,** 423-439. doi:10.1007/s10652-008-9080-9

Marba, N. and C.M. Duarte. 1998. Rhizome elongation and seagrass clonal growth. *Mar. Ecol. Prog. Ser.* **174**:269–280. doi:10.3354/meps174269.

Mars, M., M. Kuruvilla and H. Goen. 1999. The role of submergent macrophyte *triglochin huegelii* in domestic greywater treatment. *Ecol. Eng.*, **12**, 57-66.

Massel, S., Furukawa, K., and R. Brinkman. 1999. Surface wave propogation in mangrove forests. *Fluid Dyn. Res.* 24:219–249. doi:10.1016/S0169-5983(98)00024-0.

Mazda, Y., Wolanksi, E., King, B., Sase, A., Ohtsuka, D., and M. Magi. 1997. Drag forces due to vegetation in mangrove swamps. *Mangr. Salt Marsh.* **1**:193–199. doi:10.1023/A:1009949411068.

McBride, M., Hession, W.C., Rizzo, D.M. and D.M Thompson. 2007. The influence of riparian vegetation on near-bank turbulence: a flume experiment. *Earth Surf. Process. Landforms.* **32**, 2019-2037.

Mitsch, W.J. and S.E. Jorgensen. 2004. Ecological engineering and ecosystem restoration. Wiley, Hoboken.

Murphy, E., Nepf, H. and M. Ghisalberti. 2007. Longitudinal dispersion in vegetated channels, *Water Res. Res.*, **43**, W05438, doi:10.1029/2006WR005229.

Nappo, C.J., Miller D.R., and A.L. Hiscox. 2008. Atmospheric turbulence and diffusion estimates derived from plume image analysis, *15th Joint Conference on the Applications of Air Pollution Meteorology with the A&WMA.* Retrieved February 12, 2009, from

http://ams.confex.com/ams/pdfpapers/128980.pdf.

Nikora V., McEwan I., McLean S., Coleman S., Pokrajac D. and R. Walters. 2007. Double-averaging concept for rough-bed open-channel and oveland flow. *J Hydr. Eng.* ASCE 133: 873–883.

Nilsson, C. 1987. Distribution of stream-edge vegetation along a gradient of current velocity. *J of Ecol.*, **75**, 513-522.

Odum, E.P. 1981. Foreword. Pages xi-xiii. In: J.R. Clark and J. Benforado, eds., *Wetlands of Bottomland Hardwood Forests*. Elsevier, Amsterdam.

Othman, MA. 1994. Value of mangroves in coastal protection. *Hydrobiologia,* 285:277–282. doi:10.1007/BF00005674.

Poggi, D., G. Katul, and J. Albertson. 2004. A note on the contribution of dispersive fluxes to momentum transfer within canopies. *Bound. Lay. Met.*, 111, 615-621.

Pollen, N. and A. Simon. 2005. Estimating the mechanical effects of riparian vegetation on stream bank stability using a fiber bundle model. *Water Res. Res.*, **41**, W07025, doi:10.1029/2004WR003801.

Raupach, M., and R. Shaw. 1982. Averaging procedures for flow within vegetation canopies, *Bound. Lay. Met.*, **22**, 79-90.

Rominger, J., Lightbody, A., & H.M. Nepf. 2009. The Effects of Added Vegetation on Sand Bar Stability and Stream Hydrodynamics. *J. of Hydraulic Eng.* Under Review.

Scoffin, T.P. 1970. The trapping and binding of subtidal carbonate sediments by marine vegetation in Bimini Lagoon, Bahamas. *J. Sediment Petrol.* **40**:249–273.

Shiono, K., Chan, T.L., Spooner, J, Rameshwaran, P. and J.H. Chandler. 2009a. The effect of floodplain roughness on flow structures, bedforms and sediment transport rates in meandering channels with overbank flows: Part I. *J. of Hydr. Res.* **47**(1), 5-19.

Shiono, K., Chan, T.L., Spooner, J, Rameshwaran, P. and J.H. Chandler. 2009b. The effect of floodplain roughness on flow structures, bedforms and sediment transport rates in meandering channels with overbank flows: Part II. *J. of Hydr. Res.* **47**(1), 20-28.

Simon, A. and A.J.C. Collison. 2002. Quantifying the mechanical and hydrologic effects of riparian vegetation on streambank stability. *Earth Surf. Process. Landforms*, **27**, 527-546.

Sintes, T., Marba, N., Duarte, C.M., and G.A. Kendrick. 2005. Nonlinear processes in seagrass colonization explained by simple clonal growth rules. *Oikos* 108:165–175. doi:10.1111/j.0030-1299.2005.13331.x

Smith, J.D. and S.R. McLean. 1983. A model for meandering streams. *Water Res. Res.*, **20**(9) 1301-1315.

Stauffer, D. and A. Aharony. 1985. Introduction to percolation theory. Taylor and Francis, London.

Sundaravadivel, M. and S. Vigneswaran. 2001. Constructed wetlands for wastewater treatment. *Critical Reviews in Environmental Science and Technology.* **31**(4), 351-409.

Tal, M. and C. Paola, 2007. Dynamic single-thread channels maintained by the interaction of flow and vegetation. *Geology*, **35**(4), 347-350.

Tanino, Y. and H.M. Nepf. 2008. Laboratory investigation of mean drag in a random array of rigid emergent cylinders. *Journal of Hydraulic Engineering.* **134**(1), 34-41.

Taylor, G.I. 1935. Statistical theory of turbulence. *Proc. R. Soc. Lond.* **151**(873), 421-444.

Turker, U., Yagci, O., and M. Kabdasli. 2006. Analysis of coastal damage of a beach profile under the protection of emergent vegetation. *Ocean Eng.* 33:810–828. doi:10.1016/j.oceaneng.2005.04.019

Valiela, I., Teal, J. and W. Deuser. 1978. The nature of growth forms in the salt marsh grass *Spartina alterniflora*. *Am. Nat.* **112**:461–470. doi:10.1086/283290.

Werner, S.R., Beardsley, R.C., and A.J. Williams. 2003. Bottom friction and bed forms on the southern flank of Georges Bank. *J. Geophys. Res.* **108**(C11):8004. doi:10.1029/2000JC000692.

White, B. 2006. Momentum and mass transport by coherent structures in a shallow vegetated shear flow. Ph.D. Thesis, Massachusetts Institute of Technology.

White, B. and H. Nepf. 2007. Shear instability and coherent structures in a flow adjacent to a porous layer. *J. Fluid Mech.* **593**, 1–32.

White, B. and H. Nepf. 2008. A vortex based model of velocity and shear stress in a partially vegetated shallow channel. *Water Res. Res.* **44**, W01412. doi:10.1029/2006WR005651.

Windham, L., Weis, J.S., and P. Weis. 2003. Uptake and distribution of metals in two dominant salt marsh macrophytes, *Spartina alterniflora* (cordgrass) and *Phragmites australis* (common reed). *Estuarine, Coastal and Shelf Science*, **56**, 63-72.

Wu, F.C., Shen, H.W., and Y.J. Chou. 1999. Variation of roughness coefficients for unsubmerged and submerged vegetation. *J. Hydr. Eng.*, **125**(9), 934-942.

Zimmerman, R.C., Kohrs, D.G., Steller, D.L. and R.S. Alberte. 1997. Impacts of CO2

enrichment on productivity and light requirements for eelgrass. *Plant Physiol.* 115:599–607.

Appendix A: Data from Chapter 2 Outdoor StreamLab Experiments

A.1. *Surveyed Point Bar Width Data*

Table A.1: Tabulated data from Figure 2-3 showing the measured widths of the emergent point bars in Apex 2 and Apex 3. The error in the data was attributed solely to human error and variability while holding the surveying rod, and was calculated using the standard error in survey measurements at an upstream point at a fixed location.

	12-Jul	18-Jul	23-Jul	25-Jul	**Vegetation Added**	6-Aug	14-Aug	28-Aug
Apex 2 Widths (m)	1.6978	1.1194	1.5778	1.535		NaN	0.9751	1.0158
Apex 3 Widths (m)	0.9158	1.1299	1.2361	1.0296		0.9894	0.9729	0.8423

Apex 2 Pre-Vegetation Mean (m)	1.4825		Apex 2 With-Vegetation Mean (m)	0.9955
Apex 2 Pre-Vegetation Std. Err. (m)	0.0953		Apex 2 With-Vegetation Std. Err. (m)	0.0953
Apex 3 Pre-Vegetation Mean (m)	1.0778		Apex 3 With-Vegetation Mean (m)	0.9349
Apex 3 Pre-Vegetation Std. Err. (m)	0.0231		Apex 3 With-Vegetation Std. Err. (m)	0.0231

A.2. *Velocity Data*

Table A.2a: July 16, 2006 ADV data measured at flood level in the apex of Meander 2. Recorded using SAFL Vectrino side-looking ADV at 25 Hz. This data is shown in Chapter 2, Figure 2-6.

Point	1	2	3	4	5	6	7	8	9	10
y (cm)	-112.5	-87.5	-62.5	-37.5	-12.5	12.5	37.5	62.5	87.5	112.5
Traverse y (mm)	205	455	705	955	1205	1455	1705	1955	2205	2455
Water depth (cm)	29	26	24	20	15	12	10	9.5	10	13
Traverse z (cm)	457	457	457	457	457	457	457	457	457	457
	461	461	460	460	459	459	459	459	459	459
	465	465	463	463	461	461	461	460	461	461
	469	469	466	466	463	463	462	461	462	464
	473	473	469	468	465	464	NaN	NaN	NaN	NaN
	477	476	472	NaN	466	NaN	NaN	NaN	NaN	NaN
	*Water surface at z = 457 cm, points measured down from there									

Table A.2b: Velocity data from July 16, 2008. All three components are shown below at the locations summarized in Table A.2a.

U (cm/s)										
	68.5305	61.3273	57.3524	56.6646	57.5254	52.8276	50.4816	46.1804	39.6436	27.7292
	64.0797	60.1262	56.1672	58.2306	54.6961	52.3356	48.0169	43.4405	37.0616	25.12
	49.1629	57.4615	55.5786	56.7692	53.8062	48.5391	43.3502	42.3392	31.1973	23.1378
	54.2992	53.0915	56.0175	52.4409	51.3737	42.1511	35.2619	37.9789	5.5946	16.5361
	50.7825	46.32	51.7796	35.2376	43.2555	27.141	NaN	NaN	NaN	NaN
	38.5808	35.7172	40.6483	NaN	21.3118	NaN	NaN	NaN	NaN	NaN
V (cm/s)										
	-6.758	-11.9048	-10.809	-7.5293	-5.5559	-1.8782	-0.1686	-0.1097	-1.697	-3.5262
	-5.0245	-7.1923	-6.6877	-5.355	-3.1949	-1.1903	0.9499	0.2269	-1.2503	-4.0247
	-1.2121	-2.1446	-2.4568	-1.3655	-0.6832	0.1576	1.9863	0.7856	-0.7294	-5.0219
	5.0176	3.3513	1.4976	2.0388	2.2247	2.6442	2.3494	3.1735	-0.3129	-5.1628
	10.254	8.2611	5.4438	4.4931	4.5619	3.5869	NaN	NaN	NaN	NaN
	15.8384	10.8317	9.9251	NaN	3.4968	NaN	NaN	NaN	NaN	NaN
W (cm/s)										
	-1.0802	0.6087	0.9758	0.0847	0.5934	-0.0713	0.3116	-0.4459	-1.3145	0.797
	-2.5347	0.4718	0.905	-0.3281	0.6409	0.4152	-0.4068	-0.5778	-0.6191	-0.5489
	-2.6321	0.5647	-0.105	0.0674	0.3567	-0.7418	-0.5126	-1.2202	-1.137	0.184
	-5.7032	0.4556	0.0644	-1.2942	-0.1076	-0.9152	-1.0643	-1.2179	0.1069	-2.1626
	-6.3975	0.8407	0.7392	-0.3086	-0.3204	-0.7739	NaN	NaN	NaN	NaN
	-6.6679	0.7413	0.2763	NaN	0.4681	NaN	NaN	NaN	NaN	NaN

Table A.2c: Turbulence data for velocities measured on July 16, 2008 at the locations summarized in Table A.2a.

U'U' (m^2 / s^2)										
	0.0039	0.004	0.0037	0.0041	0.0037	0.0026	0.0022	0.0019	0.0012	0.0015
	0.0178	0.0045	0.0043	0.0039	0.0032	0.0036	0.0027	0.0021	0.0014	0.0014
	0.0146	0.006	0.0045	0.004	0.0031	0.0042	0.0034	0.0025	0.0016	0.0014
	0.0043	0.0084	0.0054	0.0052	0.0038	0.0057	0.0032	0.0029	0.0007	0.0015
	0.0056	0.0104	0.0055	0.006	0.0049	0.0078	NaN	NaN	NaN	NaN
	0.0083	0.0091	0.0065	NaN	0.0065	NaN	NaN	NaN	NaN	NaN
V'V' (m^2 / s^2)										
	0.0052	0.0045	0.0039	0.0037	0.0029	0.0021	0.0016	0.0012	0.0008	0.0009
	0.0082	0.0048	0.0043	0.0038	0.0029	0.0024	0.0017	0.0012	0.0009	0.0008
	0.0072	0.0054	0.0043	0.0039	0.003	0.0027	0.0018	0.0012	0.0008	0.0008
	0.0043	0.0056	0.0047	0.004	0.0031	0.0027	0.0014	0.0012	0	0.0006
	0.0046	0.0061	0.005	0.002	0.0025	0.0017	NaN	NaN	NaN	NaN
	0.0055	0.0065	0.0035	NaN	0.0011	NaN	NaN	NaN	NaN	NaN
W'W' (m^2 / s^2)										
	0.0023	0.0024	0.0026	0.0023	0.0021	0.0018	0.0013	0.0009	0.0006	0.0009
	0.0035	0.0027	0.0027	0.0022	0.0022	0.0018	0.0013	0.001	0.0007	0.0009
	0.0044	0.0033	0.0027	0.0021	0.0018	0.0017	0.0016	0.0012	0.0009	0.0009
	0.0029	0.0038	0.0027	0.0022	0.0019	0.0022	0.002	0.0015	0.0008	0.0016
	0.0034	0.0046	0.0029	0.0027	0.002	0.0025	NaN	NaN	NaN	NaN
	0.0042	0.006	0.0031	NaN	0.0021	NaN	NaN	NaN	NaN	NaN

Table A.3a: August 26, 2008 ADV data measured at flood level in the apex of Meander 2. These measurements were taken after the vegetation was added. Recorded using SAFL Vectrino side-looking ADV at 25 Hz. This data is plotted in Chapter 2, Figure 2-7.

Point	1	2	3	4	5	6	7	8	9	10
y (cm)	-99	-77	-55	-33	-11	11	33	55	77	99
Traverse Location y (mm)	100	320	540	760	980	1200	1420	1640	1860	2080
Water depth (cm)	31	26	24	19	17	14	12	10	7	8
z (cm)	447	447	447	447	447	447	447	447	447	447
	450	450	450	450	450	450	450	450	448	NaN
	453	453	453	453	453	453	453	452	NaN	NaN
	456	456	456	456	456	456	NaN	NaN	NaN	NaN
	459	459	459	459	459	NaN	NaN	NaN	NaN	NaN
	462	462	462	462	NaN	NaN	NaN	NaN	NaN	NaN
	466	466	466	NaN	NaN	NaN	NaN	NaN	NaN	NaN
	470	470	NaN	NaN	NaN	NaN	NaN	NaN	NaN	NaN
	472	NaN	NaN	NaN	NaN	NaN	NaN	NaN	NaN	NaN
	*Water surface at z = 447 cm, points measured down from there									

Table A.3b: Velocity data from August 26, 2008. All three components are shown below at the locations summarized in Table A.3a.

U (cm/s)										
	67.8146	68.0188	67.5522	62.2714	59.8927	60.691	57.5078	53.3264	26.0477	0.6313
	66.4263	66.118	67.6105	63.6299	59.0591	60.1671	55.8207	52.7725	30.8392	NaN
	64.8483	63.5192	65.3204	62.5092	65.5153	53.296	52.9434	50.4623	NaN	NaN
	69.7201	60.448	52.305	55.966	41.8161	57.0928	NaN	NaN	NaN	NaN
	59.9042	60.365	58.0885	52.6463	NaN	NaN	NaN	NaN	NaN	NaN
	54.7506	59.7177	51.5908	NaN	NaN	NaN	NaN	NaN	NaN	NaN
	39.1682	54.6293	27.688	NaN	NaN	NaN	NaN	NaN	NaN	NaN
	30.5396	41.4705	NaN	NaN	NaN	NaN	NaN	NaN	NaN	NaN
	29.5817	NaN	NaN	NaN	NaN	NaN	NaN	NaN	NaN	NaN
V (cm/s)										
	-6.7503	-12.887	-11.867	-11.130	-8.9324	-10.109	-13.822	-11.921	-6.2466	0.0069
	-4.0455	-9.0534	-9.7107	-8.9541	-6.1843	-9.4065	-10.136	-9.9131	-5.9609	NaN
	-2.0938	-6.9039	-6.0946	-4.2455	-6.6739	-7.9648	-9.0083	-8.3269	NaN	NaN
	-1.2191	-4.3003	-3.2792	-4.702	-0.2811	-2.3624	NaN	NaN	NaN	NaN
	1.1834	-1.8526	-0.4072	-1.942	NaN	NaN	NaN	NaN	NaN	NaN
	3.2796	1.8501	3.4625	NaN	NaN	NaN	NaN	NaN	NaN	NaN
	4.9824	6.1858	3.5094	NaN	NaN	NaN	NaN	NaN	NaN	NaN
	5.2663	9.1656	NaN	NaN	NaN	NaN	NaN	NaN	NaN	NaN
	3.4559	NaN	NaN	NaN	NaN	NaN	NaN	NaN	NaN	NaN
W (cm/s)										
	0.0146	1.1784	1.9614	0.8979	0.4912	0.8496	1.092	-0.5522	0.5281	1.9201
	-1.1051	0.2347	1.4692	1.1043	0.3967	0.6873	0.9442	-0.3355	0.9161	NaN
	-1.4078	0.1716	1.6838	0.5575	0.3022	-1.0821	-0.1062	0.178	NaN	NaN
	-0.1962	-0.6479	1.3286	-1.6564	0.331	1.4312	NaN	NaN	NaN	NaN
	-2.7821	-0.4073	1.2744	-1.2869	NaN	NaN	NaN	NaN	NaN	NaN
	-3.9905	-0.4747	1.5771	NaN	NaN	NaN	NaN	NaN	NaN	NaN
	-4.3032	-0.5113	-1.1339	NaN	NaN	NaN	NaN	NaN	NaN	NaN
	-2.729	-1.6869	NaN	NaN	NaN	NaN	NaN	NaN	NaN	NaN
	-1.5513	NaN	NaN	NaN	NaN	NaN	NaN	NaN	NaN	NaN

Table A.3c: Turbulence data for velocities measured on August 26, 2008 at the locations summarized in Table A.3a.

U'U' (m^2 / s^2)										
	0.004	0.0036	0.0037	0.0061	0.0043	0.0041	0.0026	0.0044	0.0038	0.0009
	0.0041	0.0036	0.0033	0.0046	0.0053	0.0024	0.0025	0.0032	0.0042	NaN
	0.004	0.0038	0.0038	0.0052	0.0062	0.0039	0.0031	0.0031	NaN	NaN
	0.006	0.0031	0.0035	0.005	0.0113	0.0088	NaN	NaN	NaN	NaN
	0.0084	0.0046	0.0058	0.0076	NaN	NaN	NaN	NaN	NaN	NaN
	0.0142	0.0055	0.0095	0.0219	NaN	NaN	NaN	NaN	NaN	NaN
	0.0251	0.007	0.0045	NaN	NaN	NaN	NaN	NaN	NaN	NaN
	0.0149	0.0109	NaN	NaN	NaN	NaN	NaN	NaN	NaN	NaN
	0.011	NaN	NaN	NaN	NaN	NaN	NaN	NaN	NaN	NaN
V'V' (m^2 / s^2)										
	0.0048	0.0049	0.0036	0.0039	0.0042	0.004	0.0015	0.0018	0.0007	0.0001
	0.0041	0.0042	0.0034	0.0049	0.004	0.002	0.0016	0.0013	0.0008	NaN
	0.0036	0.0042	0.0049	0.0046	0.0056	0.0028	0.002	0.0014	NaN	NaN
	0.0031	0.0021	0.0036	0.0055	0.0057	0.0033	NaN	NaN	NaN	NaN
	0.0042	0.0043	0.0053	0.006	NaN	NaN	NaN	NaN	NaN	NaN
	0.0054	0.0046	0.0047	0.0083	NaN	NaN	NaN	NaN	NaN	NaN
	0.0056	0.0045	0.002	NaN	NaN	NaN	NaN	NaN	NaN	NaN
	0.0037	0.005	NaN	NaN	NaN	NaN	NaN	NaN	NaN	NaN
	0.003	NaN	NaN	NaN	NaN	NaN	NaN	NaN	NaN	NaN
W'W' (m^2 / s^2)										
	0.0017	0.0023	0.0022	0.0054	0.002	0.0021	0.0009	0.0015	0.0014	0.0017
	0.0018	0.0017	0.0017	0.0026	0.0023	0.0009	0.001	0.0016	0.0019	NaN
	0.0019	0.0021	0.0023	0.0028	0.0017	0.0017	0.001	0.0008	NaN	NaN
	0.0024	0.0016	0.0015	0.0018	0.0037	0.0017	NaN	NaN	NaN	NaN
	0.0031	0.0024	0.0021	0.0029	NaN	NaN	NaN	NaN	NaN	NaN
	0.0047	0.0026	0.0025	0.0116	NaN	NaN	NaN	NaN	NaN	NaN
	0.0075	0.0024	0.0013	NaN	NaN	NaN	NaN	NaN	NaN	NaN
	0.0074	0.0023	NaN	NaN	NaN	NaN	NaN	NaN	NaN	NaN
	0.0039	NaN	NaN	NaN	NaN	NaN	NaN	NaN	NaN	NaN

Table A.4a: July 14, 2008 ADV data measured at base level in the apex of Meander 2. These measurements were taken before the vegetation was added to Apex 2, but the vegetation did not affect base flow at all, so this data was not expected to change. Recorded using SAFL Vectrino side-looking ADV at 25 Hz.

Point	1	2	3	4	5	6
y (cm)	-114	-94	-74	-54	-34	-14
Traverse y (mm)	140	340	540	740	940	1140
Traverse z (cm)	462	462	462	462	462	462
	459	459	459	459	459	461
	456	456	456	456	458	NaN
	NaN	453	453	NaN	NaN	NaN
	NaN	450	NaN	NaN	NaN	NaN
	*Water surface at z = 462 cm, points measured down from there					

Table A.4b: Velocity data from July 14, 2008, base flow at the apex of Meander 2. All three components are shown below at the locations summarized in Table A.4a.

U (m/s)	0.187	0.2807	0.3095	0.283	0.2527	0.1813
	0.2152	0.274	0.3059	0.2253	0.1966	0.1721
	0.227	0.2383	0.2576	0.1685	0.1513	NaN
	NaN	0.236	0.1862	NaN	NaN	NaN
	NaN	0.1651	NaN	NaN	NaN	NaN
V (m/s)						
	-0.0098	-0.0818	-0.0903	-0.0796	-0.0644	-0.0438
	-0.0216	-0.0547	-0.0603	-0.0344	-0.018	-0.0342
	-0.0117	-0.0214	-0.0154	0.0128	-0.0062	NaN
	NaN	0.0255	0.016	NaN	NaN	NaN
	NaN	0.0654	NaN	NaN	NaN	NaN
W (m/s)						
	0.0108	0.0016	-0.0114	-0.0037	-0.0073	-0.0166
	0.0195	-0.0132	-0.0094	-0.0012	-0.0114	-0.0111
	-0.0147	-0.0218	-0.0249	-0.003	-0.0088	NaN
	NaN	-0.048	-0.0055	NaN	NaN	NaN
	NaN	-0.0345	NaN	NaN	NaN	NaN

Table A.4c: Turbulence data for velocities measured on July 14, 2008 at the locations summarized in Table A.4a.

U'U' (m^2 / s^2)						
	0.0026	0.0006	0.0007	0.0014	0.0008	0.0005
	0.0018	0.0009	0.0007	0.0016	0.0019	0.0007
	0.0016	0.0009	0.001	0.0015	0.0019	NaN
	NaN	0.0009	0.0017	NaN	NaN	NaN
	NaN	0.0029	NaN	NaN	NaN	NaN
V'V' (m^2 / s^2)						
	0.0008368	0.0003777	0.0006433	0.0009717	0.0003879	0.0001416
	0.0005434	0.0006441	0.0005324	0.0009737	0.0005967	0.0001954
	0.0004826	0.0005812	0.000625	0.0005781	0.0005271	NaN
	NaN	0.0005745	0.0006458	NaN	NaN	NaN
	NaN	0.0006838	NaN	NaN	NaN	NaN
W'W' (m^2 / s^2)						
	0.0051	0.0008	0.001	0.0013	0.001	0.0008
	0.0033	0.0012	0.0009	0.0016	0.0019	0.0009
	0.002	0.0011	0.0011	0.0017	0.0024	NaN
	NaN	0.0015	0.0017	NaN	NaN	NaN
	NaN	0.0029	NaN	NaN	NaN	NaN

Table A.5a: July 10, 2008 ADV data measured at flood level in the apex of Meander 3. Vegetation was not added to Meander 3 so these measurements were not expected to change across the season. Recorded using SAFL Vectrino side-looking ADV at 25 Hz.

Point	1	2	3	4	5	6	7	8	9	10
y (cm)	-100	-78	-56	-34	-12	10	32	54	76	98
Traverse y (mm)	290	510	730	950	1170	1390	1610	1830	2050	2270
Water depth (cm)										
Traverse z (cm)	450	450	450	450	450	450	450	450	450	450
	448	448	448	448	448	448	448	448	448	448
	446	446	446	446	446	446	446	446	446	446
	444	444	444	444	444	444	444	444	444	444
	NaN	NaN	NaN	NaN	NaN	442	442	442	442	442
	NaN	NaN	NaN	NaN	NaN	440	440	440	440	440
	NaN	NaN	NaN	NaN	NaN	438	438	438	438	438
	NaN	NaN	NaN	NaN	NaN	NaN	436	436	436	436
	NaN	NaN	NaN	NaN	NaN	NaN	434	434	434	434
	NaN	NaN	NaN	NaN	NaN	NaN	NaN	432	432	432
	NaN	NaN	NaN	NaN	NaN	NaN	NaN	430	430	NaN
	NaN	NaN	NaN	NaN	NaN	NaN	NaN	NaN	428	NaN
	NaN	NaN	NaN	NaN	NaN	NaN	NaN	NaN	426	NaN
	*Water surface at z = 450 cm and points measured down from there									

Table A.5b: Velocity data from July 10, 2008, flood level flow at the apex of Meander 3. All three components are shown below at the locations summarized in Table A.5a.

U (m/s)										
	0.042	0.2425	0.5405	0.6244	0.6136	0.6434	0.6955	0.7076	0.7048	0.6886
	0.2867	0.3851	0.4636	0.6277	0.6317	0.6859	0.6702	0.7015	0.7478	0.7619
	0.3257	0.4803	0.4588	0.4145	0.5675	0.6444	0.596	0.6747	0.7191	0.7438
	0.0122	0.0288	NaN	0.18	0.537	0.5899	0.5966	0.6784	0.6903	0.6827
	NaN	NaN	NaN	NaN	NaN	0.5592	0.5836	0.6346	0.6872	0.6981
	NaN	NaN	NaN	NaN	NaN	0.4717	0.561	0.595	0.6978	0.6479
	NaN	NaN	NaN	NaN	NaN	0.3677	0.5397	0.5352	0.6336	0.6237
	NaN	NaN	NaN	NaN	NaN	NaN	0.4829	0.5336	0.6167	0.5396
	NaN	NaN	NaN	NaN	NaN	NaN	0.3829	0.5096	0.6131	0.4705
	NaN	NaN	NaN	NaN	NaN	NaN	NaN	0.4391	0.5882	0.4091
	NaN	NaN	NaN	NaN	NaN	NaN	NaN	NaN	0.5226	NaN
	NaN	NaN	NaN	NaN	NaN	NaN	NaN	NaN	0.42	NaN
	NaN	NaN	NaN	NaN	NaN	NaN	NaN	NaN	0.1593	NaN
V (m/s)										
	-0.0032	0.0152	0.0524	0.0234	-0.0312	-0.0098	0.0227	0.0561	0.0315	-0.0354
	-0.0491	-0.0578	-0.0532	-0.0228	0.0265	0.0752	0.0627	0.0508	0.0922	0.0394
	-0.0358	-0.0114	-0.0284	-0.0017	-0.0259	0.0215	-0.0022	0.0511	0.0556	0.0227
	0.0008	0.0111	NaN	-0.0074	-0.0369	-0.0087	0.0171	0.0374	0.0543	-0.0627
	NaN	NaN	NaN	NaN	NaN	-0.0333	-0.0261	0.0225	0.0269	0.0028
	NaN	NaN	NaN	NaN	NaN	-0.0532	-0.069	-0.056	-0.0123	-0.0218
	NaN	NaN	NaN	NaN	NaN	-0.0452	-0.0563	-0.0317	-0.0209	-0.0382
	NaN	NaN	NaN	NaN	NaN	NaN	-0.0715	-0.0496	-0.0405	-0.0468
	NaN	NaN	NaN	NaN	NaN	NaN	-0.0878	-0.0845	-0.0619	-0.0604
	NaN	NaN	NaN	NaN	NaN	NaN	NaN	-0.1054	-0.0843	-0.0645
	NaN	NaN	NaN	NaN	NaN	NaN	NaN	NaN	-0.1059	NaN
	NaN	NaN	NaN	NaN	NaN	NaN	NaN	NaN	-0.1181	NaN
	NaN	NaN	NaN	NaN	NaN	NaN	NaN	NaN	-0.06	NaN

Table A.5b cont'd.

W (m/s)										
	-0.0107	-0.0067	-0.0246	-0.026	0.0053	0.0082	0.0061	-0.0041	-0.0087	-0.0134
	0.0014	0.0092	0.0069	-0.0269	-0.0081	-0.0154	-0.0127	-0.0259	-0.0422	-0.0699
	0.0019	-0.0366	-0.0129	-0.0206	0.0013	-0.0367	0.002	-0.0261	-0.0467	-0.0661
	-0.0059	-0.0795	NaN	-0.0337	-0.0135	-0.008	-0.0028	-0.0058	-0.0475	-0.0258
	NaN	NaN	NaN	NaN	NaN	-0.0023	-0.0309	-0.0035	-0.0508	-0.0612
	NaN	NaN	NaN	NaN	NaN	0.01	-0.0015	0.0193	-0.0481	-0.0598
	NaN	NaN	NaN	NaN	NaN	0.0246	0.0362	0.0184	-0.0294	-0.0444
	NaN	NaN	NaN	NaN	NaN	NaN	0.0218	0.0193	-0.0291	-0.0408
	NaN	NaN	NaN	NaN	NaN	NaN	-0.01	0.0151	-0.0276	-0.0403
	NaN	NaN	NaN	NaN	NaN	NaN	NaN	0.0047	-0.0243	-0.0413
	NaN	NaN	NaN	NaN	NaN	NaN	NaN	NaN	-0.0185	NaN
	NaN	NaN	NaN	NaN	NaN	NaN	NaN	NaN	-0.0174	NaN
	NaN	NaN	NaN	NaN	NaN	NaN	NaN	NaN	-0.02	NaN

Table A.5c: Turbulence data for Meander 3 flood level velocities measured on July 10, 2008 at the locations summarized in Table A.5a.

U'U' (m^2 / s^2)										
	0.0044	0.0026	0.0035	0.005	0.0025	0.0036	0.005	0.0056	0.0046	0.0044
	0.0017	0.0013	0.0018	0.006	0.0045	0.0061	0.006	0.006	0.005	0.0038
	0.0025	0.0026	0.0041	0.0159	0.007	0.0065	0.0064	0.005	0.0041	0.004
	0.0182	0.0093	NaN	0.015	0.0057	0.0061	0.0048	0.0047	0.0041	0.0054
	NaN	NaN	NaN	NaN	NaN	0.0077	0.0053	0.0052	0.0038	0.0073
	NaN	NaN	NaN	NaN	NaN	0.0089	0.0067	0.0052	0.0037	0.0093
	NaN	NaN	NaN	NaN	NaN	0.0144	0.0063	0.0044	0.0037	0.0104
	NaN	NaN	NaN	NaN	NaN	NaN	0.0067	0.0063	0.0041	0.0134
	NaN	NaN	NaN	NaN	NaN	NaN	0.0082	0.0065	0.0057	0.015
	NaN	NaN	NaN	NaN	NaN	NaN	NaN	0.0078	0.0064	0.015
	NaN	NaN	NaN	NaN	NaN	NaN	NaN	NaN	0.0079	NaN
	NaN	NaN	NaN	NaN	NaN	NaN	NaN	NaN	0.0109	NaN
	NaN	NaN	NaN	NaN	NaN	NaN	NaN	NaN	0.0129	NaN
V'V' (m^2 / s^2)										
	0.0006	0.0015	0.0021	0.0034	0.0016	0.0022	0.0031	0.004	0.0059	0.0046
	0.0006	0.0007	0.0008	0.0029	0.005	0.0032	0.0045	0.0044	0.0043	0.0045
	0.0009	0.0011	0.0025	0.004	0.0037	0.0034	0.0055	0.0039	0.0043	0.0046
	0.0009	0.0007	NaN	0.0021	0.0031	0.0036	0.0044	0.0038	0.0046	0.0039
	NaN	NaN	NaN	NaN	NaN	0.0035	0.0039	0.0042	0.0041	0.0044
	NaN	NaN	NaN	NaN	NaN	0.0029	0.0039	0.004	0.0035	0.0048
	NaN	NaN	NaN	NaN	NaN	0.0037	0.004	0.0042	0.0038	0.0053
	NaN	NaN	NaN	NaN	NaN	NaN	0.0035	0.0042	0.0034	0.0062
	NaN	NaN	NaN	NaN	NaN	NaN	0.0031	0.0041	0.0036	0.0067
	NaN	NaN	NaN	NaN	NaN	NaN	NaN	0.0037	0.0036	0.0071
	NaN	NaN	NaN	NaN	NaN	NaN	NaN	NaN	0.0045	NaN
	NaN	NaN	NaN	NaN	NaN	NaN	NaN	NaN	0.0063	NaN
	NaN	NaN	NaN	NaN	NaN	NaN	NaN	NaN	0.0058	NaN

Table A.5c cont'd.

W'W' (m^2 / s^2)										
	0.0009	0.0016	0.0018	0.003	0.0017	0.0025	0.003	0.0035	0.0026	0.0022
	0.0009	0.0007	0.001	0.0023	0.0034	0.0035	0.0041	0.0044	0.0037	0.0026
	0.0016	0.001	0.0019	0.006	0.0039	0.0039	0.0044	0.0035	0.0032	0.003
	0.0295	0.0189	NaN	0.0092	0.003	0.0031	0.0037	0.0039	0.003	0.0033
	NaN	NaN	NaN	NaN	NaN	0.0031	0.003	0.0034	0.0031	0.0042
	NaN	NaN	NaN	NaN	NaN	0.0034	0.0039	0.0036	0.0029	0.0055
	NaN	NaN	NaN	NaN	NaN	0.0039	0.0027	0.0034	0.0031	0.0058
	NaN	NaN	NaN	NaN	NaN	NaN	0.0028	0.0035	0.003	0.0087
	NaN	NaN	NaN	NaN	NaN	NaN	0.0046	0.0032	0.0048	0.0104
	NaN	NaN	NaN	NaN	NaN	NaN	NaN	0.0037	0.0037	0.012
	NaN	NaN	NaN	NaN	NaN	NaN	NaN	NaN	0.0045	NaN
	NaN	NaN	NaN	NaN	NaN	NaN	NaN	NaN	0.0065	NaN
	NaN	NaN	NaN	NaN	NaN	NaN	NaN	NaN	0.0174	NaN

Table A.6a: July 14, 2008 ADV data measured at base level in the apex of Meander 3. Vegetation was not added to Meander 3 so these measurements were not expected to change across the season. Recorded using SAFL Vectrino side-looking ADV at 25 Hz.

Point	6	7	8	9	10
y (cm)	10	32	54	76	98
Traverse y (mm)	1390	1610	1830	2050	2270
Traverse z (cm)	441	441	441	441	441
	439	439	439	439	439
	NaN	437	437	437	437
	NaN	435	435	435	435
	NaN	NaN	433	433	434
	NaN	NaN	NaN	431	NaN
	NaN	NaN	NaN	430	NaN

Table A.6b: Velocity data from July 14, 2008, base level flow at the apex of Meander 3. All three components are shown below at the locations summarized in Table A.6a.

U (m/s)					
	0.2199	0.3301	0.3775	0.3836	0.3424
	0.0027	0.2964	0.3527	0.3681	0.334
	NaN	0.2625	0.3235	0.3491	0.3179
	NaN	0.0292	0.3134	0.3179	0.2955
	NaN	NaN	0.2128	0.2551	0.2698
	NaN	NaN	NaN	0.1564	NaN
	NaN	NaN	NaN	-0.002	NaN
V (m/s)					
	0.0062	0.0007	0.0001	0.0041	-0.0255
	0.0002	-0.0165	-0.0108	-0.0074	-0.0237
	NaN	-0.0385	-0.0258	-0.0225	-0.0219
	NaN	-0.0041	-0.0525	-0.0394	-0.0208
	NaN	NaN	-0.0447	-0.0429	-0.0146
	NaN	NaN	NaN	-0.0242	NaN
	NaN	NaN	NaN	0.0005	NaN
W (m/s)					
	0.0012	-0.0287	-0.002	0.0012	-0.0071
	-0.0257	0.0114	0.0036	0.0078	-0.0124
	NaN	-0.0148	0.0061	0.0154	-0.0125
	NaN	-0.0662	0.0298	0.0139	-0.0078
	NaN	NaN	0.0305	0.0152	-0.0058
	NaN	NaN	NaN	0.0257	NaN
	NaN	NaN	NaN	-0.0017	NaN

Table A.6c: Turbulence data for Meander 3 base level velocities measured on July 14, 2008 at the locations summarized in Table A.6a.

U'U' (m^2 / s^2)					
	0.001	0.001	0.0009	0.0009	0.0041
	0	0.0017	0.0014	0.0013	0.0043
	NaN	0.0019	0.0015	0.0015	0.0047
	NaN	0.0007	0.0012	0.0025	0.0049
	NaN	NaN	0.0026	0.0037	0.0052
	NaN	NaN	NaN	0.0027	NaN
	NaN	NaN	NaN	0	NaN
V'V' (m^2 / s^2)					
	0.0003	0.0005	0.0005	0.0006	0.0015
	0	0.0006	0.0006	0.0006	0.0017
	NaN	0.0006	0.0007	0.0008	0.0017
	NaN	0.0001	0.0008	0.0011	0.0016
	NaN	NaN	0.0009	0.0014	0.0014
	NaN	NaN	NaN	0.0012	NaN
	NaN	NaN	NaN	0	NaN
W'W' (m^2 / s^2)					
	0.0008	0.0008	0.0006	0.0007	0.0022
	0.0004	0.0012	0.0009	0.0009	0.0028
	NaN	0.0013	0.0013	0.0012	0.0035
	NaN	0.0026	0.0015	0.0017	0.0035
	NaN	NaN	0.0021	0.0026	0.0032
	NaN	NaN	NaN	0.0025	NaN
	NaN	NaN	NaN	0.0001	NaN

Table A.7: July 16, 2008 ADV data measured at flood level at the midpoint of Riffle 1. This data was not expected to change with the addition of vegetation. Recorded using SAFL Vectrino side-looking ADV at 25 Hz. Velocity and turbulence values are shown below.

Point	1	2	3	4	5	6	7	8	9	10
y (cm)	-76.5	-59.5	-42.5	-25.5	-8.5	8.5	25.5	42.5	59.5	76.5
Traverse y (mm)	465	635	805	975	1145	1315	1485	1655	1825	1995
Water depth (cm)	11	13	14	12	14	15	16	16	16	16
z (cm)	469	469	469	469	469	469	469	469	469	469
	473	473	473	473	473	473	473	473	473	473
		*Water surface at z = 469 cm, points measured down from there.								
U (m/s)										
	0.8734	0.9578	0.892	0.9494	0.8823	0.8165	0.822	0.7681	0.7822	0.7997
	0.5794	0.8089	0.7421	0.7483	0.6708	0.7429	0.6133	0.7063	0.4978	0.6694
V (m/s)										
	-0.001	0.0006	-0.0365	-0.076	-0.08	-0.0821	-0.124	-0.1297	-0.1425	-0.1717
	-0.0823	-0.0519	-0.0587	-0.1268	-0.0967	-0.1195	-0.2413	-0.2124	-0.1319	-0.2375
W (m/s)										
	0.0457	-0.0216	-0.0082	0.0049	0.0082	-0.0138	-0.0175	-0.0143	0.0238	-0.0306
	-0.0003	-0.0195	-0.0407	0.03	0.0236	-0.0024	0.148	-0.0166	0.0419	-0.044
U'U' (m^2 / s^2)										
	0.0102	0.0078	0.0094	0.0098	0.0136	0.0079	0.0162	0.0126	0.0202	0.0137
	0.0073	0.0071	0.0179	0.0168	0.0335	0.0104	0.0163	0.0117	0.0323	0.0157
V'V' (m^2 / s^2)										
	0.0031	0.0034	0.005	0.004	0.0055	0.0042	0.0062	0.0064	0.0065	0.0075
	0.0035	0.0053	0.0063	0.0062	0.0089	0.0057	0.0097	0.0082	0.0115	0.0087
W'W' (m^2 / s^2)										
	0.0042	0.0052	0.0053	0.0046	0.0078	0.0049	0.0083	0.0077	0.0085	0.0075
	0.0047	0.0068	0.009	0.0099	0.0278	0.0054	0.0125	0.0087	0.0205	0.0093

Table A.8: July 14, 2008 ADV data measured at base level at the midpoint of Riffle 1. This data was not expected to change with the addition of vegetation. Recorded using SAFL Vectrino side-looking ADV at 25 Hz. Velocity and turbulence values are shown below.

Point	1	2	3	4	5	6	7	8
y (cm)	-70	-50	-30	-10	10	30	50	70
Depth	3.5	5.5	6	6	4.5	4.5	4.5	4.5
Traverse z (cm)	451.5	451.5	450.5	451.5	451.5	451.5	452	452.5
		*Water surface around 452 cm, points measured down from there						
U (m/s)								
	0.3357	0.1475	0.3975	0.4891	0.2066	0.2258	0.5433	0.5307
V (m/s)								
	0.1124	0.0242	0.0319	-0.0008	0.011	-0.0591	-0.0767	-0.0307
W (m/s)								
	-0.0094	0.0125	-0.017	-0.0004	-0.0079	0.0475	-0.0153	0.0302
U'U' (m^2 / s^2)								
	0.0082	0.0064	0.0322	0.0132	0.0093	0.0093	0.0066	0.0025
V'V' (m^2 / s^2)								
	0.004	0.0007	0.0074	0.0031	0.0049	0.0025	0.0026	0.0012
W'W' (m^2 / s^2)								
	0.013	0.008	0.0636	0.0228	0.0089	0.0197	0.0051	0.0021

Table A.9: July 16, 2008 ADV data measured at flood level at the midpoint of Riffle 2. This data was not expected to change with the addition of vegetation. Recorded using SAFL Vectrino side-looking ADV at 25 Hz. Velocity and turbulence values are shown below.

Point	1	2	3	4	5	6	7	8	9	10
y (cm)	-81	-63	-45	-27	-9	9	27	45	63	81
Traverse y (mm)	580	760	940	1120	1300	1480	1660	1840	2020	2200
Water depth (cm)	11	16	15	16	16	14	14	14	14	15
z (cm)	480	480	480	480	480	480	480	480	480	480
	483	484	484	484	484	484	484	484	484	483
			*Water surface at z = 480 cm and points measured down from there							
U (m/s)	1.0327	0.9987	0.9204	0.871	0.8529	0.819	0.907	0.9658	0.9524	0.9772
	0.8862	0.6828	0.7234	0.633	0.8006	0.6586	0.6636	0.6963	0.9428	0.93
V (m/s)	0.2514	0.1854	0.1669	0.1047	0.0833	0.1084	0.074	0.0653	0.0484	0.0619
	0.2408	0.167	0.1219	0.0552	0.1079	0.0636	0.0534	0.0653	0.0384	0.0895
W (m/s)	-0.0003	0.0147	0.0197	0.0804	0.0209	-0.0512	0.0009	-0.0279	-0.0129	-0.0163
	-0.0154	-0.0046	0.0201	0.0461	-0.0389	-0.0687	-0.0009	-0.0335	-0.02	-0.0183
U'U' (m^2 / s^2)										
	0.0048	0.0103	0.0094	0.016	0.0098	0.0127	0.0127	0.0056	0.0031	0.0017
	0.0132	0.028	0.016	0.0454	0.015	0.0177	0.0341	0.0226	0.0081	0.0054
V'V' (m^2 / s^2)										
	0.0026	0.0042	0.0042	0.0062	0.0054	0.0051	0.0055	0.0028	0.002	0.0012
	0.0046	0.0099	0.0063	0.0147	0.0084	0.0079	0.0117	0.008	0.0021	0.0019
W'W' (m^2 / s^2)										
	0.0032	0.0048	0.0054	0.0091	0.0054	0.0066	0.0062	0.0029	0.002	0.0014
	0.0067	0.0227	0.0104	0.048	0.0128	0.0127	0.0244	0.0157	0.0115	0.0029

Table A.10: July 15, 2008 ADV data measured at base level at the midpoint of Riffle 2. This data was not expected to change with the addition of vegetation. Recorded using SAFL Vectrino side-looking ADV at 25 Hz. Velocity and turbulence values are shown below.

Point	1	2	3	4	5	6	7	8
y (cm)	-77	-55	-33	-11	11	33	55	77
Depth	4	4.5	5	5	6	4	5	5
Traverse z (cm)	443	443	443	443	443	443	443	443
		*Water surface at z = 443 cm, points measured down from there						
U (m/s)								
	0.2304	0.1107	0.2398	0.5222	0.4515	0.4091	0.3413	0.3675
V (m/s)								
	0.1105	-0.0314	-0.0693	-0.0375	-0.0213	-0.1114	-0.0743	-0.0588
W (m/s)								
	-0.0217	0.101	-0.0335	-0.1634	-0.0366	-0.1002	0.0324	-0.0087
U'U' (m^2 / s^2)								
	0.0062	0.0057	0.0064	0.0061	0.0023	0.0106	0.0044	0.0044
V'V' (m^2 / s^2)								
	0.0025	0.0038	0.0024	0.0016	0.001	0.0026	0.0029	0.0018
W'W' (m^2 / s^2)								
	0.01	0.0093	0.0078	0.0058	0.003	0.0091	0.0056	0.0039

Table A.11a: August 1, 2008 ADV data taken in the entrance plane (Plane A of Figure 2-1) to Meander 2 at flood level before the addition of vegetation. Recorded using Nepf Lab Sontek MicroADV at 25 Hz.

Point	1	2	3	4	5	6	7	8	9	10	11	12
y (cm)	-100	-90	-70	-50	-30	-10	10	30	50	70	90	100
Traverse y (mm)	360	460	660	860	1060	1260	1460	1660	1860	2060	2260	2360
Depth (cm)	9	12	31	31	27	26	29	30	32	19	19	10
Traverse z (cm)	478	478	479	479	479	479	479	479	479	479	479	479
	480	480	485	485	485	485	485	485	485	482	482	481
	482	482	490	490	490	490	490	490	490	485	485	
	484	484	495	495	492	492	494	494	494			
			498				498	498				
			*Water surface at z = 473 cm, and points measured down from there									

Table A.11b: Velocity data from August 1, 2008, flood level flow at the entrance plane (Plane A of Figure 2-1) of Meander 2. All three components are shown below at the locations summarized in Table A.11a.

U (cm/s)												
	-7.6256	6.7208	83.2828	80.724	72.8478	63.5624	95.317	70.3197	9.836	-6.1094	-25.3025	-5.1638
	-12.8121	4.8341	65.9877	57.459	54.8016	42.2369	77.5938	70.214	7.1772	-5.3114	-17.6158	-0.3167
	-14.5663	5.4644	53.0943	38.5738	36.9698	32.613	61.8663	59.4099	17.2346	-5.8192	-19.6265	NaN
	-14.547	2.8581	45.4087	4.0838	38.5456	34.8622	43.9751	45.5765	17.1041	NaN	NaN	NaN
	NaN	NaN	26.8356	NaN	NaN	NaN	33.7088	30.1911	NaN	NaN	NaN	NaN
V (cm/s)												
	0.8071	0.3147	-5.3579	-6.7847	-8.5486	-5.9176	-10.4267	-8.5872	-3.7385	4.6172	-1.9929	-1.3153
	1.3488	0.5201	-8.2645	-6.1121	-4.056	-1.7527	-4.7509	-3.9649	-1.2921	4.4711	-4.7404	0.2379
	4.0854	0.9021	-9.4215	-2.4757	0.692	0.694	-1.6746	0.9703	6.347	4.0258	-4.5875	NaN
	3.4538	1.3495	-1.3078	0.4353	2.4031	-1.1478	-0.7309	5.1517	12.7713	NaN	NaN	NaN
	NaN	NaN	4.8516	NaN	NaN	NaN	1.3514	9.1878	NaN	NaN	NaN	NaN
W (cm/s)												
	-0.5789	-0.0298	-2.412	5.237	1.0189	-3.4421	-3.6047	-2.5848	-1.0768	-0.2711	-3.1576	0.1232
	-4.3707	-1.7829	-6.7563	2.5946	0.3236	1.7682	-5.9179	-4.6906	0.19	1.5432	-4.8848	-0.0376
	-1.801	-2.2548	-7.313	2.467	-0.488	-1.0477	-6.9255	-5.3641	4.6076	-0.2535	-4.2342	NaN
	-0.1095	1.1356	-1.9692	0.5715	-1.8404	-0.8276	-2.74	-4.2028	7.937	NaN	NaN	NaN
	NaN	NaN	0.5166	NaN	NaN	NaN	-5.1042	-0.6715	NaN	NaN	NaN	NaN

Table A.11c: Turbulence data for the entrance plane (Plane A of Figure 2-1) of Meander 2 flood level velocities measured on August 1, 2008 at the locations summarized in Table A.11a.

U'U' (m^2 / s^2)												
	0.0171	0.0321	0.0549	0.044	0.0273	0.0189	0.0205	0.0466	0.0151	0.0045	0.0029	0.0011
	0.0154	0.0491	0.1094	0.0266	0.0236	0.0204	0.0344	0.0377	0.0105	0.0041	0.0052	0.0001
	0.0123	0.0462	0.0709	0.0215	0.0159	0.0152	0.0332	0.0379	0.0133	0.0048	0.0062	NaN
	0.0121	0.0284	0.0209	0.0112	0.0125	0.0148	0.0235	0.0259	0.0115	NaN	NaN	NaN
	NaN	NaN	0.0147	NaN	NaN	NaN	0.0199	0.0154	NaN	NaN	NaN	NaN
V'V' (m^2 / s^2)												
	0.0089	0.0195	0.0316	0.0158	0.0128	0.0126	0.0187	0.0121	0.0088	0.0044	0.004	0.0004
	0.0095	0.0344	0.0659	0.0176	0.0141	0.013	0.0197	0.0193	0.0077	0.0042	0.0033	0.0001
	0.0073	0.028	0.0515	0.0167	0.0138	0.0099	0.0238	0.0232	0.0074	0.0045	0.006	NaN
	0.0076	0.0169	0.0143	0.0111	0.0102	0.0115	0.0199	0.0168	0.007	NaN	NaN	NaN
	NaN	NaN	0.0127	NaN	NaN	NaN	0.0156	0.0094	NaN	NaN	NaN	NaN
W'W' (m^2 / s^2)												
	0.0095	0.0208	0.0105	0.0074	0.0071	0.0073	0.0052	0.0091	0.0087	0.004	0.0012	0.0002
	0.0103	0.02	0.0162	0.0099	0.008	0.0088	0.0092	0.0117	0.0101	0.0042	0.0018	0
	0.0094	0.0204	0.015	0.0112	0.007	0.007	0.0113	0.0137	0.009	0.002	0.0015	NaN
	0.0094	0.0177	0.0086	0.0006	0.0036	0.0059	0.0098	0.0132	0.0045	NaN	NaN	NaN
	NaN	NaN	0.0015	NaN	NaN	NaN	0.0046	0.0088	NaN	NaN	NaN	NaN

Table A.12: August 19, 2008 ADV data taken in the entrance plane (Plane A of Figure 2-1) to Meander 2 at flood level after the addition of vegetation. Recorded using Nepf Lab Sontek MicroADV at 25 Hz. Velocity and turbulence data are show below as well.

Point	1	2	3	4	5	6	7	8	9	10	11
y (cm)	-100	-90	-70	-50	-30	-10	10	30	50	70	95
Traverse y (mm)	360	460	660	860	1060	1260	1460	1660	1860	2060	2310
Traverse z (cm)	475	475	475	475	475	475	475	475	475	475	475
	481	482	481	481	481	481	482	481	479	479	NaN
	487	488	487	487	487	489	489	486	483	NaN	NaN
			*Water surface at z = 470 cm, and points measured down from there								
U (cm/s)	42.8523	68.9188	65.8144	54.3623	73.1541	62.3095	63.2062	32.2183	12.1386	-4.4455	-0.2433
	41.2143	57.5117	55.5092	70.1333	61.2807	47.0865	56.6871	37.2582	18.7312	-6.8036	NaN
	37.1185	43.6743	45.2411	42.2823	47.3268	33.0337	47.0428	35.1215	13.8959	NaN	NaN
V (cm/s)	-8.0642	-13.1889	-26.817	-3.5734	-9.4054	-4.5088	4.9422	10.2595	13.6269	12.6643	0.1465
	-9.8616	-11.8343	-8.4979	-9.7291	-3.2942	-0.0396	6.7756	13.0303	17.6348	8.9507	NaN
	-8.599	-6.7205	1.915	1.8989	2.4695	7.4746	7.3605	14.8545	16.7993	NaN	NaN
W (cm/s)	1.1804	-2.2558	-1.9842	-1.8541	-2.9724	1.8253	2.853	4.0062	4.0998	1.5811	0.0035
	-0.6395	-3.9596	-0.6136	-1.6655	-2.8107	3.7634	3.4802	5.9025	6.9043	-0.3109	NaN
	-1.2892	-2.2335	1.2461	-1.834	-2.5371	2.5694	2.204	6.1308	5.6966	NaN	NaN
U'U' (m^2 / s^2)	0.0447	0.0429	0.0465	0.0176	0.0147	0.0333	0.0391	0.0182	0.0101	0.0058	0.0002
	0.0429	0.0434	0.022	0.0186	0.0216	0.0241	0.0396	0.0192	0.0113	0.0065	NaN
	0.022	0.0239	0.0215	0.0133	0.017	0.016	0.0293	0.0192	0.0109	NaN	NaN
V'V' (m^2 / s^2)	0.0275	0.0269	0.0696	0.0126	0.0104	0.0149	0.0147	0.01	0.0073	0.0061	0.0003
	0.0218	0.0277	0.0126	0.0111	0.0127	0.0137	0.0157	0.0099	0.0076	0.0066	NaN
	0.0189	0.0173	0.0124	0.0097	0.0109	0.0144	0.0139	0.0119	0.0082	NaN	NaN
W'W' (m^2 / s^2)	0.0169	0.0132	0.0051	0.0061	0.0054	0.009	0.0117	0.0121	0.0094	0.0044	0
	0.0174	0.0135	0.0079	0.0058	0.0068	0.0089	0.011	0.0113	0.0074	0.0031	NaN
	0.0136	0.011	0.0052	0.0047	0.0059	0.0039	0.0062	0.0045	0.0024	NaN	NaN

Table A.13a: July 28, 2008 ADV data taken in the exit plane (Plane D of Figure 2-1) of Meander 2 at flood level before the addition of vegetation. Recorded using Nepf Lab Sontek MicroADV at 25 Hz.

Point	1	2	3	4	5	6	7	8	9	10
y (cm)	-99	-77	-55	-33	-11	11	33	55	77	99
Traverse y (mm)	290	510	730	950	1170	1390	1610	1830	2050	2270
Depth (cm)	23	27	23	21	20	16	15	10	8	7
Traverse z (cm)	478	478	478	478	478	478	478	480	480	479
	480	480	480	480	480	480	480	484		
	482	482	482	482	482	482	482			
	484	484	484	484	484	484	484			
	486	486	486	486	486	486	486			
	488	488	488	488	488					
	490	490	490	490	490					
	492	492	492	492						
		494								
		496								
		498								
		*Water surface at z = 473 cm, and points measured down from there								

Table A.13b: Velocity data from July 28, 2008, flood level flow at the exit plane (Plane D of Figure 2-1) of Meander 2. All three components are shown below at the locations summarized in Table A.13a.

U (cm/s)	68.3897	65.6447	65.3367	64.0676	63.9464	58.1166	58.0606	42.7386	32.9401	3.6633
	68.3642	67.8022	64.243	65.0645	61.9447	58.5613	51.8262	6.9726	NaN	NaN
	68.5944	68.6005	63.1752	63.5978	61.0385	57.0477	51.9668	NaN	NaN	NaN
	63.1114	68.3805	62.136	57.8455	58.1941	52.5516	32.0497	NaN	NaN	NaN
	55.9645	68.4902	61.2504	55.8701	53.5287	46.5002	41.2672	NaN	NaN	NaN
	44.4308	68.3943	59.4448	51.7248	45.5633	NaN	NaN	NaN	NaN	NaN
	29.6704	66.8323	53.851	38.1655	40.3969	NaN	NaN	NaN	NaN	NaN
	16.3373	66.1266	41.7689	31.9579	NaN	NaN	NaN	NaN	NaN	NaN
	NaN	56.4334	NaN	NaN	NaN	NaN	NaN	NaN	NaN	NaN
	NaN	50.1209	NaN	NaN	NaN	NaN	NaN	NaN	NaN	NaN
	NaN	36.7074	NaN	NaN	NaN	NaN	NaN	NaN	NaN	NaN
V (cm/s)	0.6927	-2.5255	-2.6372	1.0098	1.544	0.9881	-0.4885	3.6664	1.9343	0.138
	0.905	-0.6994	-0.3387	2.278	1.9281	3.2115	3.6103	1.0686	NaN	NaN
	2.2974	1.6421	2.8519	2.2987	4.9267	5.9541	5.3109	NaN	NaN	NaN
	3.7795	3.2512	6.2894	5.4511	6.3973	6.9863	5.3201	NaN	NaN	NaN
	4.6397	5.3577	10.3778	9.5375	10.6762	8.8599	8.0403	NaN	NaN	NaN
	5.3605	8.0701	14.7235	12.3379	11.3361	NaN	NaN	NaN	NaN	NaN
	5.7383	8.8411	17.941	9.3824	12.027	NaN	NaN	NaN	NaN	NaN
	6.0358	12.2737	18.9174	13.1492	NaN	NaN	NaN	NaN	NaN	NaN
	NaN	10.6926	NaN	NaN	NaN	NaN	NaN	NaN	NaN	NaN
	NaN	11.8005	NaN	NaN	NaN	NaN	NaN	NaN	NaN	NaN
	NaN	14.3699	NaN	NaN	NaN	NaN	NaN	NaN	NaN	NaN
W (cm/s)	-5.2406	-3.3928	-1.5851	-1.855	-2.9854	-1.4054	-1.8408	-1.6781	-0.7543	-0.1477
	-5.3938	-4.4052	-1.2974	-2.601	-4.0202	-2.8399	-0.4496	0.2994	NaN	NaN
	-5.1	-5.6364	-1.0304	-1.8836	-1.6971	-3.4213	-1.171	NaN	NaN	NaN
	-4.6805	-3.9425	-0.603	-1.6081	-1.956	0.6794	-1.7888	NaN	NaN	NaN
	-4.6308	-3.9478	-0.2714	-1.4289	-3.5411	-2.2153	-1.3429	NaN	NaN	NaN
	-5.4781	-3.3617	0.2548	-1.5922	-1.4183	NaN	NaN	NaN	NaN	NaN
	-5.2028	-4.6448	0.0977	0.4952	-2.9714	NaN	NaN	NaN	NaN	NaN
	-5.2698	-4.7353	-0.1266	-0.6971	NaN	NaN	NaN	NaN	NaN	NaN
	NaN	-1.7374	NaN	NaN	NaN	NaN	NaN	NaN	NaN	NaN
	NaN	-0.7107	NaN	NaN	NaN	NaN	NaN	NaN	NaN	NaN
	NaN	0.9923	NaN	NaN	NaN	NaN	NaN	NaN	NaN	NaN

Table A.13c: Turbulence data from July 28, 2008, flood level flow at the exit plane (Plane D of Figure 2-1) of Meander 2. All three components are shown below at the locations summarized in Table A.13a.

U'U' (cm^2 / s^2)	26.1036	25.7885	32.8778	30.0665	24.0717	24.8267	18.1284	155.2557	29.8411	7.4868
	35.3003	17.8034	37.9008	23.9596	25.3735	31.4612	19.7695	69.36	NaN	NaN
	42.1106	16.4457	42.0449	26.615	35.954	40.0941	39.197	NaN	NaN	NaN
	95.2688	18.5351	47.4351	31.2954	44.5541	92.9927	90.0956	NaN	NaN	NaN
	138.6123	25.2614	49.5749	60.9596	52.1318	83.1494	40.1137	NaN	NaN	NaN
	173.52	25.9496	59.4988	71.8948	131.8129	NaN	NaN	NaN	NaN	NaN
	214.9359	31.0295	75.8968	123.5305	60.1741	NaN	NaN	NaN	NaN	NaN
	140.1737	38.6554	96.544	70.0398	NaN	NaN	NaN	NaN	NaN	NaN
	NaN	50.603	NaN	NaN	NaN	NaN	NaN	NaN	NaN	NaN
	NaN	68.198	NaN	NaN	NaN	NaN	NaN	NaN	NaN	NaN
	NaN	102.1214	NaN	NaN	NaN	NaN	NaN	NaN	NaN	NaN
V'V' (cm^2 / s^2)	24.8821	34.828	33.8571	28.3134	24.7485	20.9656	17.7872	131.1995	12.9438	5.6819
	26.9476	26.519	33.4738	39.8241	26.3106	26.1964	15.1967	61.4307	NaN	NaN
	31.8963	26.1689	37.2744	27.695	32.0552	24.4857	24.3462	NaN	NaN	NaN
	57.6564	29.6593	37.9657	28.9256	31.4874	60.1128	24.1043	NaN	NaN	NaN
	84.5871	26.5452	37.0032	29.9149	31.9244	61.1117	22.8832	NaN	NaN	NaN
	115.3696	25.7792	38.647	27.9034	95.8915	NaN	NaN	NaN	NaN	NaN
	118.6336	24.7084	40.0725	162.6634	30.7117	NaN	NaN	NaN	NaN	NaN
	87.4867	28.7352	52.546	36.479	NaN	NaN	NaN	NaN	NaN	NaN
	NaN	27.0589	NaN	NaN	NaN	NaN	NaN	NaN	NaN	NaN
	NaN	33.0261	NaN	NaN	NaN	NaN	NaN	NaN	NaN	NaN
	NaN	69.6608	NaN	NaN	NaN	NaN	NaN	NaN	NaN	NaN
W'W' (cm^2 / s^2)	11.9918	13.415	16.3098	13.9805	9.8176	8.7558	7.3509	8.9786	3.1721	0.299
	16.6834	10.0161	18.7797	11.8731	11.0449	11.5015	6.3523	2.588	NaN	NaN
	23.3753	11.4569	20.4073	9.5728	12.97	11.5984	10.4156	NaN	NaN	NaN
	40.4487	11.8855	22.1952	11.0352	13.7885	10.7468	9.1832	NaN	NaN	NaN
	52.0432	11.9912	21.3414	12.3683	15.1973	17.8923	7.4358	NaN	NaN	NaN
	69.6496	13.4187	23.0403	15.5636	13.9076	NaN	NaN	NaN	NaN	NaN
	80.6524	15.3534	20.5236	18.54	10.127	NaN	NaN	NaN	NaN	NaN
	60.5853	16.0754	15.8291	8.408	NaN	NaN	NaN	NaN	NaN	NaN
	NaN	16.4214	NaN	NaN	NaN	NaN	NaN	NaN	NaN	NaN
	NaN	17.554	NaN	NaN	NaN	NaN	NaN	NaN	NaN	NaN
	NaN	19.3293	NaN	NaN	NaN	NaN	NaN	NaN	NaN	NaN

Table A.14: August 12, 2008 ADV data taken in the exit plane (Plane D of Figure 2-1) of Meander 2 at flood level after the addition of vegetation. Recorded using Nepf Lab Sontek MicroADV at 25 Hz. Velocity and turbulence data are included below.

Point	1	2	3	4	5	6	7	8	9	10
y (cm)	-99	-77	-55	-33	-11	11	33	55	77	99
Traverse y (mm)	290	510	730	950	1170	1390	1610	1830	2050	2270
Depth (cm)	23	27	23	21	20	16	15	10	8	7
Traverse z (cm)	477	477	477	477	477	477	477	477	477	477
	483	483	483	481	481	480	480	479	478	
	487	489	487	485	485	483	483	481		
			*Water surface at z = 472 cm, and points measured down from there							
U (cm/s)	71.8289	68.8572	68.1049	67.4884	65.192	62.5844	53.7907	31.9564	16.4597	7.9756
	62.3567	72.0019	69.6033	65.7878	66.8246	60.7525	19.593	40.9286	9.591	NaN
	29.6531	70.1237	60.537	56.4311	56.8938	53.8793	11.5035	6.2926	NaN	NaN
V (cm/s)	-8.2843	-10.9579	-10.3842	-6.7551	-3.902	-2.9705	1.7298	1.3758	-5.1943	-1.9887
	-3.1777	-5.5588	-1.935	-1.3338	0.1379	2.2226	3.9304	2.8755	0.9927	NaN
	2.3239	1.1918	5.8827	-0.1506	8.2233	10.4515	0.6898	-0.968	NaN	NaN
W (cm/s)	-5.5956	-4.3172	-2.3588	-2.4257	-2.8645	-1.4798	-0.4407	-0.8881	-1.6124	-1.3107
	-4.6806	-5.0302	-1.1162	-1.8766	-2.4428	-5.5937	-2.4683	-0.7055	-1.6227	NaN
	-5.5495	-4.9246	-0.192	-2.8535	-3.0666	1.6584	0.0189	-1.1313	NaN	NaN
U'U' (cm^2 / s^2)	26.4459	18.2942	25.7126	20.0684	19.3454	23.9508	51.1038	20.2475	10.4262	8.0808
	110.9131	25.3613	55.708	49.6015	33.4755	46.038	143.3486	19.1529	5.6057	NaN
	293.2379	33.3163	84.475	72.5165	113.3721	61.9675	223.8086	86.9497	NaN	NaN
V'V' (cm^2 / s^2)	21.8143	31.0698	29.9467	23.952	19.3002	15.1088	32.4687	15.1122	7.3406	7.4463
	63.6093	31.1429	35.0749	34.7514	25.3633	37.5705	24.8885	17.9539	5.6105	NaN
	127.6255	27.5013	42.703	41.7195	59.8672	24.7677	275.8246	18.902	NaN	NaN
W'W' (cm^2 / s^2)	11.2878	11.1317	15.185	10.8278	10.2981	8.7189	24.2854	7.0379	2.2806	0.8452
	37.7912	14.245	23.4135	16.5927	11.6897	17.6477	8.5815	5.1785	0.7013	NaN
	84.4637	18.1768	26.3132	16.2654	12.0716	10.9371	11.1716	4.0345	NaN	NaN

Table A.15: Tabulated data from Figure 2-9, the depth of the bed measured at the apex of Meander 2 before and after the addition of vegetation.

Measured July 16 (cm)	29	26	24	20	15	12	10	9.5	10	13
y-location (cm)	-112.5	-87.5	-62.5	-37.5	-12.5	12.5	37.5	62.5	87.5	112.5
Interpolated July 16 (cm)	27.38	25.16	22.8	19.1	14.82	12.18	10.36	9.65	9.79	11.38
y-location (cm)	-99	-77	-55	-33	-11	11	33	55	77	99
Measured August 26 (cm)	31	26	24	19	17	14	12	10	7	8
y-location (cm)	-99	-77	-55	-33	-11	11	33	55	77	99

A.3. *Fluorometer Calibration Data and Residence Time Distributions*

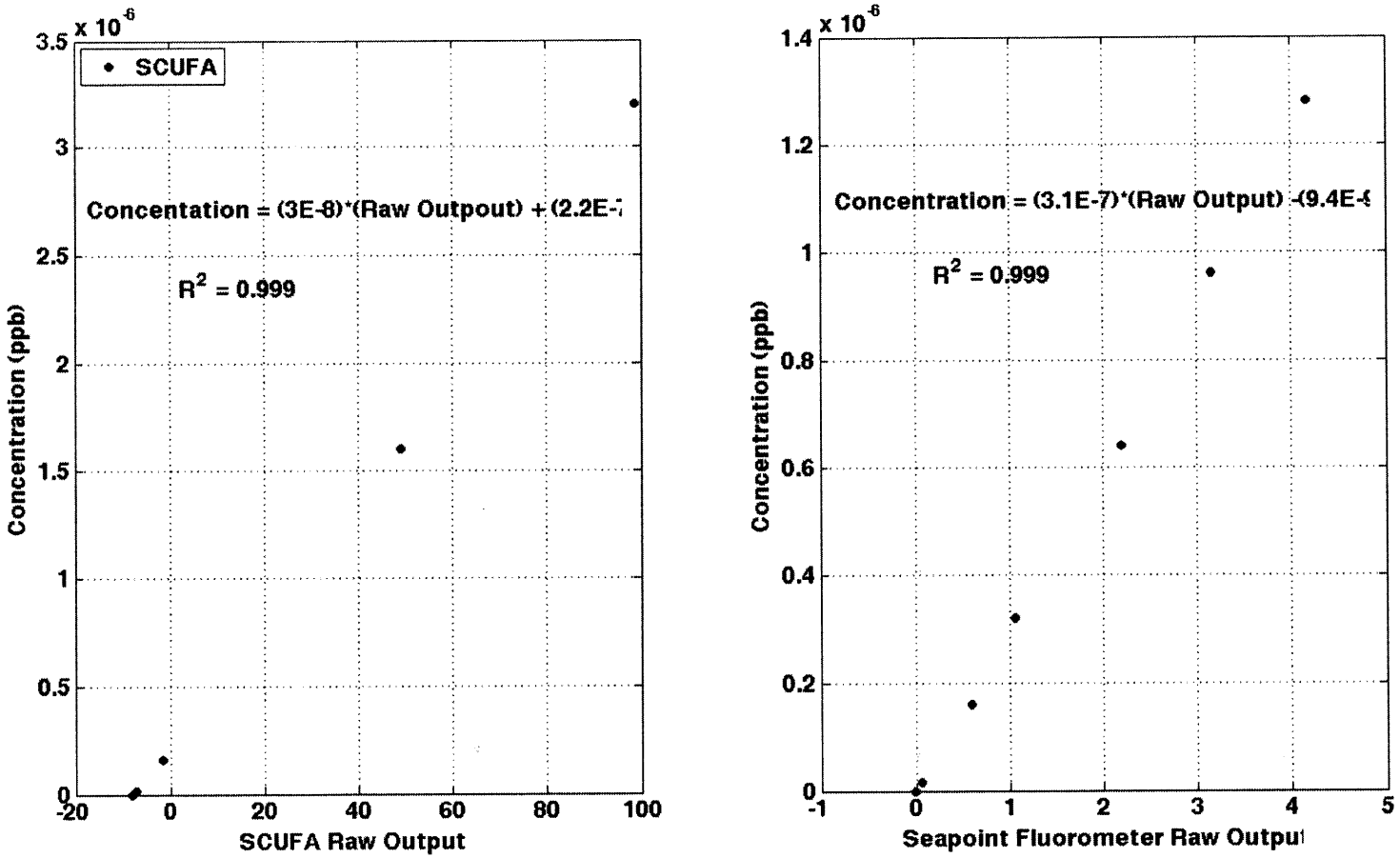

Figure A-1: Fluorometer calibration curves for both the (a) SAFL SCUFA and the (b) Nepf Lab Seapoint Systems Fluorometer.

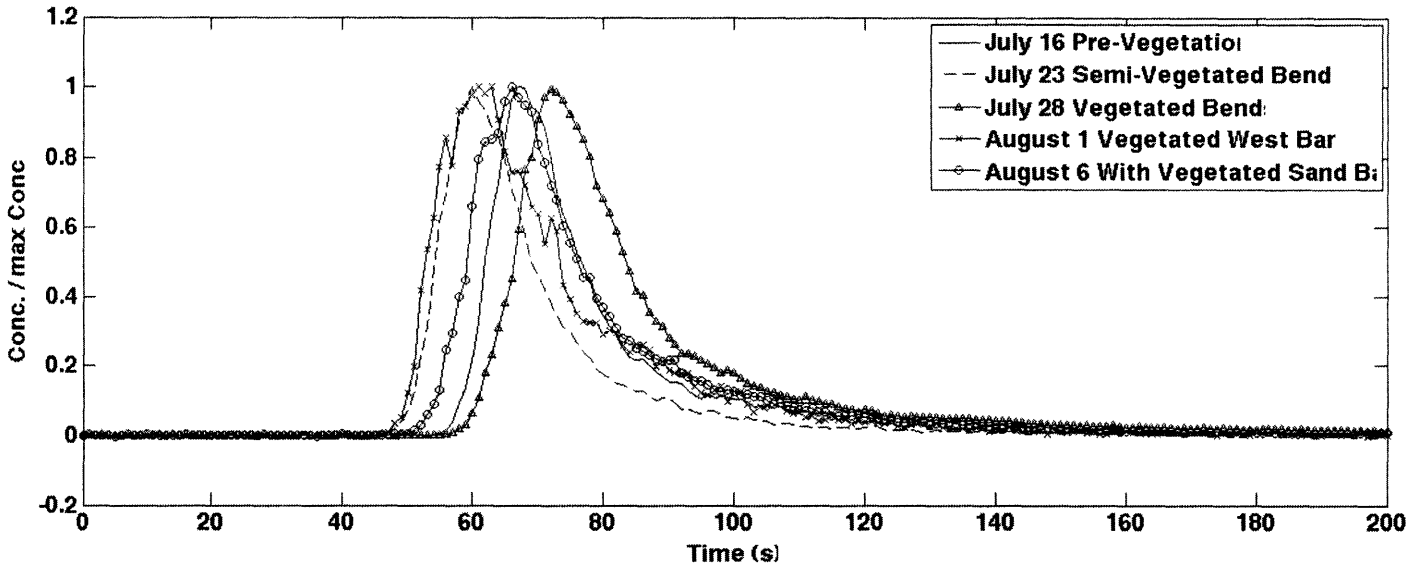

Figure A-2: Residence time distributions for the reach-scale tracer studies conducted throughout the summer. This data is summarized in Figure 2-14.

A.4. *Deposition Experiments*

Several experiments were conducted to look at the rates of sediment deposition within the plant canopy on the point bar in Meander 2 and in the corresponding locations on the unvegetated point bar in Meander 3. In these experiments, small square pieces of drywall sanding screens (4 in. by 4 in.) were backed with a vinyl liner and placed on the point bar, flush with the surface of the sand. The locations are shown below in Figures A-3a and A-3b. The screens were fastened to the bar using metal wires as anchors in the sandy substrate. Several floods were run during which different materials were added to the flow as suspended sediment (turbidity), including Kaolinite (D_{50} = 20 μm), fine sand (D_{50} = 110 μm), and organic ditch soil (D_{50} = 17 μm). . Bed load sediment was assumed constant across the season. Following the flood experiments, the flow level subsided back to base level, exposing the point bars. After the deposition screens were exposed, they were carefully collected in individual plastic bags. In the laboratory, the screens were carefully washed and all of the collected sediment was dried in an oven for 24 hours at 100 degrees C. and weighed. The collected mass of sediment at each location is shown below in Figures A-4 and A-5.

The results show no clear pattern of deposition at different points along the point bar, nor any clear pattern across the different sediments released as turbidity. On the vegetated bar, very little sediment is collected near the tailing edge of the patch, which could be because sediment has entirely settled out of the water column by that point. The most sediment is collected on the vegetated bar near the leading edge and the outer middle edge, which are exposed to the highest velocities. On the unvegetated, "bare," bar, the most sediment is collected near the leading edge and the tailing edge regions, with little collected near the middle of the bar.

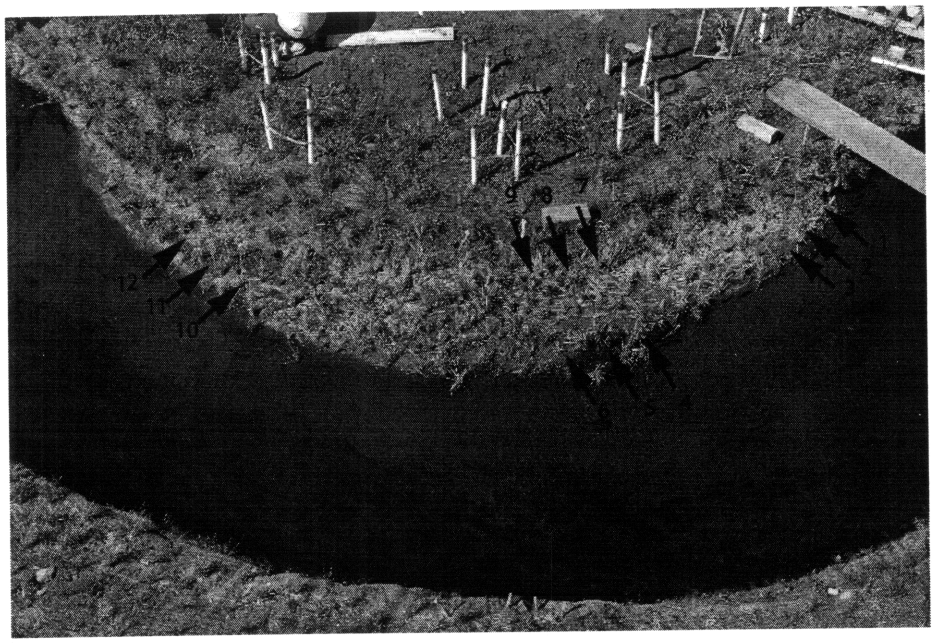

Figure A-3a: Sediment deposition screen locations in the vegetated point bar of Meander 2. Flow is from right to left in this image.

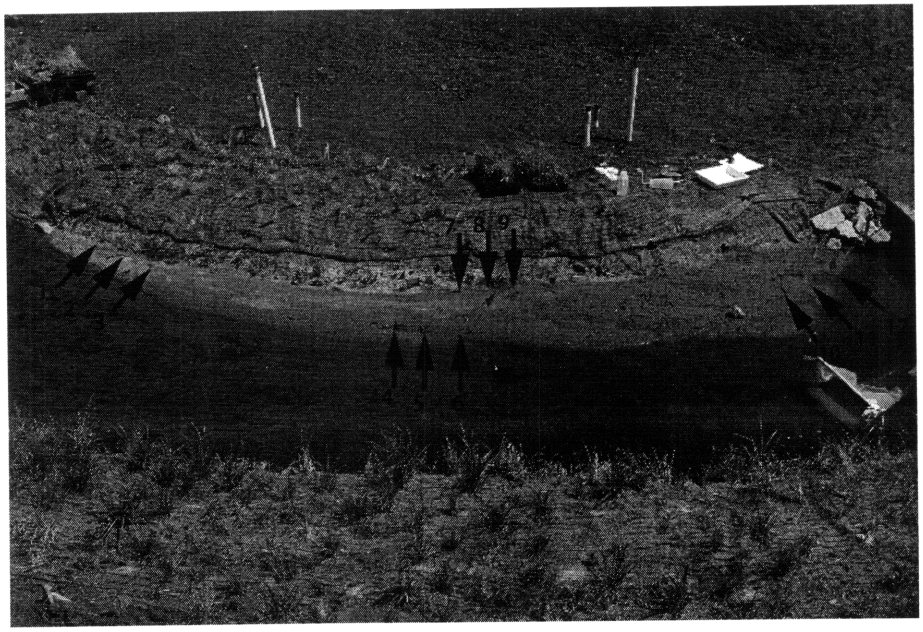

Figure A-3b: Sediment deposition screen locations in the un-vegetated point bar of Meander 3. The flow is from left to right in this image.

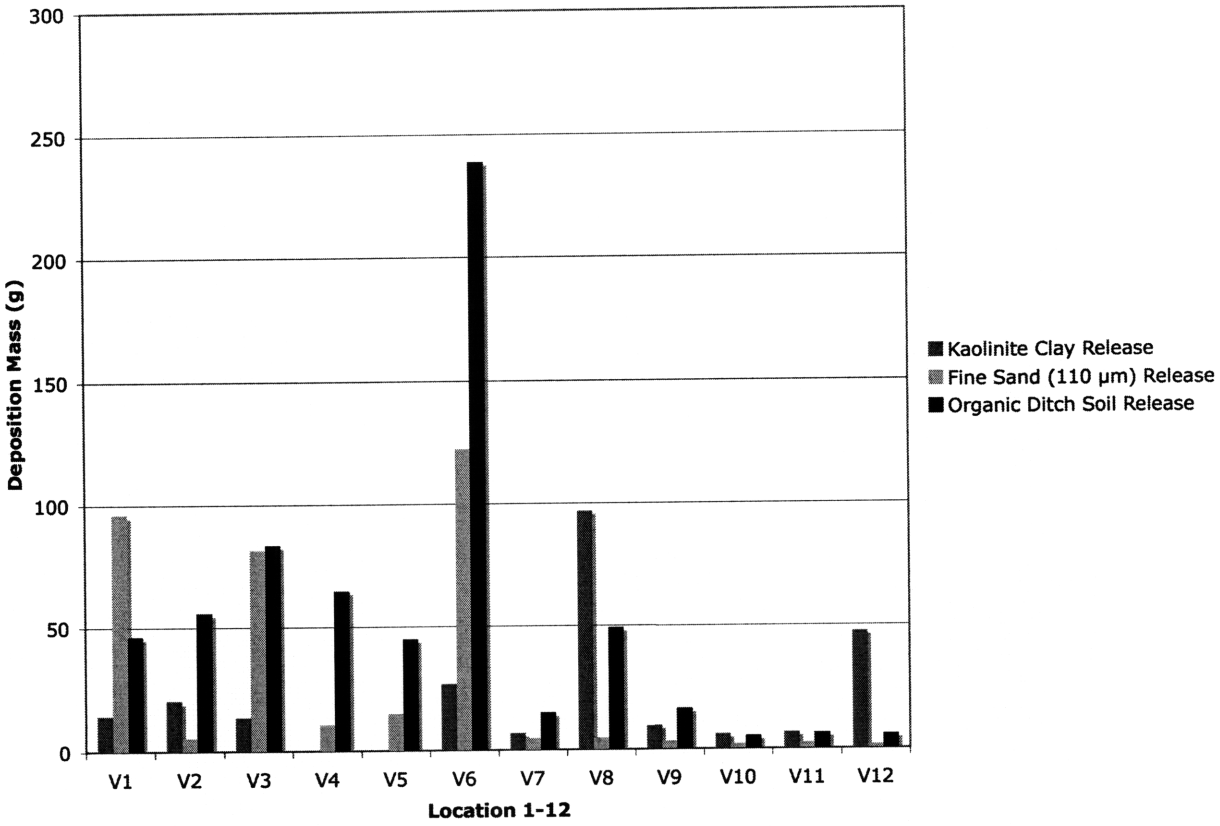

Figure A-4: Vegetated sand bar deposition screen results at each of the screen locations shown in Figure A-3a.

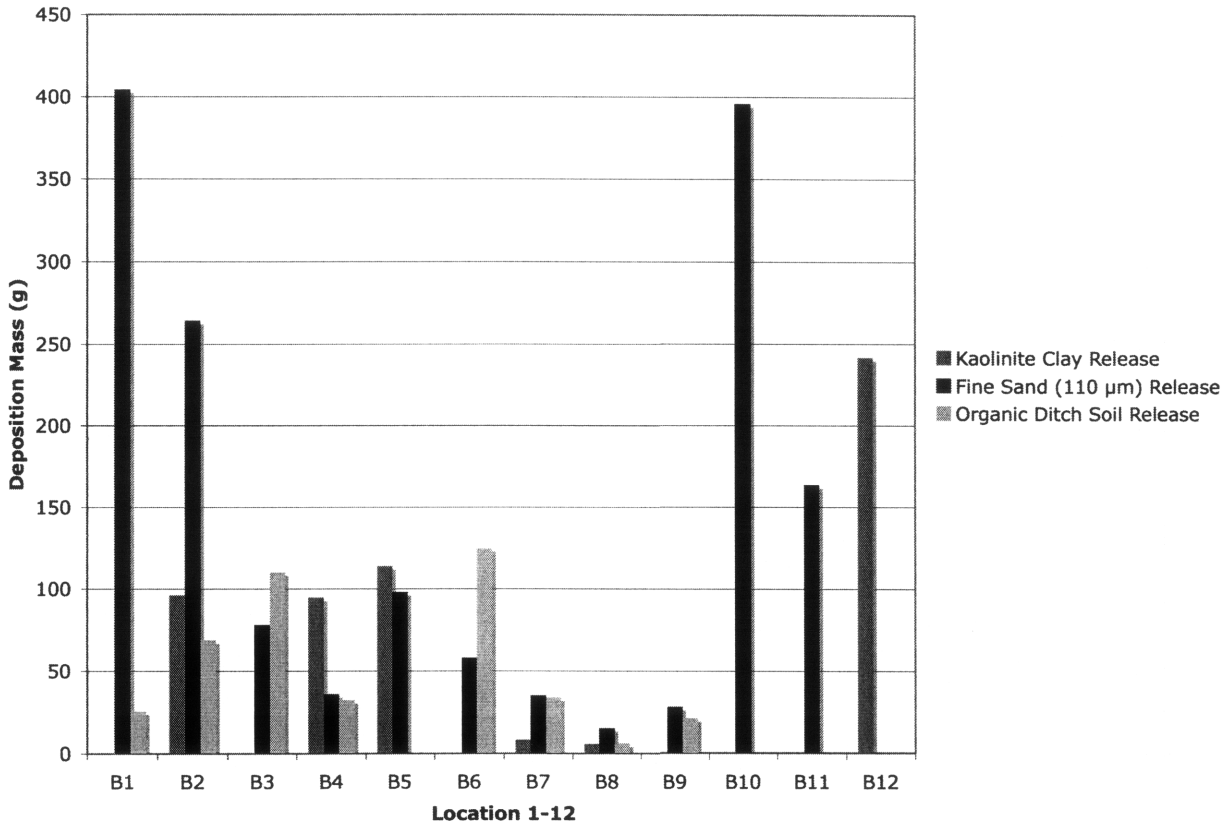

Figure A-5: Unvegetated, "bare," sand bar deposition screen results at each of the screen locations shown in Figure A-3b.

Appendix B: Data from Chapter 3 Seagrass Meadow Coverage

B.1. *Probability Density Plot Data*

Table B.1: Probability Density Plot data, from Figure 3-3. Source of Data is Fonseca and Bell (1998) figure 3b.

Coverage	#
0-10%	4
10-20%	4
20-30%	6
30-40%	10
40-50%	8
50-60%	4
60-70%	6
70-80%	5
80-90%	3
90-100%	17

Appendix C: Chapter 4 MATLAB Codes

C.1. *MATLAB Code for Model 1*

```
%jtr 12/11/08
%to predict velocities in open channel and in vegetation in a stream cross
%section with known and fixed Q, h=constant and the width of
%the vegetation, b, as some portion of the entire (constant) width of the
%channel, W.

%S can vary with changing b, but S is constant across the width of the
%channel.

clear all
Q=.2;
h=.18;
CDa=5;  %[m^-1]
Cf=.005;
g=9.8;

W=2.5; %set width =1
b=0:.001:W; %set width of vegetation to vary between nothing and full coverage
bnorm=b./W;

%%%%%%%%now define the constant in the quadratic equation for U
A1=-0.5.*CDa.*(h.^2).*b.*((W-b).^3);
A2=0.5*(b.^3).*(W-b).*Cf.*h;
A3=W.*(((b.^2).*(h.^2))+2.*b.*(h.^2).*(W-b)+(h.^2).*((W-b).^2));
A=A1+A2+A3;

B1=-W.*((2.*b.*h.*Q)+(2.*Q.*h.*(W-b)));
B2=-(b.^2).*(W-b).*Cf.*Q;
B=B1+B2;

C1=W.*(Q.^2);
C2=0.5.*b.*(W-b).*Cf.*(1./h).*(Q.^2);
C=C1+C2;
%%%%

%Now do the quadratic equation to solve for U
U2=((-B)-(((B.^2)-(4.*A.*C)).^0.5))./(2.*A);

Uo2=(Q-(U2.*b.*h))./((W-b).*h);

%plot the results
figure(1);
hold on
plot(bnorm,Uo2,'k');
plot(bnorm,U2,'--k');
```

C.2. *MATLAB Code for Model 2*

```
%jtr 3/31/09
%streamvelocities_iteration_part3
%the open channel bed, the vegetation, and the outer bank can all erode at
%the same rate.  The code will "erode" these boundaries incrementally until
%the velocity reduce below the critical velocity.
%Q and h are known and constant.  S can vary with varying b, but is
%constant across the width of the channel.

clear all

%hydraulic parameters
step=.0001;
Q=.2;
CDa=5;  %[m^-1]
Cf=.005;
ho=.18:step:10;
hv=.18;
Ucr=.53; %arbitrary critical velocity threshold

W=2.5:step:4; %set width
b_added=0:step:1.5; %set width of vegetation to vary

for j=1:length(b_added)
    Uo(j)=.7; %dummy velocity to initiate while loop
    i=1;
    b=b_added(j):-step:0;
    ho_baseline(j)=ho(1);

    while Uo(j)>Ucr

        %%%%%%%%%define the constant in the quadratic equation for Uv
        A1=CDa;
        A2=-(1./b(i));
        A3=-((hv^2).*(b(i))).//((ho(i)^2).*((W(i)-b(i)).^2));
        A4=-2.*hv./(ho(i).*(W(i)-b(i)));
        A5=-Cf.*(b(i).^2).*(hv.^2)./((ho(i).^3).*((W(i)-b(i)).^2));
        A6=-(hv.^2).*(b(i).^2)./((ho(i).^2).*((W(i)-b(i)).^3));
        A7=-2.*hv.*b(i)./(ho(i).*((W(i)-b(i)).^2));
        A=A1+A2+A3+A4+A5+A6+A7;

        B1=(2*Q*hv)./((ho(i)^2).*((W(i)-b(i)).^2));
        B2=(2*Q)./(ho(i).*(W(i)-b(i)).*b(i));
        B3=(2*Q*hv*Cf).*b(i)./((ho(i).^3).*((W(i)-b(i)).^2));
        B4=(2*Q*hv).*b(i)./((ho(i).^2).*((W(i)-b(i)).^3));
        B5=(2*Q)./(ho(i).*((W(i)-b(i)).^2));
        B=B1+B2+B3+B4+B5;

        C1=-(Q^2)./((ho(i)^2).*((W(i)-b(i)).^2).*b(i));
        C2=-(Cf*(Q^2))./((ho(i).^3).*((W(i)-b(i)).^2));
        C3=-(Q^2)./((ho(i).^2).*((W(i)-b(i)).^3));
        C=C1+C2+C3;
        %%%%

        %Now do the quadratic equation to solve for Uv and Uo
        Uv(j)=((-B)+(((B.^2)-(4.*A.*C)).^0.5))./(2.*A);
        Uo(j)=(Q-(Uv(j).*b(i).*hv))./((W(i)-b(i)).*ho(i));

        i=i+1;
```

```
    end
    ho_result(j)=ho(i-1);
    b_result(j)=b(i-1);
    W_result(j)=W(i-1);
end
```